Diffusion and perfusion-weighted imaging in the structural and functional characterization of diffuse gliomas for differential diagnosis and treatment planning

Anna Latysheva

Doctoral Thesis

Faculty of Medicine, University of Oslo

2020

Department of Radiology and Nuclear Medicine,

Oslo University Hospital - Rikshospitalet

Oslo, Norway

Series of dissertations submitted to the
Faculty of Medicine, University of Oslo

ISBN 978-82-8377-727-7

Cover: Hanne Baadsgaard Utigard.
Print production: Reprosentralen, University of Oslo.

Fields of knowledge exist and advance because we find beauty and joy within them.

Thomas P. Naidich

The idea must be very high, much higher than the ways to realize it.

Fyodor M. Dostoevsky

TABLE OF CONTENTS

ACKNOWLEDGEMENTS

This thesis was initiated and carried out at the Section of Neuroradiology, Department of Radiology in collaboration with the Department of Diagnostic Physics and Department of Neurosurgery at the Oslo University Hospital - Rikshospitalet from 2015 to 2020.

First of all, I would like to express my gratitude towards all the patients participating in this project and thus contributing to the increased knowledge of MR imaging of diffuse glioma.

This work is the result of the contribution of many scientists and skilled people I have the privilege of working together with both on my project and every day work and I would like to express my sincere gratitude.

My deepest thankfulness goes to my principal supervisor, Andrés Server Alonso, for all encouragement and for sharing your endless knowledge. You have always found time for me in your very busy days, where many other colleagues ask for your help and expertise as well. These studies could not have been carried out without your invaluable help. You are a role model in my professional and academic career. I am very lucky to have you as my supervisor and colleague.

I am also very grateful for my supervisor John K Hald for introducing me to the brain tumor imaging research group and for all your support. You inspired me to begin, go through and complete this work. You have provided a lot of help and support to this project even after your retirement, and it is highly appreciated.

My warmest gratitude goes to my co-supervisor Kyrre Eeg Emblem. You are one of the most enthusiastic and inspiring persons I know. Your knowledge and skills in so many different fields as physics, mathematics, statistics and radiology impress me a lot. I have also learned much from your talent in networking and cooperation. Thank you very much for your contributions in all aspects of this work.

I am very thankful for my co-supervisor, Einar Osland Vik-Mo. Your great clinical knowledge and experience, practical approach and the endless optimism continues to impress me. You have been very important in the clinical aspects of this thesis. Thank you for the close collaboration in the past five years and for always giving constructive feedback.

I would also express my sincere thanks to my co-supervisor Oliver Marcel Geier. Despite your continually involvement in many different research projects, you always had time and capacity to come up with questions, scientific remarks and suggestions. Your assistance with image postprocessing is invaluable. Thank you for your patience and willingness to explain me ‘’the banal things’’ within MRI physics over and over again.

I would like to acknowledge the valuable contributions from all my co-authors Petter Brandal, Torstein R. Meling, Jens Pahnke, Kjetil Røysland, Tuva Hope, Marta Brunetti and Francesca Micci. Thank you for your knowledge, extensive experience, clear views, reliability and quick response to questions and drafts.

I will express my gratitude to the previous and present heads of the Department of Radiology, Paulina B Due-Tønnessen and Einar Hopp and to the heads of Section of Neuroradiology, Mona K Beyer and Bjørn Tennøe for giving me the time to complete this study. Your sincere and warm wishes to do good for everyone in our department are remarkable.

I am also very grateful to my close colleagues and friends at the section of neuroradiology: Vanja Cengija, Øivind Gjertsen, Oksana Lapina, Pål Bache Martinssen, Bård Nedregaard, Terje Nome, Geir Andre Ringstad, Thomas Sakinis, Thor Håkon Skattør, Ruth Sletteberg and Martin Sökjer. Thank you for your encouragement, believing in me, good discussions and always good company. I would never have time to finish this thesis without your cooperation. What a wonderful place to work!

Special thanks go to Alexandra Hankin for all your linguistic support and many good conversations (with your corrections) at our office.

Also, huge thanks to our MRI radiographers. Without your enthusiastic help in our busy every-day, willingly including patients, this study would not have been possible.

To my parents, Larisa and Viktor whose value to me only grows with age. Thank you for allowing me to be what I was meant to be. I am so lucky to have you! My especial thanks to my closest family Gunnar and Randi, my children's wonderful grandparents, for your presence and constantly positive support. And to my brothers Sergey and Nikolay, for stimulating my competitive spirit (you got your PhDs a long time ago) and for great inspiration.

To my dear children Andrè, Max and Emilie, thank you for all fun distractions and for reminding me of what is important in life. Thanks for your daily question: have you finished your thesis? Finally, I can give you a positive answer.

My dearest Henning, words are not sufficient, for your endless patience, love and support. You are my best friend and I feel so lucky.

Anna Latysheva – Oslo, April 2020

ABBREVIATIONS

2D	2-dimentional
3D	3-dimentional
ADC	Apparent diffusion coefficient
ADC_{Mean}	ADC mean value of the normalized histogram
ADC_{Peak}	ADC maximum peak heights of the normalized histogram
AI	Artificial intelligence
ASL	Arterial spin-labeling
APT	Amide proton transfer
AUC	Area under the curve
BBB	Blood-brain barrier
BOLD	Blood oxygen level dependent
CBF	Cerebral blood flow
CBV	Cerebral blood volume
CT	Computed tomography
CET	Contrast-enhancing tumor core
CEST	Chemical exchange saturation transfer
cNAZ	Normal-appearing white matter contralateral to the tumor
CPH	Cox proportional hazard regression analysis
CNS	Central nervous system
DCE MRI	Dynamic contrast-enhanced perfusion MR imaging
DSC MRI	Dynamic susceptibility contrast perfusion MR imaging
DSI	Diffusion spectrum imaging
DWI	Diffusion-weighted imaging
DTI	Diffusion tensor imaging
DKI	Diffusional kurtosis imaging
EPI	Echo-planar imaging
ECM	Extracellular matrix
FA	Fractional anisotropy
fMRI	Functional MRI
FZ	Far zone
FOV	Field of view
FLAIR	Fluid attenuated inversion recovery
HARDI	High angular resolution diffusion imaging
HR	Hazard ratio
GBCA	Gadolinium-based contrast agent
IDH1 and IDH2	Isocitrate dehydrogenase 1 and 2
iNAZ	Ipsilateral normal-appearing zone
iRANO	Immunotherapy response assessment for neuro-oncology
ITSS	Intratumoral susceptibility signal
IVIM	Intravoxel incoherent motion
K^{trans}	Volume transfer constant
LOOCV	Leave-one-out cross-validation
MGMT	O^6-Methylguanine-DNA-Methyltransferase promoter
MD	Mean diffusivity
ML	Machine learning
MLPA	Multiplex ligation-dependent probe amplification
MRI	Magnetic resonance imaging
MTT	Mean transit time

NZ	Near zone
NMR	Nuclear magnetic resonance
OS	Overall survival
OD	Odds ratio
PFS	Progression-free survival
PEZ	Peri-enhancing zone
PBZ	Peritumoral brain zone
PCR	Polymerase chain reaction
RANO	Response assessment for neuro-oncology
rCBV	Relative cerebral blood volume
ROC	Receiver operator characteristic
ROI	Region of interest
RSI	Restriction spectrum imaging
SD	Standard deviation
SWI	Susceptibility weighted imaging
T1	Longitudinal relaxation time in units of ms
T1W	T1-weighted
T1 MPRAGE	3D-T1 magnetization-prepared rapid gradient-echo
T1 SPACE	3D-T1 Sampling perfection with application of optimized contrast using different flip angle evolution
T2	Transverse relaxation time in units of ms
T2W	T2-weighted
TE	Echo time in units of ms
TERT	Telomerase reverse transcriptase
TR	Repetition time in units of ms
VEGF	Vascular endothelial growth factor
VOI	Volume of interest
WHO	World Health Organization

SUMMARY IN ENGLISH

Diffuse infiltrative gliomas are the most common primary brain tumors in adult population and represent a range from slow-growing lesions to highly invasive tumors with poor prognosis. The growth potential and aggressiveness of gliomas depend on World Health Organization (WHO) grade and molecular features. The standard radiographic characterization of glioma is based on magnetic resonance imaging (MRI); a widely utilized examination for both the initial diagnosis and for ongoing post-treatment management of these patients. Despite the growing success and number of applications in neuro-oncologic imaging there are still many challenges that need to be solved with regard to diagnosis, preoperative delineation and posttreatment monitoring of gliomas.

The objectives of this thesis were to evaluate the value of the advanced MR techniques, as perfusion and diffusion imaging, to characterize diffuse gliomas with respect to WHO grading systems, morphologic and genetic features and to find new imaging prognostic biomarkers in order to individualize medical management.

In study I we retrospectively evaluated the ability of Apparent Diffusion Coefficient (ADC) and relative Cerebral Blood Flow (rCBV) parameters derived from whole-tumor normalized histograms to stratify progression-free survival (PFS) and overall survival (OS) in patients with diffuse gliomas grade II and III. In patients with oligodendrogliomas we found that tumors with heterogeneous perfusion signatures and high average perfusion values were associated with longer PFS, while in patients with astrocytomas, heterogeneous perfusion distribution was associated with poorer outcomes. We did not find a significant association between ADC from diffusion MRI and patient survival. Our results indicate that perfusion MRI might serve as an independent factor to predict prognosis in patients with diffuse gliomas.

Study II was based on the same retrospective material as for study I. The aim was to determine whether the rCBV and ADC parameters could help differentiate genetically defined oligodendrogliomas from astrocytomas and to distinguish between WHO grade II and grade III diffuse gliomas. Several large clinical trials have demonstrated that patients with oligodendrogliomas *(Isocitrate dehydrogenase (IDH)*-mutant and 1p19q codeleted gliomas*)* derive more benefit from chemotherapy when compared to their genetic astrocytoma counterparts. Differentiation between these two entities affects treatment strategy and prognosis. We found that patients with oligodendrogliomas showed significantly higher microvascularity and higher vascular heterogenity than patients with astrocytomas. Among diffuse gliomas, oligodendrogliomas revealed a higher cellular density. Combined use of ADC and rCBV histogram parameters had superior diagnostic performance to identify oligodendroglial tumors. Thus, imaging-based biomarkers of vascularity and cellularity may constitute a non-invasive supplement to histopathologic and molecular genetic markers and provide important information to guide future treatment.

In study III we prospectively included forty-two patients with untreated IDH wild-type glioblastoma to evaluate the ability of MRI-based Restriction Spectrum Imaging (RSI) to estimate the level of cellularity (cell density in tissue) in the different tumoral zones. We also investigated the prognostic value of RSI to assess the potentially aggressive behavior of the tumor and compared it to established diffusion metrics such as mean diffusivity (MD) and fractional anisotropy (FA). The highest RSI-cellularity index was measured in the contrast-enhanced zone with a negative gradient from the tumor core to the periphery of the peritumoral zone. Shorter survival outcomes were significantly associated with higher RSI-cellularity index in the contrast-enhanced zone, but also in the peri-enhancing zone and near peri-tumoral zone. In contrast, MD and FA in the near peri-tumoral zone did not show any predictive value to survival outcome, which may indicate a more severe affection of MD and FA values by extracellular edema than for RSI-cellularity index. RSI provided a promising prognostic biomarker to depict tumor infiltration in the peritumoral brain zone, which can be helpful to optimize surgical procedures and radiation field mapping with significant benefits for treatment.

In conclusion, our results suggest that both perfusion and diffusion MRI provide reliable non-invasive biomarkers of glioma status and the information from the two imaging techniques appear to be complementary. Additionally, to further implementation of these modalities in a diagnostic work-flow, multicenter studies are warranted that would assist in standardizing imaging protocols as well as postprocessing procedures.

SAMMENDRAG PÅ NORSK

Diffust infiltrerende gliomer er den vanligste primære hjernesvulsten hos voksne. Gliom spenner fra langsomt voksende lesjoner til aggressive svulster med særdeles dårlig prognose. Vekstpotensialet og aggressivitet er avhengig av Verdens helseorganisasjon (WHO)-grad og molekylære egenskaper. Standard radiologisk utredning er basert på forskjellige magnetresonanstomografi (MR) teknikker, både ved initial diagnostikk og ved senere kontroller etter behandling. Til tross for stadig utvikling av MR teknikker og økende bruk innen nevroonkologisk avbildning, er det fortsatt mange utfordringer knyttet til diagnostikk, pre-operativ kartlegging og oppfølging i behandlingen av gliomer.

Dette arbeidet har hatt som mål å evaluere bruken av avanserte MR-sekvenser med perfusjon- og diffusjon-vekting for karakterisering av diffuse gliomer, vurdert opp mot WHO-grad, morfologi og genetiske egenskaper. I tillegg har vi hatt som mål å finne radiologiske parameter som kan navigere persontilpasset kreftbehandling. Dersom man kan identifisere gliomtype og WHO grad preoperativt kan dette legge grunnlag for viktige behandlingsvalg ved kirurgi.

Den første studien er retrospektiv og vurderte om Apparent Diffusion Coefficient (ADC) og relative Cerebral Blood Flow (rCBV) verdiene avledet fra normalisert histogram av hele tumor kan brukes til å forutsi progresjons-fri overlevelse (PFO) og total overlevelse (TO) hos pasienter med diffuse gliomer WHO grad II og III. Vi fant at svulster med en heterogen perfusjonssignatur og høye gjennomsnittlige rCBV-verdier var assosiert med lengre PFO hos pasienter med oligodendrogliom. Hos pasienter med astrocytom var det omvendt, der heterogen perfusjonsfordeling var assosiert med dårligere utfall. Vi fant ingen assosiasjon mellom ADC-verdier og overlevelse. Resultatene våre indikerer at perfusjon parameter kan brukes som en uavhengig prognostisk faktor for pasienter med diffust gliom.

Den andre studien bygger på det samme retrospektive materialet som studie en. Intensjonen var å finne ut om rCBV- og ADC-histogram parameter kan bidra til å skille genetisk definerte oligodendrogliom fra astrocytomer, og mellom WHO grad II og grad III. Vi fant ut at oligodendrogliomer har signifikant høyere mikrovaskularitet og høyere vaskulær heterogenitet enn astrocytomer. Diffuse gliomer med høy celletetthet var mer sannsynlig oligodendrogliomer enn astrocytomer. Kombinert bruk av ADC- og rCBV-histogram parametere var den klart beste metoden til å identifisere oligodendrogliale svulster. MR-baserte ikke-invasive biomarkører for vaskularitet og cellularitet kan derfor gi viktig informasjon ved vurdering av videre behandling.

Den tredje studien inkluderte vi prospektivt 42 pasienter med ubehandlet *IDH-villtype* glioblastom og vurderte i hvilken grad Restriction Spectrum Imaging (RSI) kan estimere forskjellige nivåer av cellularitet (celle tetthet) i ulike deler av svulsten. Vi undersøkte også

den prognostiske verdien av RSI med tanke på aggressiv tumor atferd og sammenlignet RSI med de etablerte diffusjons-parameter som mean diffusivity (MD) og fractional anisotropy (FA). Den høyeste RSI-cellularity index ble målt i soner med kontrastoppladning med en negativ gradient fra kjernen av svulsten og ut til perifere deler av området rundt svulsten (peritumoral zone). Kortere overlevelse var signifikant assosiert med høyere «RSI-cellularity index» både i den kontrastladende sonen og i nærområdet omkring svulsten. I motsetning, hadde MD og FA i nærområdet ikke noen prognostisk verdi for overlevelse. Dette indikerer at MD og FA i større grad påvirkes av ekstracellulært ødem enn RSI. Derfor ser det ut til at RSI kan være en god prognostisk markør og nyttig for å karakterisere tumorinfiltrasjon. Videre kan denne parameteren potensielt også kan bidra til å optimalisere planlegging av kirurgiske inngrep og kartlegging av strålefelt, som igjen kan gi bedre behandlingsresultater.

Både perfusjon- og diffusjon-MR gir potensielle ikke-invasive biomarkører som komplementerer hverandre. Dette kan med fordel implementeres i vanlig diagnostisk arbeidsflyt for diffuse gliomer. Vi håper også at metodene som vi utarbeidet, kan brukes med fordel i fremtidige studier for å validere og standardisere nye MR teknikker.

LIST OF PUBLICATIONS

I. Latysheva A, Emblem KE, Server A, Brandal P, Meling TR, Pahnke J, Hald JK. Survival Associations Using Perfusion and Diffusion Magnetic Resonance Imaging in Patients With Histologic and Genetic Defined Diffuse Glioma World Health Organization Grades II and III. J Comput Assist Tomogr. 2018 Sep/Oct;42(5):807-815.

II. Latysheva A, Emblem KE, Brandal P, Vik-Mo EO, Pahnke J, Røysland K, Hald JK, Server A. Dynamic susceptibility contrast and diffusion MR imaging identify oligodendroglioma as defined by the 2016 WHO classification for brain tumors: histogram analysis approach. Neuroradiology. 2019 May; 61(5):545-555.

III. Latysheva A, Geier OM, Hope T, Brunetti M, Micci F, Vik-Mo EO, Emblem KE, Server A. Diagnostic utility of Restriction Spectrum Imaging in the characterization of the peritumoral brain zone in glioblastoma: Analysis of overall and progression-free survival (accepted for publication in European Journal of Radiology).

1. INTRODUCTION

1.1 Diffuse infiltrative glioma

1.1.1 Epidemiology of diffuse infiltrative gliomas

Diffuse infiltrative gliomas represent 31% of all central nervous system (CNS) tumors and are the most common primary brain tumors in adults, especially the most malignant form, glioblastoma [1]. The annual incidence of low grade gliomas in Norway is 1 per 100,000 persons with an average age of 45 years, while for high grade gliomas the same rate is 3.8 per 100,000 with a significantly higher average age of 62 years (approximately 200 new cases each year) [2]. Incidence has almost doubled since 1980 in Norway, most likely due to an ageing population and the increased availability of accurate and more modern neuroimaging techniques, aiding in the detection of smaller tumors.

There are several potential risk factors for the development of glioma. Ionizing radiation related to both radiotherapy and high environmental radiation are the most established agents. Recently, it has been suggested that allergies may be protective against different cancer types, including glioma. Less than 5% of all gliomas are associated with genetic inherited cancer syndromes, such as neurofibromatosis, Li-Fraumeni syndrome and Ollier disease/Maffucci syndrome [3].

Median survival in patients with low-grade gliomas is 11.3 years. [4]. After the introduction of adjuvant treatment with Temozolomide in 2005, median overall survival in patients with glioblastoma increased from just 8.3 months to 10.1 months [5]. However, 5 year survival from time of diagnosis is still not more than 6.1 % [2]. The most favorable prognostic factors are younger age at time of diagnosis (below 50 years), a Karnofsky performance status of at least 70 points and non-eloquent tumor location [6].

1.1.2 Histopathological features and diagnostic challenges of diffuse gliomas

Histopathological classification of gliomas are based on presence of nuclear atypia, mitotic activity, microvascular proliferation and necrosis (figure 1) [7].

Microvascular proliferation is an important histopathological criterion to establish the diagnosis of high- grade glioma. However, quantitative structural studies have reported, that while some focal tumoral parts have extreme angiogenesis, there are many tumor regions that have vascular density at the same level as normal brain tissue. Highly invasive glioma cells also incorporate preexisting parenchymal vessels to obtain intratumoral blood supply [8].

Necrosis is another characteristic of high-grade gliomas and is defined as accidental cell death that occurs within sheets of cells. Although cancer treatment has a goal to induce tumor cell death, biological natural necrosis in glioblastomas is not a favorable finding for

patient outcome. Several studies have demonstrated that the extension of necrosis correlates with poor survival, mostly likely due to hypoxia as a result of procoagulation which preferentially selects for tumor cells that are more aggressive and more resistant to therapies [9-11]. Necrotic foci are typically surrounded by ‘’pseudopalisading” - cells, a configuration that is relatively unique for malignant gliomas and associated with unfavorable prognosis [12].

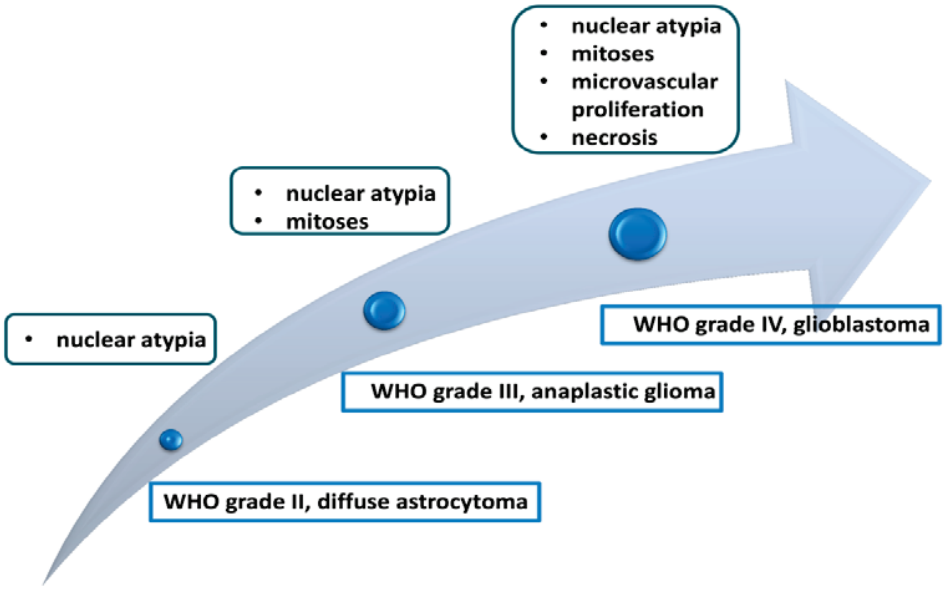

Figure 1. Histopathological classification of diffuse gliomas. The histologic features of mitotic activity and necrosis are used for grading of diffuse gliomas. A diffuse astrocytoma without these features is defined as low-grade (WHO grade II). With increased mitotic activity, the diagnosis of an anaplastic tumor is rendered. The presence of necrosis and/or microvascular proliferation leads to a diagnosis of glioblastoma.

Diffuse Infiltrative growth in the neuropil is a feature almost unique to gliomas and is a critical factor in therapeutic failure. So called ‘’pseudogliomatous’’ growth pattern can sometimes be observed in primary CNS lymphoma and small cell lung carcinoma. In these cases neoplastic cells change their shape in order to overcome obstacles in the preexisting tissue structure [13]. In contrast, glioma cells generate ‘’proper structures’’ (canalicular and papillary formation) that are not dependent on preexisting brain texture. ‘’Secondary’’ formations depend on surrounding tissue architecture, and appear as perineuronal, pial, intrafascicular and perivascular growth. Typical growth patterns are represented in figure 2 [8]. Even ‘’tertiary formations’’, caused by the interaction of glioma cells with proliferative mesenchymal tissue of the tumor can be created [14]. Multifocal satellites occur by the dissemination of glioma cells via white matter tracts, cerebrospinal fluid pathways and meninges. Multiple gliomas may be classified as synchronous, metachronous and metacentric. The latter is rare and occurs only in patients with glioblastoma. Metastasis

outside neuropil is extremely seldom but can occur in some cases after craniotomy or shunting due to damage of the basement membrane allowing for seeding [15]. Studies using high-resolution time-lapse intravital imaging suggest that there are two distinct cell invasion patterns: a slow course with directed movement, and a fast course with less directed movement. These patterns are related to different types of tumor borders: those with invasive margin and those with a diffuse infiltrating margin, respectively [16]. Molecular biology underlying glioma cell migration is still unknown. Molecules such as nuclear factor kappa B, macrophage chemoattractant protein-1, stem cell factor and stromal cell-derived factor-1 may play an important role in the regulation of infiltration, but their specific contributions are not well understood [8, 17, 18].

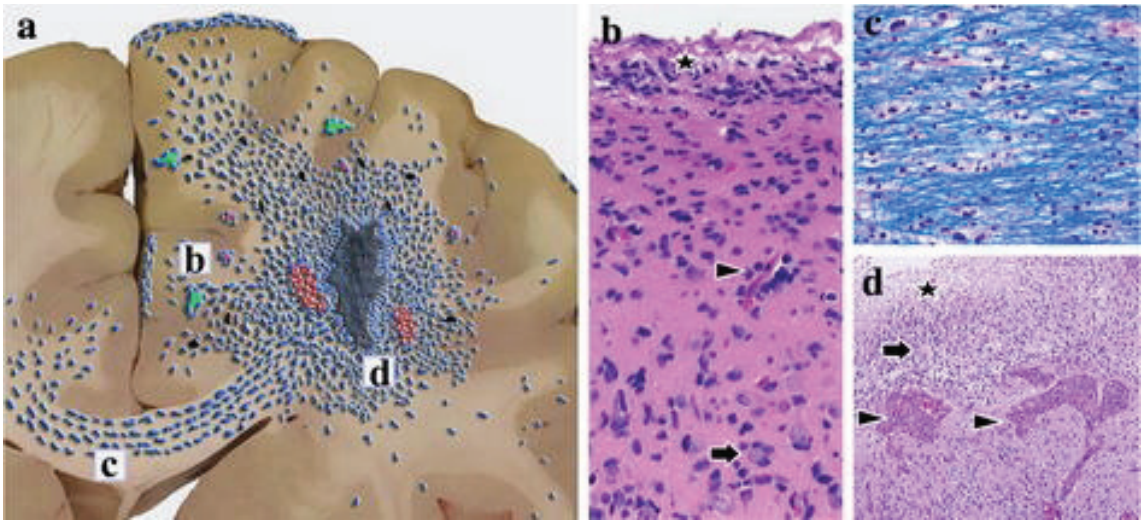

Figure 2. Schematic representation of the growth pattern of a glioblastoma (a), including the following secondary structures of Scherer: perivascular accumulation of tumor cells (example in area indicated by b; vessels in red, tumor cells in blue), perineuronal satellitosis (b; neurons in green), subpial growth of tumor cells (b), and intrafascicular growth in the corpus callosum (c). Mitotic tumor cells are depicted in black. Furthermore, in GBMs necrosis (dark grey area) surrounded by pseudopalisading tumor cells and adjacent Xorid/glomeruloid microvascular proliferation (d) are often present. Images b–d on the right represent the histology of these features: in b asterisk indicates subpial growth, arrow indicates perineuronal satellitosis, arrowhead indicates perivascular accumulation of tumor cells; image c shows increased cellularity with diffuse infiltration of tumor cells in the relatively well preserved myelinated tracts of the corpus callosum; in image d asterisk indicates area of necrosis, arrow indicates peri-necrotic pseudopalisading tumor cells, arrowheads indicate glomeruloid microvascular proliferation [b, d: H&E staining, c: combined Luxol Fast Blue and H&E staining; original magnification £200 (b, c) and £100 (c)]. Figure and text from Acta Neuropathologic, diffuse glioma growth: a guerilla war, Claes et al, Nov 2007. Creative Commons Attribution 4.0 International License.

Tumor heterogeneity at multiple levels (genomic, cellular, morphological, functional and clinical) often hinders the diagnosis and adequate therapeutic intervention for glioma. Intertumoral heterogeneity refers to the variability between tumor-to-tumor genomic and histopathological diversity. Intratumoral heterogeneity is attributed to variability between cells from the same tumor, that may have differences in both origin and genetic alteration and that may also express various phenotypic and epigenetic states [19]. Histopathological evidence of extensive heterogeneity has been demonstrated at the regional and cellular level, including variable amounts of necrosis, hemorrhage, thrombosis, glomeruloid microvascular proliferation, and pleomorphic tumor cells [20, 21]. Immunohistochemistry and molecular biology studies have shown uneven distribution of genetic markers [20]. New data also reflects that this complex heterogeneity is present at the single-cell level [22, 23].

The genomic road leading to tumor recurrence is highly idiosyncratic but can be broadly classified into linear recurrences - those that share extensive genetic similarity with the primary tumor and divergent recurrences - those that share few genetic alterations with the primary tumor and originate from cells that branched off early during tumorigenesis. Divergent recurrences may compromise the value of molecular information obtained from initial surgery in the setting of tumor recurrence [24, 25]. However, deeper understanding of heterogeneity complexity is challenging because of technological limitations in the tracing of tumor cell populations within a human tumor mass [26].

1.1.3 Molecular features of diffuse gliomas

Our understanding of genetic alterations in gliomas and their prognostic and predictive value has increased significantly in the past two decades. The most important genetic alterations influencing classification, treatment and prognosis for gliomas are referred to below.

Isocitrate dehydrogenase 1 or 2 (*IDH1*/*IDH2*) are currently the earliest known events in glioma genesis and were first identified in 2008 [27]. This genetic alteration affects the active site of the Krebs cycle enzyme *IDH*. A lack of *IDH*-mutation occurs in *de novo* glioblastomas and is associated with poor prognosis. Glioblastomas with *IDH*-mutation or secondary glioblastomas are less common (just about 8-13 % of all glioblastomas) and typically affect younger patients. There is a controversy regarding the classification of WHO grade II and III gliomas with an absence of *IDH* 1 or 2 mutations. A recent meta-analysis showed that heterogeneous subtypes have different prognosis, and further stratification is necessary [28]. Favorable outcomes were observed in patients of younger age, oligodendroglial phenotype and who had a WHO grade II histology [29].

*1p19q codeletion (*combined loss of the short arm of chromosome 1 (1p) and the long arm of chromosome 19 (19q)) in combination with *IDH* mutation defines the diagnosis of oligodendroglioma according to the updated 2016 WHO Classification of Tumors of the CNS, and is associated with a better response to chemotherapy as well as improved survival [30, 31]. There is a strong association between 1p19q codeletion and classical

oligodendroglial morphology - the combination of the round nuclei and perinuclear haloes results in a fried-egg appearance for individual cells and the presence of a branching network of delicate capillaries (chicken-wire pattern) [32, 33]. A partial deletion of 1p and/or 19q chromosomal arms, in contrast to a whole arm deletion, commonly occurs in astrocytic tumors and is not associated with a better prognosis [34].

ATRX mutational status is one of the critical markers that define the molecular classification of gliomas. ATRX mutation are most common in grade II-III astrocytomas (71%) and secondary glioblastomas (57%), and in combination with *IDH1* mutations it is mutually exclusive with 1p19q. ATRX mutation combined with TP53 mutation is characteristic for diffuse astrocytoma, but not mandatory for the diagnosis [35, 36].

The *TP53 t*umor suppressor gene is involved early in astrocytomas development. *TP53* plays a role in halting cell cycle, thus protecting cells from accumulation of DNA damage. Mutations of *TP53* may therefore lead to tumor progression through genomic instability [37]. TP53 mutation together with ATRX mutation supports the diagnosis of astrocytoma and differentiates it from oligodendroglioma. It can be detected in both primary and secondary glioblastoma [38].

O^6-Methylguanine-DNA- Methyltransferase (MGMT) is a DNA repair enzyme, which gene is located on chromosome 10q26 [39]. MGMT can protect cells against alkylating agents and impede the effectiveness of alkylating chemotherapeutic agent, such as temozolomide. Up to 45-47% of glioblastomas exhibit methylation of the MGMT promotor gene. In patients treated with temozolomide and radiotherapy, PFS and OS significantly increase when tumor contains a methylated MGMT promoter. In the absence of methylation of the MGMT promoter, there is a smaller but statistically insignificant difference in survival with TMZ treatment [39, 40].

1.1.4 The updated 2016 WHO Classification of tumors of the CNS

The WHO published the first classification system of tumors of the CNS in 1979, and since then several updates have been made. Before 2016, the classification was based on morphological criteria that could only be assessed by microscopy alone.

The knowledge based around brain tumor genetics has increased remarkably over the past two decades. The last update to the WHO classification of tumors of the CNS was published in May 2016, and placed greater emphasis on molecular/genetic parameters as opposed to the previous focus on morphological features identifiable by light microscope [38] . The reason for a more ‘’integrated approach’’ is to provide more biological homogeneous diagnostic entities with common behaviors, response to treatment and prognosis. Because neuroimaging plays a key role in brain tumor diagnosis and management, radiologists need to stay abreast of these developments and collaborate with specialists from other medical disciplines. The most remarkable changes in the updated

classification concern diffuse infiltrating gliomas. Several entities were eliminated and others were redefined by genetic features for the first time [38, 41]. The main changes are:

- That the presence of *IDH* mutation is now required for diagnosis of diffuse infiltrating glioma, where a combination with 1p19q codeletion identifies oligodendrogliomas and an absence of 1p19q codeletion results in a diagnosis of astrocytoma.
- The use of oligoastrocytoma as a diagnosis is now strongly discouraged and can be used only for tumors with both astrocytic and oligodendroglial genotypes (so called dual genotype).
- Glioblastomas are subdivided in *IDH*-wild type and *IDH*-mutant, which mostly correspond to the previously recognized genetically different primary and secondary glioblastoma multiforme, respectively.
- The gliomatosis cerebri diagnosis is has been removed but the term gliomatosis cerebri is still appropriate for use by radiologists to describe a widely infiltrating glioma.

The diagnostic approach for an integrated histological and molecular classification of diffuse gliomas according to the 2016 updated classification is shown in figure 3. This classification represents the primary source of updates on diagnostic classes, grades and criteria. However, it is worth noting that rapid and ongoing advances in molecular pathogenesis warrant faster incorporation of this information into clinical practice than WHO updates can keep pace with. To allow for this, the Consortium to Inform Molecular and Practical Approaches to CNS Tumor Taxonomy (cIMPACT-NOW) was created under the sponsorship of the International Society of Neuropathology. From 2016 to 2019, cIMPACT has published four updates to the WHO criteria [42].

There are several controversies that still need to be resolved, especially between tumor behavior and the new classification. For example, WHO grade II and III astrocytoma *IDH*-wild type behave more aggressive than their counterparts with IDH mutation. Several experts suggest treating these tumors as glioblastomas, regardless of their histopathologic grade [43]. In such cases supplementary molecular analysis are useful, although this is not yet formally incorporated into the WHO criteria [44].

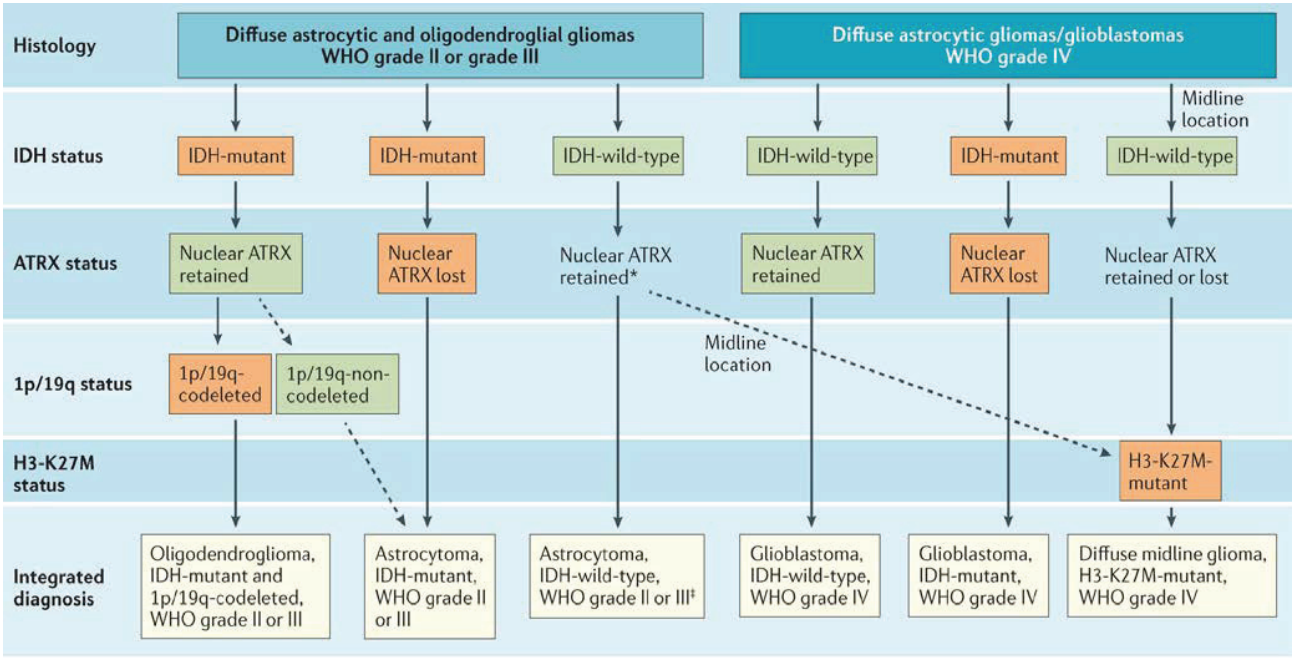

Figure 3. Diagnostic approach for integrated histological and molecular classification of diffuse gliomas according to the 2016 WHO Classification of Tumors of the Central Nervous System. In addition to histological typing and grading, diffuse gliomas are evaluated for isocitrate dehydrogenase 1 or 2 (IDH)-mutation status. Nuclear transcriptional regulator ATRX expression is determined by immunohistochemistry. Testing for 1p/19q codeletion is performed in patients with IDH-mutant tumors with retained nuclear ATRX expression to further refine the classification of these tumors. IDH-wild-type gliomas located in midline structures (thalamus, brainstem, or spinal cord) are additionally tested for histone-H3-K27M mutations. Dashed lines indicate smaller subgroups of tumors with the respective diagnoses. *Nuclear ATRX expression is retained in most IDH-wild-type WHO grade II or III astrocytic tumors. ‡IDH-wild-type WHO grade II or III astrocytoma is considered a provisional entity in the 2016 WHO Classification of Tumors of the Central Nervous System. Figure and text from Nature Reviews Clinical Oncology, Advances in the molecular genetics of gliomas — implications for classification and therapy, Reifenberger et al, 2016 [45] . Copyright license Number 4775930600068.

1.2 MRI in diffuse infiltrative glioma

1.2.1 History and evolution of brain tumor imaging

Neuroradiology has progressively moved from a purely anatomy-based discipline to one that combines anatomy, physiology and function; all of which play an important role in the assessment and management of neurologic disease , especially brain tumors [46]. Below, we will present some of the pioneers in the history of neuroradiology, with focus on neurooncology.

The X-ray was discovered by the German physicist Wilhelm Röntgen in 1895 at Würzburg. Neuroradiology began at the turn of the 20th century with the publication of 'Röntgen-diagnostik der Erkrankungen des Kopfes` in 1912 by Arthur Schüller [47]. This was the first comprehensive study of intracranial pathology by X-ray diagnosis including the differential diagnosis of intra and extra-sellar tumors, the displacement of pineal calcifications by masses, and more besides.

In 1918, neurosurgeon Walter E. Dandy introduced ventriculography [48] and the result was an increase in the detection of brain tumors by one-third. One year later in 1919, he introduced pneumoencephalography to diagnose brain tumors as well as abnormalities of CSF flow using air displacement as an aid to diagnosis [49]. It is worth noting that ventriculography and pneumoencephalography were not without substantial risk to the patient.

In 1927, Egas Moniz, a Portuguese neurologist introduced cerebral angiography. This was performed by injecting sodium iodide directly into the carotid artery via a surgical exposure after failing the percutaneous approach. On July 7, 1927, Moniz presented his paper entitled ‘’Arterial Encephalography: Its importance in localization of cerebral tumors’’ to the Neurological Society of Paris [50]. Per Amundsen, a Norwegian neuroradiologist, was the first to catheterize and examine cerebral vessels, carotid and vertebral arteries via a femoral approach, via a procedure he developed at Ullevål Hospital in Norway in 1964 [51].

The first major advance in neuroimaging of the brain itself was computed tomography (CT), which revolutionized the field by allowing the anatomic localization of brain tumors without the previous requirement of direct visualization via surgery. In 1979, Allan MacLeod Cormack, a physicist, and Godfrey Hounsfield, a computer engineer, were jointly awarded the Nobel Prize for Medicine for their pioneering contributions to the development of CT [52]. The first CT was installed in the UK in 1971, in the United States in 1973, and the first CT in Norway in 1975 at Ullevål University Hospital. CT scanning of the brain forever changed the way we examine and diagnose brain tumors and other neurological diseases [46].

The next important advance in anatomic neuroimaging came with the development of MRI. In addition to the higher anatomical resolution that was now available, this also opened new

opportunities for physiological imaging. In 1973 Paul C. Lauterbur reported the first images of a mouse obtained with MR imaging. In England, Peter Mansfield developed the mathematic algorithms that allowed rapid imaging and, in 1977, the first human MR images were reported. Lauterbur and Mansfield received the Nobel Prize in 2003 [53, 54], figure 4.

The first articles showed the essential role of contrast agent administration for detection of primary cerebral tumors came in 1985 [55, 56]. Russell et al pointed out that contrast agent administration was essential for depiction of intracerebral metastases, especially those smaller than 10 mm in diameter and without accompanying cerebral edema [57].

The first images from **diffusion-weighted MR imaging (DWI)** were presented by Denis Le Bihan at the 1985 Radiological Society of North America Annual Meeting [46]. Although originally conceived for liver imaging, DWI soon found considerable utility in neuroimaging. Again, it was Le Bihan and his group who showed that **diffusion-tensor imaging (DTI)** could produce maps with white matter fiber direction. In 1991, the first tractographic images of white matter appeared [58].

Figure 4. Sir Peter Mansfield (to the left) and Paul Lauterbur (to the right), Picture from: Questions and answers in MRI, courtesy of Allen D.Elster, MRIquestions.com

The basis of **blood perfusion imaging** was reported in 1980 by Leon Axel and its neuroimaging applications coincided with the development of spiral CT and MR echo-planar imaging capabilities [59]. Both MR imaging and CT can be used to measure the amount of contrast agent traveling through blood vessels contained in voxels producing parametric maps of cerebral blood flow, volume, mean transit time, as well as time to peak. One of the first articles that addressed dynamic contrast-enhanced perfusion imaging was published in Radiology in 1990 and demonstrated increased perfusion in brain tumors [60].

MR-spectroscopy utilizing nuclear magnetic resonance was first described in 1946 simultaneously by Edward Purcell and Felix Bloch. At that time, spectroscopy was only used by physicists for the purposes of determining the nuclear magnetic moments of nuclei. It was not until the mid-1970s that spectroscopy started to be used in vivo, after the introduction of MRI [61].

Blood Oxygen Level Dependent (BOLD) functional magnetic resonance imaging (fMRI) depicts changes in deoxyhemoglobin concentration subsequent to task-induced or spontaneous modulation of neural metabolism [62]. The primary form of functional fMRI was incepted by Seiji Ogawa in 1990 [63-65]. This method has been widely used in studies of cognition for clinical applications such as surgical planning, for monitoring treatment outcomes, and as a biomarker in pharmacologic programs. Technical developments have solved many of the challenges encountered in applying fMRI in practice, such as the low contrast to noise ratio of BOLD signals, image distortion, and signal dropout [62]. Although now widely used for functional mapping, anatomical localization at a detailed level is still challenging for complex brain functions [66].

Visualization and quantification by MR imaging of biological, cellular, and molecular traits of brain tumors are in rapid development. Hopefully, several more informative, specific and robust imaging techniques will be developed in the future.

1.2.2 Basic principles of MRI

The concept of nuclear magnetic resonance (NMR) stems from spin angular momentum of atomic nuclei in quantum physics mechanics. The MR active nuclei are characterized by their tendency to align their axis of rotation in the presence of an external magnetic field, causing induction of a net magnetization in the field direction. The magnetic moment of atoms is called the net magnetization vector (NMV). In clinical MRI the hydrogen nucleus is the preferred MR active nucleus, because it is abundant in the human body and have relatively large magnetic moment. The NMV is a vector quantity and consists of two main components: magnetization in the longitudinal plane and magnetization in the transverse plane. After the application of a distinct radio-frequency pulse, NMV is flipped into the transverse plane with less or no longitudinal magnetization. Following the radio-frequency pulse, the NMV then gradually recovers its longitudinal magnetization back to its thermal equilibrium. The T1 relaxation effect describes the recovery of longitudinal magnetization due to energy dissipation to the surrounding lattice, while the T2 relaxation effect describes the loss of transverse magnetization due to dephasing of static local magnetic fields caused by interactions of adjacent nuclei [67]. T1 and T2 relaxation times are constant for a certain magnetic field strength and temperature, and depend on the local chemical microenvironment, which varies between tissue types or with the introduction of an NMR based contrast agent. Various methods are used to emphasize one property over another

in a given MRI paradigm (“pulse sequence”). Spin-echo and gradient-echo are two basic pulse sequences that manipulate the NMV to acquire different image readouts [68].

1.2.3 Brain tumor MRI protocol

MRI is essential for the identification and characterization of gliomas, their consequential surgical management and for evaluation of treatment response. Typical tumor protocols usually include both anatomical and functional sequences, which are valuable tools for diagnosis, tentative WHO grading, tumor affection of surrounding regions and planning of optimal biopsy tracts or extent of surgery.

Conventional MRI sequences commonly used for evaluation of gliomas include T1-weighted (T1W), T2-weighted (T2W), fluid attenuated inversion recovery (FLAIR), and post-contrast T1W images. These sequences provide exquisite anatomic detail and give important information about different tumor components (hemorrhage, calcifications, edema, cysts etc). The use of a gadolinium-based contrast agent allows detection of areas where the blood-brain barrier is compromised and indicate high-grade gliomas [69].

Susceptibility-weighted imaging (SWI) provides insight into glioma pathophysiology and internal tumoral architecture. Intratumoral susceptibility signal (ITSS) may correspond to intralesional hemorrhage, calcification, or tumoral neovascularity [70]. MR spectroscopic imaging (MRS) provides metabolic information regarding the brain tissue, that allows to characterize glioma with respect to WHO grade, genetic status and also differentiate glioma from another condition [71-74].

However, there is currently a lack of MRI protocol standardization between different institutions both on a national level here in Norway as well as internationally. This lack of consensus may affect image interpretation and assessment of follow-up examinations [75]. The American National Brain tumor Society (NBTS), the American Society for Neuro-oncology (ASNO), and the European Organization for Research and Treatment of Cancer (EORTC) jointly published in 2015 the ‘’EORTC-NBTS Consensus Recommendations for a standardized Brain Tumor Imaging protocol’’, which primary was developed for the using in clinical trials [76].

Specific sequence parameters in advanced tumor protocols with both anatomical and functional techniques in our institution are summarized in Table 1.

Table 1. Advanced preoperative tumor protocol on a 1.5T scanner with both anatomical and functional techniques at Oslo University Hospital - Rikshospitalet.

Sequence	Repetition time (ms)	Echo time (ms)	Field of view (mm)	Flip angle(°)	Voxel size (mm)	Bandwidth (Hz/Px)
T1 3D MPRAGE*	1900	2.36	256	10	0.5x0.5x1.0	180
3D FLAIR	5000	337	230		0.5x0.5x1.0	592
DWI/DTI	6170	59	230	180	1.6x1.6x4.0	940
DSC	1600	30	230	90	1.8x1.8x5.0	1502
SWI	49	40	230	15	0.7x0.7x1.6	80
T2 TSE	4840	87	230	139	0.3x0.3x4.0	192
Spectroscopy	1500	135	220	90	10.0x10.0x15.0	1000

*before and after gadolinium-based contrast agent (Clariscan 279.3 mg/mL, 0.2 mL/kg bodyweight, GE Healthcare, USA) administration

1.2.4 Advanced MR imaging of diffuse gliomas

The advanced MRI techniques with main applications and limitations, which were used in this thesis are described in this section.

1.2.4.1 Diffusion-weighted imaging

In 1986 Denis Le Bihan with colleagues published an article in Radiology with the title: ‘’MR imaging of intravoxel incoherent motions: application to diffusion and perfusion in neurologic disorders’’. They described differences in water diffusion between various normal and pathologic tissues imaged via magnetic resonance. This work has been cited in approximately 24.500 later articles in Pub Med and contributed to a dramatic growth of MRI diffusion technics and their application in neuro-oncology [77].

MRI diffusion techniques are based on the physical principle of random Brownian motion of water molecules, a molecular displacement, which obeys a Gaussian distribution. Modern diffusion-weighted imaging based on pulsed gradient spin echo technique was developed by Edward Stejskal and John Tanner in the mid-1960. Clinical diffusion imaging sequences rely on spin-echo signal formation with balanced diffusion-encoding magnetic field gradients on each side of the refocusing radio-frequency pulse [78]. A DWI is the unprocessed result of the application of a single pulsed gradient SE sequence in one gradient direction, and it corresponds to one point in q-space [79]. The most common DWI technique is the pulsed-gradient spin echo pulse sequence with a single-shot, echo-planar imaging (EPI) readout.

The rapid acquisition of diffusion data and the inherent motion robustness is the main advantages of this method [80]. The last ten years, using of bipolar (twice refocused) diffusion encoding effectively reduce eddy current distortions compared to the monopolar Stejskal-Tanner approach [81]. For this purpose, additional spoiler gradients required in order to suppress unwanted stimulated echo contributions increase TE and correspondingly reduce SNR [82].

Diffusion in a homogeneous medium is dependent on the type of molecule, the temperature of the medium and the time allowed for diffusion [79]. However, in brain tissue movement of water molecules is limited by the presence of molecular and cellular obstacles. Neuronal tissue has fibrillar structure and consists of tightly packed and coherently aligned axons that are surrounded by glia. As a result, the micrometric movements of water molecules are more hindered in the direction perpendicular to the axonal orientation than parallel to it. Movement of water molecules is also limited by tortuosity in the extracellular interstitium [79].

The ADC was introduced along with the diffusion MRI concept to facilitate clinical application of the technique. ADC is derived from the equation ADC= - 1/b ln (S_{DWI}/ S_0), where S_{DWI} is signal from the trace-DW image, and S_0 is a the signal from each corresponding point in the b0 image [83]. Thus, to obtain an ADC image, a minimum of two acquisitions with different b-values are necessary [79]. National Cancer Institute (at the 2008 ISMRM conference in Toronto) consensus recommends the use of DWI with a maximum b value of 1000 s/mm^2 and preferably the use of three different b-values (0, 500 and 1,000 s/mm^2) [84]. ADC inversely correlates to tumoral cellularity, and as a result it decreases in tumor parts with high cellular density [85]. Quantitative measurements of ADC are preferable for characterization of tumor, because the potential pitfalls of visual assessment. In clinical practice the most usual way to estimate ADC is by utilizing 2-dimentional (2D) region of interest (ROI) - based methods. The whole tumor histograms method, demands more complicated post processing and is more time consuming. To date, the histogram method is mostly used for research purpose.

The main clinical applications for DWI in current neuro-oncology are to differentiate glioma from other neoplastic and non-neoplastic conditions [86, 87]; WHO grading [88-90]; characterization of tumor microstructure; prediction of molecular subtypes [91]; follow up monitoring with differentiation between progression versus pseudoprogression; response versus pseudoresponse; and for prognostication [92].

1.2.4.2 Diffusion tensor imaging

Diffusion tensor imaging is widely used to explore the structural connectivity of the brain with applications in both clinical and basic neuroscience. Molecular displacement parallel to the fiber direction is typically greater than that perpendicular to it. Anisotropy is the predominant condition, when diffusive properties change with the direction of diffusion. Anisotropy and associated displacement distribution is no longer isotropic but cigar shaped

[79]. In contrast to isotropic diffusion vector (chaotic trajectories), the anisotropy of diffusion can be imaged [93]. Contributors to diffusion tensor anisotropy include cellular membranes, axons, myelin sheaths and other factors [94]. In addition to the measurement of fractional anisotropy (FA) and mean diffusivity (MD), DTI provides a visual color-coding map, where red corresponds to diffusion along inferior-superior axis, blue to diffusion along the transverse axis, and green to diffusion along the anterior-posterior axis. The intensity of the color is proportional to the fractional anisotropy. The best visualization of fibers may be achieved in regions where fibers are aligned along a single axis and it fails in regions with several fiber populations aligned along intersecting axes. Techniques with better angular resolution are preferable for these areas [79].

DTI is widely used for preoperative planning, especially for identification of eloquent white matter tracts (functional neuro-navigation), such as the corticospinal tract, the optic tract and the arcuate fasciculus. An increasing number of studies shows, that incorporation of DTI into surgical planning could alter the surgical approach, thereby allowing for more accurate resection and limiting postoperative deficits in these patients. However, there are still important limitations related to standardization and clinical integration of tractography for neurosurgical decision-making [95-97]. Some studies also demonstrate the usefulness of DTI to analyze tumor infiltration in peritumoral regions, but lack of histopathologic confirmation reduce the validity of these studies [98, 99]. FA reduction occurs not only in tumor affected areas but also in the surrounding edema associated with inflammation, mass effect and tumor infiltration all of which adds to interpretation difficulties.

A number of validation studies have been conducted with the aim to evaluate the reliability of tractography and these studies have revealed uncertainties and sources of error in the tractography process that may limit anatomical accuracy [100-102]. In addition to artifacts affecting EPI acquisitions (susceptibility gradients, head motion and eddy currents), another pitfall includes drawing conclusions about local fiber orientation from the diffusion displacement profile. Fibers with crossing, fanning and curving configurations are especially challenging to interpret in this situation [103].

1.2.4.3 Restriction spectrum imaging (RSI)

The improvement in gradient performance and coil technology, allow for higher b-values with shorter diffusion time and higher field strengths with better signal-to-noise ratios. This allows for developing innovative diffusion methods that provide more direct measures of tumor cellularity, such as RSI [104]. The main principle of RSI is to separate the ‘’fast’’ hindered and ‘’slow’ ’restricted diffusion compartments in tissues over a range or “spectrum” of length (size) scales with spherical and cylindrical geometries. The diffusion properties are fundamentally different between water molecules that are hindered versus restricted. The hindered or free molecules (extracellular/ekstraaxonal) follow a Gaussian displacement probability distribution, while restricted (intracellular/intraaxonal) water molecules shows non-Gaussian displacement probability because these water molecules are trapped by

plasma membranes. The restriction spectrum model, shown in figure 5 is written as a linear mixture of the Gaussian response functions with different transverse diffusivities [105]. To achieve this, RSI is required to collect data over an extended b-value range (b over3000 s/mm2) with multiple diffusion directions at each b-value at a fixed intermediate diffusion time (~90 ms). As a result, RSI is less influenced by changes in edema, necrosis and cysts, compared to ADC [104, 105]. RSI provide a ‘’cellularity index map’’ whereby the cellularity index is a measure of cellular density in tissue. RSI shows promising results to improve conspicuity of high-grade tumors and delineation of white matter tracts [106, 107], interpreting true tumor response in the setting of anti-angiogenic treatment and as a survival biomarker in patients with glioblastoma [108, 109].

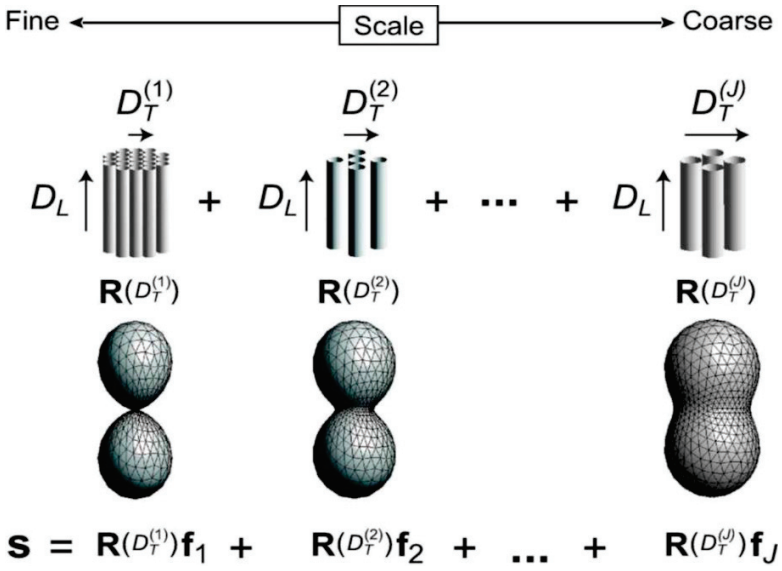

Figure 5. Restriction spectrum model. The oriented component of the diffusion signal is written as a linear mixture (spectrum) of cylindrically symmetric Gaussian response functions R with different fixed transverse diffusivities DT and unknown volume fraction and orientation distribution (f). From Human Brain mapping, Probing Tissue Microstructure with Restriction Spectrum Imaging: Histological and Theoretical Validation, White et al, 2013 Copyright license Number 4780801340083.

1.2.4.4 Dynamic Susceptibility Contrast perfusion MR imaging (DSC-MRI)

DSC-MRI was the most used perfusion method in a European survey on glioma MRI practice for initial grading and/or gliomas follow-up (over 80 %), with almost 50 % of all users acquiring it for all glioma indications [95]. The technique was first described by Villringer et al in 1988 [110]. DSC is based on the susceptibility induced signal attenuation on spin echo or gradient echo planar images, which results from a bolus of a paramagnetic

contrast agent with a high magnetic moment. Typically, a gadolinium-based contrast is used for passing through a microvasculature. The level of signal loss is proportional to the amount of contrast located primarily in the capillary bed. The application of a kinetic model allows generating intensity-time curves and estimation of relative or semi-quantitative maps of CBV, cerebral blood flow (CBF) and mean transit time (MTT) [111, 112]. Because the arterial input function is often not measured, these maps show relative CBV values and are therefore usually termed rCBV maps [113].

DSC MRI noninvasively provides in vivo metrics that depicts overall tumor vascularity and permits the indirect assessment of tumor angiogenesis and vascular permeability [114]. The main clinical applications of DSC brain tumors are as follows: differentiating solitary metastatic brain lesion and primary CNS lymfoma from high-grade glioma, preoperative grading of glioma, predicting prognostic molecular markers and noninvasive therapeutic monitoring. rCBV in patients with glioblastoma were significantly higher than in patients with primary CNS lymphoma [115]. In a meta-analysis study, where twenty-two studies with 1182 patients were included, a diagnostic performance with a sensitivity of 92% and a specificity of 95% to differentiate primary CNS lymphoma from glioblastoma was demonstrated [116] . Evaluation of max rCBV within the peritumoral zone is helpful to distinguish GBMs showing peritumoral infiltration from metastases surrounded by pure edema [117, 118]. High-grade glioma can be differentiated from low-grade glioma using rCBV values with high (95 %) sensitivity however specificity is relatively low (70 %)[119]; in another study the authors found a sensitivity of 98,4% for discrimination of grade II from grades III-IV, thus indicating high true-positive and low-false negative rates [120]. However, low-grade gliomas with elevated rCBV can be misclassified mostly because diffuse oligodendrogliomas may demonstrate a high microvascular profile [121]. Preliminary results are promising in the differentiation of gliomas on the basis of IDH mutation status, overall sensitivity and specificity rates for the rCBV for IDH stratification were 68% and 81%, respectively [122]. Furthermore, a lower degree of perfusion in MGMT methylated glioblastomas compared with unmethylated tumors (mean rCBV ratio) was also reported [123]. DSC studies have consistently demonstrated that rCBV is the most validated perfusion parameter for the distinction of therapy-related changes from tumor progression [124]. rCBV is also reviewed by several studies to be a reliable biomarker to stratify PFS and OS in patients with gliomas [125, 126].

Despite its widespread use, DSC has well-known pitfalls that limit the interpretations of this technique. The analysis of DSC-MRI data is based on the assumptions that the contrast agent remains inside the vascular bed during its passage through the brain. However, in the case of high-grade gliomas, the blood-brain barrier (BBB) is commonly disrupted, resulting in leakage of gadolinium-based contrast agent (GBCA) into the extravascular extracellular compartment. Such extravasation of GBCA results in accurate CBV, CBF, and MTT maps. CBV is underestimated in tumors where T1-weighted effects induced by increased vessels permeability dominate and overestimated if T2*-weighted effects dominate. These effects of

contrast agent leakage may be corrected to some extent by injecting a small dose of contrast agent prior to the acquisition of the first-pass DSC-MRI series [127]. Leakage-correction method based on analysis of the tissue residue function enables semiquantitative determination of the transfer constant and can be used to distinguish between T_1- and T^*_2-dominant extravasation effects, while being insensitive to variations in tissue MTT [128].

CBV measurements can also be confounded by susceptibility artifacts due to presence of blood products, calcifications, bone-air-brain interfaces, melanin and metal, when obtained values will be unreliable. Assessment of CBV in cortical areas is further challenged by the presence of large veins.

Alternative perfusion techniques such as dynamic contrast-enhanced (DCE) perfusion MRI and arterial spin labelling (ASL) are less established. DCE imaging measures T1 changes in tissues over time after bolus administration of gadolinium. The volume transfer coefficient of contrast between the blood plasma and the extracellular extravascular space (K^{trans}) derived from DCE represents the permeability of the tumor vasculature and has become increasingly important in the evaluation of tumor response to therapy. K^{trans} is higher in tumor recurrence than in radiation necrosis [129-131]. The disadvantages of DCE are mostly related to its being an immature technology with considerable technical issues around measuring K^{trans} related to data collection and analysis. Compared with dynamic contrast-enhanced approaches, the main advantage of ASL is that this technique does not require the use of contrast agent and therefore noninvasively quantifies CBF. In addition, a recent meta-analysis has demonstrated an excellent diagnostic performance in differentiating gliomas grades [132].The main disadvantage is low SNR, requiring a number of averages to produce a good-quality image and taking approximately 10 min for whole-brain coverage [133]. Figure 6 demonstrates standard imaging including diffusion and perfusion sequences in a patient with glioblastoma.

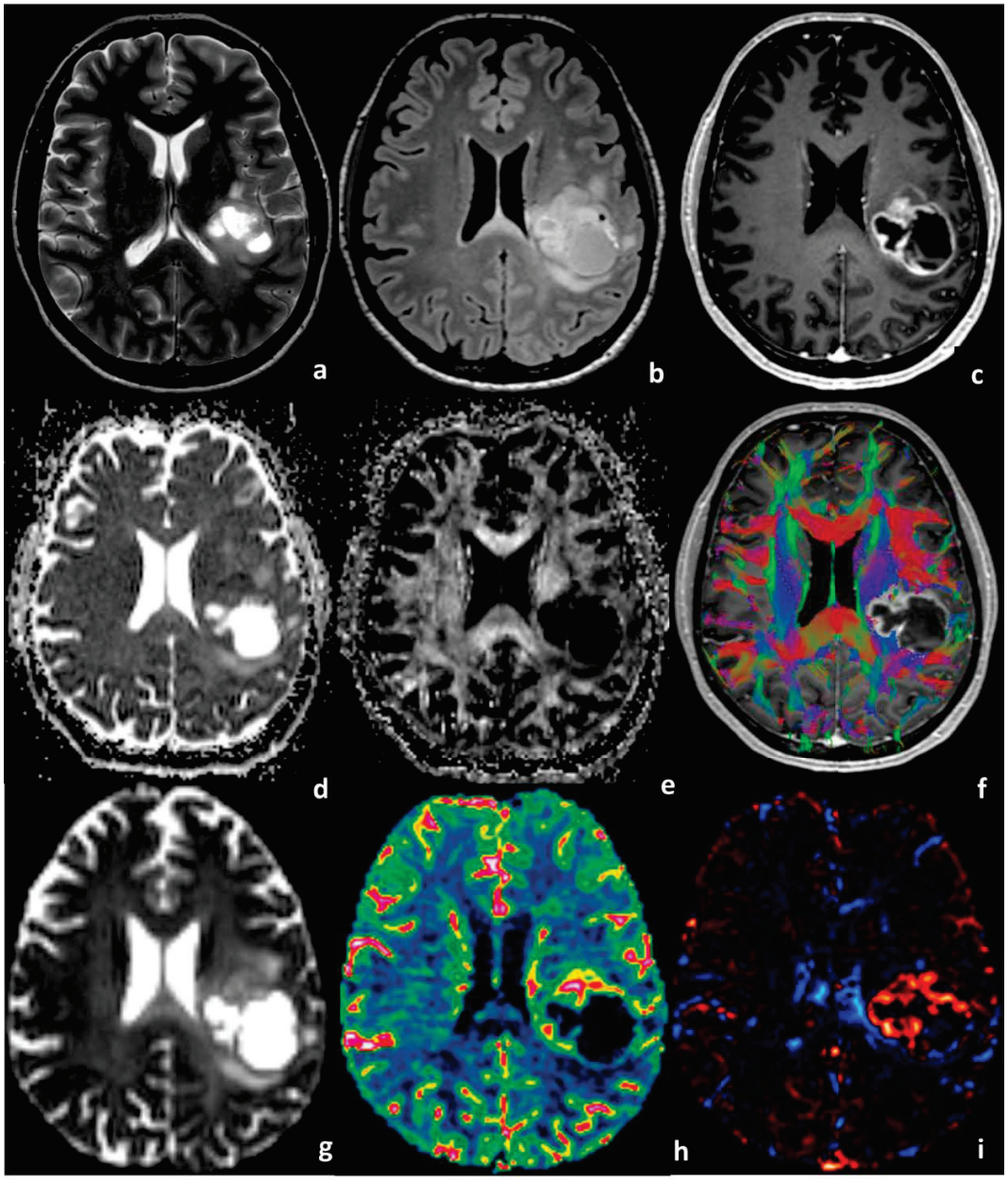

Figure 6. A 67-year-old man with a glioblastoma IDH wild type. a) Axial T2-weighted imaging shows an intraaxial heterogeneous tumor in the left frontal lobe. b) FLAIR image shows peritumoral hyperintensity, which suggests combination of tumor infiltration, edema and inflammation; c) contrast 3D MPRAGE shows irregular enhancement with central necrosis; d) ADC map, mean ADC in contrast-enhancing tumor core measured $0.87x10^{-3}mm^2/sec$, indicating high tumoral cellularity, and in peri-enhancing zone $1.16x10^{-3}mm^2/sec$, suggesting tumor infiltration; e-f) FA map with also directionally color-encoded map show FA abnormality in the tumor and in the peritumoral edema; g) RSI map; h) rCBV map clearly demonstrates areas of increased blood volume in contrast-enhancing tumor core; i) K2 map shows high capillary permeability in contrast-enhancing tumor core due to BBB damage.

1.2.5 Response assessment criteria for neuro-oncology (RANO)

RANO was published by the Neuro-Oncology working group in 2010 for use in clinical trials [75]. This first version was designed for high-grade gliomas. Overview of the RANO criteria for high-grade glioma is shown in Table 2 [75].

Table 2. Response assessment criteria based on MR imaging for high-grade glioma, adapted from Wen et al [75].

MRI and clinical features	Type of response			
	Complete respons	Partial respons	Stable disease	Progressive disease
T1 postgadolinium	Complete ↓	≥ 50 % ↓	< 50 % ↓, < 25 % ↑	≥ 25 ↑*
T2/FLAIR	Stable or ↓	Stable or ↓	Stable or ↓	Significant ↑*
New lesion	No	No	No	Yes*
Corticosteroids	No	Stable or ↓	Stable or ↓ dose	-
Clinical status	Stable or ↑	Stable or ↑	Stable or ↑	Significant ↓*
Requirements for response	All	All	All	Any

Abbreviations: ↓decrease; ↑increase; * Progression occurs when this criterion is met.

Postcontrast T1 weighted images are used for assessment of contrast-enhanced components of the tumor and T2/FLAIR to evaluate extension of non-enhanced tumor changes. The measurement technique for tumor size is bi-dimensional and represents the sum of the largest perpendicular diameters in axial MR imaging. Special instructions have been developed for so-called non-measurable lesions, for example lesions with central necrosis or irregular T2/FLAIR intensity changes [134-136].

Initially, RANO criteria were developed based on the mechanism of cytotoxic chemoradiotherapy, where the primary goal is reduction of tumor volume. Despite the widespread use of RANO criteria in clinical trials they are not adapted to innovative therapeutic agents such as tyrosine kinase inhibitors, antiangiogenics and immune-based therapy. Immunotherapy response assessment for neuro-oncology (iRANO) criteria was developed to address challenges related to emerging immunotherapy for high-grade gliomas and represents a modification of the RANO criteria [137]. RANO criteria for brain

metastases, leptomeningeal metastases, response assessment in pediatric neurooncology, meningioma and spine response assessment in neuro-oncology is outside the scope of this thesis.

There are two special conditions: pseudoprogression and pseudoresponse. These are regularly seen in patients treated for high-grade gliomas where it gives rise to additional challenges to classify patients as non-responders or responders, respectively [137, 138]. Pseudoprogression is defined as a transient increase in size of the contrast tumor enhancing component with or without associated T2/FLAIR changes mimicking tumor progression, but usually without clinical deterioration. It is associated with radiotherapy with or without temozolomide and is seen in 20–30% of patients with glioblastoma [139, 140]. Patients with a MGMT methylated tumor have an additional risk of developing pseudoprogression [141]. In most cases, pseudoprogression resolves spontaneously within 3 months even if treatment is continued and it will usually not cause any long-term neurologic decline. To avoid misclassification between true progression and pseudoprogression, the RANO criteria for HGG in clinical trials allow the assessment of images only 3 months or more after radiotherapy commencement, unless these two exceptions exist: a histological confirmation of tumor progression or the appearance of new lesions outside the radiation field [136].

In contrast, pseudoresponse refers to a decrease of both contrast-enhanced parts of the tumor and non-enhancing T2/FLAIR hyperintense portions of the tumor without true regression or even with progression. It is seen in 20–60% of patients who receive VEGF-targeted therapy and it is caused by normalization of abnormally permeable blood vessels within the tumor. Use of MR perfusion and spectroscopy is therefore of particular importance for assessment of residuals with and without contrast-enhancement [136].

1.2.6 Endpoints in clinical oncology: progression free survival and overall survival

While RANO criteria were developed to follow up treatment, overall survival (OS) and its surrogate progression free survival (PFS) have been used as endpoints to evaluate treatment success, as well as for assessment of the prognostic value of different clinical, laboratory and imaging parameters.

PFS is the time from either the date of diagnosis or the start of treatment to tumor progression. PFS has many advantages over OS, including earlier assessment of efficacy, greater statistical power at the time of analysis, and lack of influence from post progression therapies. Minimization of time between clinical and radiologic assessment is important in order to avoid large interpatient variabilities [142].

OS is a direct measure of clinical benefit to a patient and is defined as the time from either the date of diagnosis or the start of treatment to death from any cause. As an endpoint, OS is easily measured, unambiguous, objective and unaffected by the timing of assessment.

However, it is often limited by long trial times and confounding effects of post protocol events, such as subsequent therapies [142, 143].

The relationship between PFS and OS has been studied in various tumors and the results vary greatly depending on the tumor type [144, 145]. Meta-analysis of published phase II and III trials demonstrated good correlation between hazard ratio (HR) of PFS and OS and between median PFS and OS in patients with glioblastoma [142].

1.2.7 Radiomics and radiogenomics

A large number of studies have demonstrated beneficial use of a combination of parameters either derived from a single MRI technique or from several different MRI techniques. Multiparametric analysis commonly provides more information about glioma structure before treatment and is also more beneficial in analyzing specific tissue changes after chemoradiotherapy than single values or methods [146-148].

Imaging information could also be extracted as quantitative features, processed with machine-learning methods and linked to clinical markers (WHO grade, survival time, recurrence etc). This concept is called radiomics, a novel high-throughput method, which has recently developed from the field of oncology and incorporates several disciplines, including radiology, computer vision and machine learning. Radiogenomics is a subgroup of radiomics, and represents image based quantitative indicators that are capable of predicting clinical relevant genomic features of tumors tissue [149-151]. The central hypothesis of radiomics is that tumor imaging can reflect the underlying morphology and dynamics of smaller-scale biologic phenomena, such as gene expression patterns, tumor cell proliferation, and blood vessel formation [152] . There are two primary extraction strategies of image features. The first, local level image extraction, provides an image descriptor used to compare a pixel being tested with its pixel neighborhood and allows identification of a small niche area of biologic importance within an otherwise homogeneous appearing tumor. The second strategy, global-level feature extraction, represents quantification of the overall composition of an entire ROI [149].

There are several different approaches for discovering predictive radiomic features. For example, biologically inspired feature descriptors based on specific biological hypotheses that transfer the recognized radiologal knowledge into quantitative correlation. Understanding disease characteristics is necessary to propose biologically inspired features because they can be disease-specific. In contrast, machine-learning approaches build on searching imaging features statistically associated with clinical outcome but without prior biological hypothesis. A specification of the medical diagnostic task is necessary before evaluation of machine-learning models for appropriate model training. The fundamental strategies are supervised, unsupervised, and semisupervised learning models, used in line with the different levels of available clinical outcome labels [149].

Classification of gliomas by WHO grade and genotype, tumor-tissue discriminative analysis and prediction of survival outcome are typical clinical applications of radiogenomics [153-157].

There are several substantial challenges limiting the use of radiomics in clinical practice. Lack of annotated data necessary for proper training and limited generalizability of algorithms are the most recognizable problems [158].

1.2.8 MRI biomarkers in therapeutic decision-making and in clinical trials: the requirements, challenges and new solutions

The American Food and Drug Administration-National Institute of Health Biomarkers Working Group defines a biomarker as “a defined characteristic that is measured as an indicator of normal biological processes, pathogenic processes, or responses to an exposure or intervention, including therapeutic interventions. Molecular, histologic, radiographic, or physiologic characteristics are types of biomarkers but a biomarker is not an assessment of how an individual feels, functions, or survives”[159].

The use of radiologic biomarkers in neuro-oncology has increased dramatically in the last two decades. There is a need for non-invasive markers for primary tumor diagnostic and especially for treatment monitoring. Conventional evaluation of ex vivo tissue specimens by microscopic and next-generation sequencing methods as a standard reference for diagnosis and evaluation of glioma progression is being challenged. These methods are invasive with risk to the patient. Moreover, a tissue sample represents a small and localized region of the tumor and does not address inter- and intratumoral heterogeneity. Recently, liquid biopsy has emerged as a promising approach to detect, molecularly characterize and monitor brain tumor. However, accessibility of tumor-derived materials in blood outside BBB and even in CSF is difficult. Levels of plasma components, in particular tumor-derived nucleic acids, may be insufficient to perform genotyping. In addition a lack of standardized cut-off levels makes its implementation in clinical practice problematic [160, 161].

Radiologic biomarkers can be divided into three main groups: 1) diagnostic biomarkers, that provide more accurate classification of tumor; 2) predictive biomarkers, that can guide the therapeutic decision in early stages, adapted to patient specific biology and, 3) prognostic biomarkers, that provide information about clinical outcome.

Several important requirements need to be fulfilled before we can use quantitative MRI data for reliable decision-making biomarkers. Firstly, we need rigorous guidelines for standardization and validation, including brain tumor protocols, imaging postprocessing and analysis, in addition to standardized reports with specific endpoints measures. Secondly, we need presence of reproducibility and repeatability of qualitative and quantitative MRI data. Using phantoms, and test and retest of the same patients can be useful to assess baseline variation of each MR sequence in a particular machine. Quality control procedures need to be performed systematically. Thirdly, a better understanding of the biological substrates behind imaging biomarkers and their relation to clinical outcome will help to

select appropriate MRI techniques. Lastly, high dimensional data are beyond human ability alone for interpretation. The ability to translate big data generated by multiple MR sequences into a clinically suitable form is essential for reliable interpretation and further decision-making [162-164].

Development of databases and sharing of data, standardized brain image protocols and infrastructure organized across many clinical centers, cooperation between different specialists such as radiologist oncologist, neurosurgeon, imaging technologists and statisticians are essential for the development of reliable biomarkers.

Several multidisciplinary organizations, such as Quantitative Imaging Network, Quantitative Imaging Biomarkers Alliance (USA) and The European Imaging Biomarkers Alliance have as their primary goals to make radiology a more quantitative science, to facilitate imaging biomarker development and to standardize and promote their use in clinical trials and in clinical practice.

Quantitative Imaging Network:
https://imaging.cancer.gov/programs_resources/specialized_initiatives/qin/about/background.htm#h03

Quantitative Imaging Biomarkers Alliance:

https://www.rsna.org/en/research/quantitative-imaging-biomarkers-alliance

The European Imaging Biomarkers Alliance:

https://qibawiki.rsna.org/images/6/69/EIBALL_Poster2019.pdf

2. AIMS OF THE THESIS

The aim of this study was to evaluate the role of advanced MR techniques such as perfusion and advanced diffusion imaging, in order to characterize diffuse gliomas. Particularly the correlation of the imaging metrics to WHO grade, differential diagnosis, morphologic features and genetic features was assessed. An additional goal was to develop imaging prognostic biomarkers in order to improve preoperative planning, perioperative navigation and follow-up treatment in adult patients with diffuse glioma.

The specific aims for each of the studies were as follows:

Paper I: To evaluate whether ADC and rCBV histogram-based analyses can stratify progression-free survival (PFS) and overall survival (OS) in patients with diffuse gliomas grade II and III with respect to both oligodendroglial and astrocytic tumors.

Paper II: To determine whether the rCBV and ADC values analyzed by histogram method could separate genetic defined oligodendrogliomas from astrocytomas, as well as WHO grade.

Paper III: To evaluate the ability of RSI to provide information that highlights heterogeneity related to cellular density within the peritumoral brain zone. Further, to investigate the prognostic value of RSI in order to correlate with the tumors' potential aggressive behavior and compared it with clinical established diffusion metrics such as MD and FA. In addition, to evaluate the association between RSI metrics and MGMT promoter methylation status.

3. MATERIALS AND METHODS

3.1 Study design and population.

This thesis includes single center studies. Patients were included after being referral to the neurosurgery department, Oslo University Hospital, Rikshospitalet. All patients provided written informed consent for use of clinical data and imaging surveys for research purpose.

The studies presented in paper I and II were based on a retrospective material. A total of 352 adult patients with a histopathologic diagnosis of diffuse glioma were identified based on our clinical database from November 2006 until May 2013. Inclusion criteria were: 1) diagnosed oligodendroglioma, oligoastrocytoma or astrocytoma, classified according to the 2007 WHO classification of tumors of the CNS; 2) a known 1p19q status 3) a baseline pretreatment MRI examination from our institution including DSC and DWI in addition to T1- and T2-weighted images, and 4) age over 18 years. The final study cohort included 67 patients for study I and 71 patients for study II.

The study presented in paper III is a prospective cross-sectional study. A total of 92 adult patients with MRI findings suggestive of high-grade glioma from the local hospitals were identified in the period from June 2016 to December 2018. Criteria for participation were: 1) age over 18 years; 2) no significant blood products on MRI and 3) satisfactory general condition. Eighty-one patients were examined with advanced MRI tumor protocol. The diagnosis was based on histological and molecular examinations of specimens obtained by stereotactic navigated biopsy or from tumor resection. In the final study cohort forty-two patients with pretreatment glioblastoma, IDH-*wildtype,* classified according to 2016 WHO classification of tumors of the CNS were included. Thirty-one patients with another diagnosis (lymphoma, anaplastic astrocytoma, metastasis, ependymoma, glioblastoma, *IDH-mutant)* and 8 patients with reduced MRI quality were excluded.

3.2 Image acquisition

3.2.1 Study I and II

MRI was performed on a 1.5T scanner (Sonata, Symphony, or Avanto; Siemens, Erlangen, Germany) equipped with an 8-channel (Sonata and Symphony imagers) or 12-channel (Avanto) phased-array head coil. The MRI protocol included the following sequences before the injection of contrast agent: axial T2-weighted fast spin-echo (TR=4000 ms; TE=104 ms; slice thickness = 5 mm), coronal FLAIR (TR=9000; TE=108 ms; slice thickness=5 mm), and axial T1-weighted spin-echo (TR=500 ms; TE=77 ms; section thickness, 5 mm). DWI was obtained using an axial echo-planar spin-echo sequence (TR=2900 ms; TE=84 ms; section thickness 5mm). Diffusion was measured in 3 orthogonal directions using b-values 0, 500, 1000 sec/mm^2. Gradient echo EPI based DSC-MRI was acquired with TR=1430 ms; TE=46 ms (12 axial slices) to TR, 1590 ms; TE 52 ms (14 axial sections); bandwidth, 1345 Hz/pixel; voxel size, 1.80 ×1.80 × 5 mm^3; intersection gap, 1.5 mm; 50 times point). After

approximately 8 time points, 0.2 mmol/kg of gadobutrol (Gadovist; Bayer Pharma AG, Berlin, Germany) was injected at a rate of 5 mL/s, immediately followed by a 20-mL bolus of Sodiumchloride (9 mg/mL) injected at a rate of at 5 mL/s. T1-weighted spin-echo with the same parameter as the pre-contrast T1 weighted series was acquired after completion of the DSC-MRI.

3.2.2 Study III

All examinations were performed on the same 3T MR scanner (Skyra, Siemens Healthcare, Erlangen Germany) using a 20 channel head/neck coil. The following tumor protocol was carried out before gadolinium-based contrast agent (Clariscan 279.3 mg/mL, 0.2 mL/kg bodyweight, GE Healthcare, USA) administration: RSI (TR=10600 ms, TE=103 ms, FOV 256 mm, bandwidth 1480 Hz/pixel); 3D T1-MPRAGE (TR=2300 ms, TE=2.98 ms, FOV=256 mm, bandwidth 240 Hz/pixel); 3D FLAIR (TR=5000 ms, TE=387 ms, FOV=230 mm, bandwidth=751 Hz/pixel); axial T2-weighted images (TR=4090 ms, TE=88 ms, FOV=230 mm, bandwidth=349 Hz/pixel). After contrast agent injection: dynamic susceptibility contrast (DSC) MRI with a bolus injection (3ml/s) of the Gadolinium-based contrast agent, followed by 30ml of physiologic saline solution; susceptibility weighted imaging (TR=1350 ms, TE=30 ms, FOV=220 mm, bandwidth 1202 Hz/pixel); 3D T1-MPRAGE. RSI was performed using gradient spin echo planar imaging with 5 b-values of 0, 200, 800, 1500 and 3000 s/mm² and with 12 directions at each respective nonzero b-value.

3.3 Segmentation and image processing

3.3.1 Study I and II

A series of ROIs were manually drawn on every representative image slice for the entire tumor volume on ADC maps and T2-weighted images separately. The segmentation performed on T2-weighted images was co-registered with rCBV maps. The tumors were defined as regions with hyperintensities on T2-weighted images and on ADC maps, avoiding cystic appearing lesions and non-tumoral macroscopic vessels. Areas of contrast enhancement on post contrast T1-weighted images were always included. rCBV maps from DSC-MRI were created by using standard tracer kinetic models. The maps were corrected for potential contrast agent leakage and normalized with respect to blood volume values from normal-appearing tissue to obtain rCBV. Standard Stejskal-Tanner diffusion approximation was used for creating ADC maps from DWI. 100 bins histogram were created over an ADC range of 0-300 and an rCBV range of 0-7.5 (ratios; arbitrary units), respectively by using Matlab 2013 (MathWorks, Natick, Mass). The histograms were normalized by making all areas under the curves equal to one to correct for varying tumor sizes. From this the maximum peak heights of the normalized histogram $rCBV_{Peak}$ and ADC_{Peak} were statistically used as measures of vascular and cellular tumor heterogeneity, respectively. In addition, mean ADC (ADC_{Mean}) and mean rCBV (CBV_{Mean}) values of the ROI were assessed, as metrics for tumor cellularity and microvascularity, respectively [165,

166]. Tumor segmentation and processing of ADC and rCBV maps were performed using nordicICE (NordicNeuroLab AS, Bergen, Norway), figure 7.

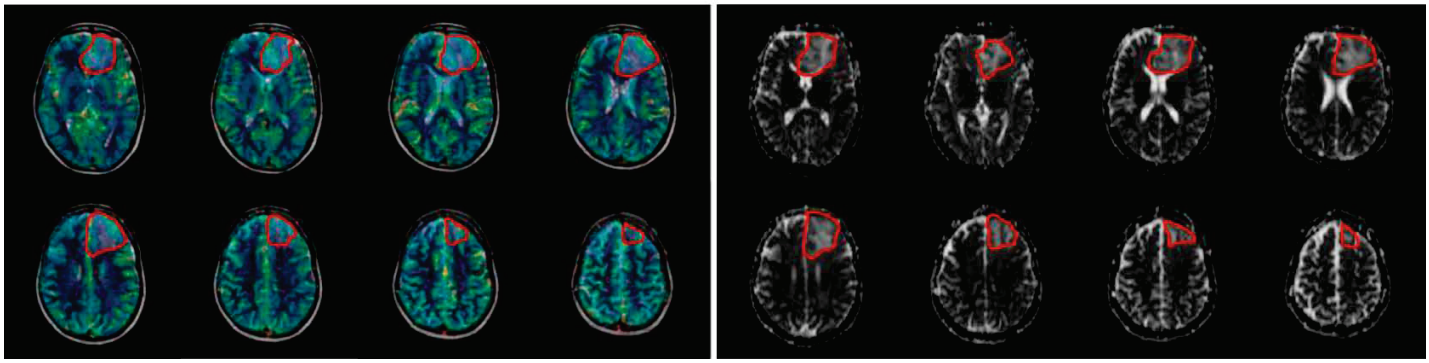

Figure 7. Segmentation of diffuse gliomas for studies I and II. A series of ROIs were manually drawn on every representative image slice for the entire tumor volume on ADC maps and T2-weighted images.

3.3.2 Study III

Tumor segmentation was performed semi-automatically on post-contrast T1- MPRAGE (1 mm thickness), using a dedicated software package nordicICE (NoridcNeuroLab AS, Bergen, Norway). The volumetric region of interest (ROI) was obtained from the contrast-enhancing portion on all representative slides and defined as contrast-enhancing tumor core (CET). ROI with extended margins were generated by means of morphological dilation using a spherical structuring element Matlab (v.R2017a, MathWorks Inc., Mass., USA) in order to derive three concentric volumetric regions with 5 mm thickness from external boarder of CET to the periphery. ROIs defined as peri-enhancing zone (PEZ), near zone (NZ) and far zone (FZ), respectively, are shown in figure 8. Circular shaped ROIs were also placed in the normal appearing tissue adjacent to the external border of pathologic FLAIR signal and in corresponding lobe of the contralateral hemisphere. These two regions served as reference examples and defined as iNAZ and cNAZ, respectively. All ROI's were then co-registered with the RSI-cellularity index, FA and ADC respective maps. Whole-tumor normalized histogram distributions of the RSI-cellularity index, FA and ADC were created and mean values were used for further analysis.

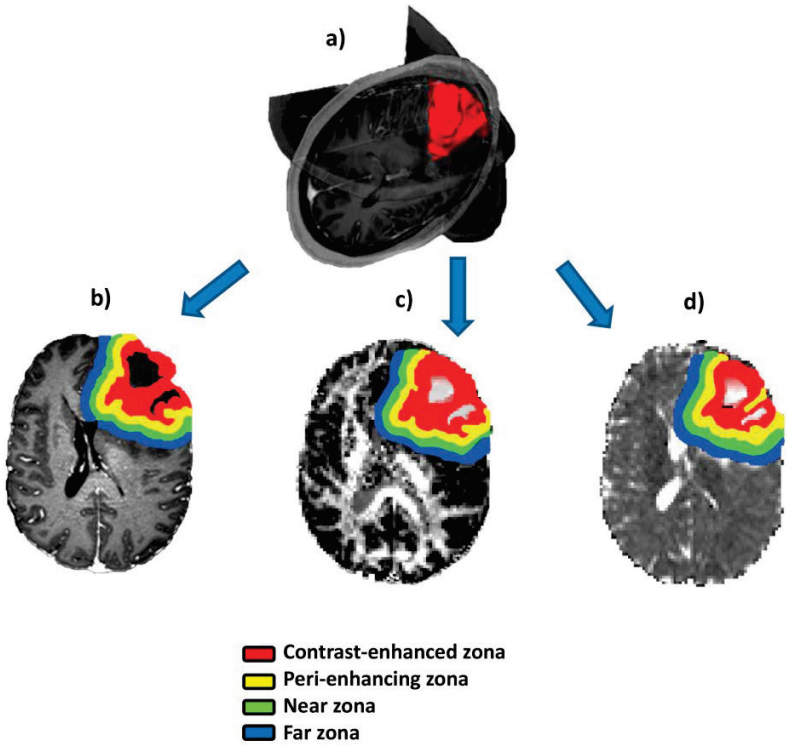

Figure 8. a) The volumetric ROI was obtained from the contrast-enhancing tumor core ROIs with extended margins were generated by morphological dilation of the contrast-enhancing tumor core, using a spherical structuring element on b) T1 MPRAGE, c) RSI-map, d) ADC-map. CET subtraction provided three concentric volumetric regions with 5 mm thickness in the peritumoral zone.

3.4 Histopathology, genetic molecular analysis and classification

Tumor tissue was obtained from needle biopsy or surgical excision, as part of the clinical routine. Specimens were formalin-fixed and paraffin-embedded, reviewed and diagnosed by experienced neuropathologists.

For patients from study I and II, in the period from 2006 to 2009, the 1p19q codeletion status analysis was performed by polymerase chain reaction (PCR) using at least 4 of 6 microsatellite markers on 1p35-36 and 19q13 [167]. From 2009, for detection of 1p19q codeletion, ATPX, TP53, IDH1 or IDH2 multiplex ligation-dependent probe amplification (MLPA) was performed. MLPA is based on the ligation of two DNA oligonucleotides that hybridize adjacently to DNA target sequence and has previously been described [168]. The MLPA kit was assembled by MRC-Holland (Amsterdam, The Netherlands). Tumors were primary classified by 2007 WHO classification of tumors of the CNS and retrospectively reclassified according updated 2016 classification with knowledge about 1p19q and IDH status in most cases. IDH status was determined for 58% of the tumors.

For the glioblastomas cohort in paper III, the DNA was extracted using the Maxwell 16 extractor (Promega, Madison, WI, USA) and the Maxwell 16 Tissue DNA Purification kit (Promega) according to the manufacturer's recommendations. The mutational analyses were performed using M13-linked Polymerase chain reaction (PCR) primers. All PCR were run on a Bio-Rad C100 Thermal Cycler (Bio-Rad Laboratories, Hercules, CA, USA). Detailed information about analysis of IDH 1, IDH2, TERT and MGMT with PCR can be seen in a previously described protocol [169]. Direct sequencing was performed using a 3500 Genetic Analyser (Applied Biosystems, Foster City, CA, USA). The BLAST (http://blast.ncbi.nlm.nih.gov/blast.cgi) and BLAT (http://genome.ucsc.edu/cgi-bin/hgblat) programs were used for computer analysis of sequence data. Tumors were classified according 2016 WHO classification of tumors of the CNS.

3.5 Survival assessment

OS and PFS were defined as the time interval (number of days) from initial diagnosis to patient death or tumor progression, respectively. Tumor progression was defined according to updated RANO criteria [75, 136]. Pseudoprogression was accounted by reviewing all available follow-up examinations and clinical information.

For study I, censoring was performed after 60 months observation and May 2017 was the date of administrative censoring. For PFS 48 months was used, because several previous studies have reported a median PFS of 27-53 months for patients with diffuse glioma [170]. For further analysis, all patients were divided in two groups per OS status: (I) long OS (over 60 months) and (II) short OS (under 60 months) and in two groups per PFS status: (I) long PFS (over 48 months) and (II) short PFS (under 48 months).

For study III, patients were censored for the death on the date of the last follow-up visit and for the progression on the date of their last central nervous system imaging study.

3.6 Statistical analysis.

Statistical analysis was performed using SPSS version 18 and 25 software (SPSS, Chicago, USA) and Stata 14 (*STATA* Corp., Texas, USA). For all cases, a two-tailed P-value of 0.05 or less was considered statistically significant including Holm-Bonferroni correction in the case of multiple comparisons.

The non-parametric Mann-Whitney U-test was used to assess the ability of histogram-derived diffusion and perfusion MRI parameters to identify patients suggestive of an oligodendroglioma independent of histopathologic grade, but also in subgroups related to the WHO grade (II and III) in study II. Mann-Whitney U-test was also used to compare diffusion parameters between different ROI inside and outside contrast enhanced tumor core in study III. The diagnostic performance was analyzed by the receiver operating characteristic curve (ROC), including values of sensitivity, specificity and area under the curve (AUC). Optimal cutoff points based on the Youden index were also estimated. Association between genetically defined subtypes, WHO grade and ADC and rCBV

parameters, were evaluated by both univariate and multivariate logistic regression. A leave-one-out cross-validation (LOOCV) algorithm with 10-fold cross-validation was used to calculate the overall diagnostic accuracy.

The independent significance of various predictors (age, extent of resection, Karnofsky performance status scale and genetic profile) on overall survival and progression-free survival were assessed by Univariate Cox proportional hazard regression analysis (CPH) in both study I and III. For study I, Cox regression with time-dependent covariates was also performed, including time and extent of surgical resection, as well as type and time of adjuvant therapy or chemoradiotherapy.

Kaplan–Meier survival analyses were performed based on the subgroups obtained from the LOOCV (study III) and ROC (study I) analysis and compared with each other's using a log-rank test.

3.7 Ethical considerations

The study was performed according to ethical standards based on the World Medical Association Declaration of Helsinki with its later amendments laid down by the 18th World General Assembly, Helsinki, Finland. The Regional Committee for Medical and Health Research Ethics (REC) for South-Eastern Norway approved these studies with REC-number 2013/81 2.2006.541 (study I and II) and REC-number 2018/2464 (study III).

MRI scanning was performed in line with current safety procedures at Oslo University Hospital and did not provide any increased risk for the patients. The study participants in studies I and II were scanned as part of their routine clinical work-up without any increasing in scanning time. For study III, research sequences prolonged the total scanning time which potentially slightly increased the discomfort for those patients. However, only patients in good general condition were recruited to the study.

4. RESULTS AND SUMMARY OF THE STUDIES

4.1 Study I

Median PFS and OS for patients with oligodendroglioma grade II were 41 and 58 months, anaplastic oligodendroglioma grade III: 43 and 57 months, diffuse astrocytoma grade II: 35 and 56 months and anaplastic astrocytoma grade III: 23 and 34 months, respectively.

Correlation between DSC parameters and survival outcome in patients with diffuse glioma WHO grade II and III

Histogram derived perfusions parameters $rCBV_{Peak}$ and $rCBV_{Mean}$ were independently associated with PFS in patients with oligodendrogliomas ($p<0.001$; $p=0.003$). Longer PFS (median, 46 versus 37 months) was associated with higher vascular heterogeneity (lower $rCBV_{Peak}$) and higher microvascularity (higher $rCBV_{Mean}$). In contrast, in the group with diffuse astrocytomas, longer PFS (median, 37 versus 26 months) was associated with lower vascular heterogeneity within the tumor (higher $rCBV_{Peak}$). Higher $rCBV_{Peak}$ and lower $rCBV_{Mean}$ values were showed statistically significant with longer OS in patients with astrocytomas grade III (median, 54 versus 37 months, $p=0.004$ and median, 48 versus 23 months, $p=0.008$, respectively). Conversely, the difference in OS was not significant in patients with diffuse astrocytoma grade II and oligodendrogliomas grade II/III.

Correlation between DWI parameters and survival outcome in patients with diffuse glioma WHO grade II and III

Histogram analysis of DWI-MR imaging parameters (ADC_{Peak}, ADC_{Mean}) did not show significant difference between patients with long and short OS and PFS for neither the oligodendroglioma, nor the astrocytoma groups. A combination of rCBV and ADC parameters did not yield a significant survival association.

Summary

Our results suggest, that perfusion MRI is a sensitive prognostic factor in patients with diffuse gliomas grade II and III, and may be used as a supplementary non-invasive vascular biomarkers to provide important information to treatment guidance.

4.2 Study II

Sixty-one patients with untreated genetic subclassified diffuse glioma: twenty-three oligodendrogliomas grade II, ten oligodendrogliomas grade III, nineteen astrocytomas grade II and nineteen astrocytomas grade III made up the study population.

Differentiation between oligodendrogliomas and astrocytomas by using DSC-MRI and DWI parameters based on histogram analysis

Oligodendrogliomas showed a significantly higher $rCBV_{Mean}$ with cut-off point ≥0.80 (AUC 79, sensitivity 68%, specificity 93%, p=0.003) and lower $rCBV_{Peak}$ with cut-off point ≥0.80(AUC 81, sensitivity 78%, specificity 78% p=0.005) compared to diffuse astrocytomas regardless of WHO grade.

Diffuse gliomas with higher cellular density (low ADC_{Mean}) cut-off point ≤ $1094 \times 10^{-6} mm^2/s$ were more likely to be found in oligodendroglioma than in astrocytoma (AUC 76, sensitivity 63%, specificity 61% p=0.009). Higher ADC_{Peak} and lower ADC_{Mean} indicated oligodendroglioma when the gliomas grade II subgroup was analyzed separately (p=0.042; p=0.001 respectively).

Linear combination of $rCBV_{Peak}$, $rCBV_{Mean}$, ADC_{Peak} and ADC_{Mean} based on logistic regression showed superior diagnostic performance in differentiating oligodendrogliomas from diffuse astrocytomas (AUC 84, sensitivity 92%, specificity 81% p=0.035).

Differentiation between WHO grade II and grade III astrocytomas by using DSC-MRI and DWI parameters based on histogram analysis

ADC_{Peak} and ADC_{Mean} values were not significantly different between WHO glioma grade II and III. A multivariate regression model including combined ADC and rCBV values was able to classify between grade II and III in the astrocytoma subgroup (Odds ratio 0.92 (CI 0.81;1.00, p=0.03), but not in the total patient population or in the oligodendroglioma subgroups.

Summary

Histogram derived DSC-MRI and DWI parameters may be used as imaging biomarkers for identification of oligodendroglioma as defined by the new WHO 2016 classification criteria. Non-invasive assessment is an important supplement to neuropathological evaluation in newly diagnosed glioma and in longitudinal follow-up.

4.3 Study III

In forty-one patients with glioblastoma, IDH-wild type, median PFS was 184 days and the median OS was 245 days. Of all clinical parameters, only total resection and Karnofsky performance status over 70 were significant associated with longer PFS (HR 3.5, 95% confidence interval (CI) 1.0-12.1; P=0.04 and HR 4.4, 95%CI 1.6-12.1, P=0.006) and longer OS (HR 3.8, 95%CI 1.1-12.9, P=0.03 and HR 3.2, 95%CI 1.3 -7.8, P=0.01).

RSI-CI, FA and ADC in contrast-enhanced zone and peritumoral zones

The RSI-cellularity index in CET was on average 24% higher than the value in PEZ (P<0.001) and 28% higher than in NZ (P=0.003) (CET > PEZ > NZ). FA was measured in CET 25 % higher (P < 0.01) compared with PEZ with a diagnostic accuracy of 82% (P < 0.01) (CET > PEZ).

Relationship between RSI-cellularity index, FA and MD values in different glioblastoma compartments and survival outcome.

Higher value of RSI-CI was significantly associated with shorter OS (215 versus 543 days, P=0.002).This association was also found for RSI-CI value measured in PEZ (OS: 298 versus 572, P=0.041) and NZ (OS: 166 versus 643, P<0.020). Lower FA value in CET and PEZ was significantly associated with poorer OS (316 versus 601 days, P=0.006). Statistical significance was reached between MD values from CET and PFS (log rank = 0.004), but not from PEZ, NZ, FZ. Patients with MD in CET under cut-of value 0.83 x 10^{-3} mm^2/s and FA cut-of value under 0.17 had the shortest survival time.

MGMT promoter methylation status and diffusion metrics

Presence of MGMT promoter methylation were significant associated with longer PFS (HR 3.3, 95% CI 1.4; 7.9, P=0.006) and longer OS (HR 3.7, 95%CI 1.6; 8.7, P=0.002). No statistically significant differences were noted between RSI-cellularity index, FA, MD and MGMT promoter methylation status obtained from different tumor zones.

Summary

In contrast to conventional diffusion metrics, RSI-cellularity index was a robust and stable measurement for tumor tissue cellularity. By analyze structural heterogeneity in the peritumoral zone, we may better assess the biological behavior of glioblastoma, and thus also its prognosis. RSI, supplemented by other MRI modalities, can be helpful to optimize the extent of surgical resection and radiation field mapping, improving the benefits for patient outcome.

5. DISCUSSION

5.1 General methodological consideration

5.1.1 Whole tumor histogram analyses (study I, II and III)

In all three studies we have used histogram analysis in order to assess the complete distribution of diffusion and perfusion values from whole-tumor volumes. Previous studies showed that histogram analysis may provide robust and reproducible estimates for the differentiation of gliomas from each other and for the prediction of prognosis for glioblastoma. However, it has been suggested that histogram parameters may be less sensitive to user-bias for diffuse glioma grading than for single ROI analysis [165, 171-174].

Whole tumor histogram profiling of ADC and CBV maps provide a comprehensible set of parameters, which allow for evaluating not only the value but also the pixel distribution that reflects heterogeneity within a ROI. In study I and II we calculated the means of ADC and CBV in whole tumor volume (ADC_{Mean} and $rCBV_{Mean}$) as metrics for tumor cellularity and microvascularity respectively. In addition, maximum peak heights of the normalized histogram (ADC_{Peak} and $rCBV_{Peak}$) were both statistically used as measures of cellular and vascular tumor heterogeneity. A visual inspection of histogram curves contributed to interpretation of heterogeneity; a flattened normalized histogram shape reflects higher heterogeneity of ADC and CBV values distribution within a tumor.

Based on previous works, we chose the ADC 10^{th} percentile and the RSI-cellularity index 90^{th} percentile value derived from whole-volume histograms for analyses in study III [109, 175]. The reason for this is the inverse relation of ADC and RSI values to one another (lower ADC values and higher RSI cellularity values are associated with higher tumor cellularity). As a result, the ADC 10^{th} percentile corresponded to the 90^{th} percentile value of the RSI cellularity histogram.

Unfortunately, histogram analysis is not available in standard PACS software at our hospital and requires dedicated segmentation software. In contrast working with single non-volumetric ROIs is quite easy for clinical applications but this approach is always prone to bias because of the high variability of diffusion values [171, 176].

5.1.2 Volumetric ROI design (study I, II and III)

Historically, several different methods for ROI design have been used to assess glioma characteristics with MRI modalities. The main differences in ROI approach concerns two-dimensional 2D-ROI versus three-dimensional 3D-ROI models; manual versus semi-automatic versus fully automatic methods; separate segmentation of contrast-enhanced tumor core and non-contrast enhanced tumor parts versus whole tumor volume segmentation [177].

Over the last decade several automatic segmentation algorithms have been proposed including support vector machines [178], level-set methods [179], the k-nearest neighbor algorithm [180] and deep learning approaches using convolutional neural networks [181, 182]. However, these automatic approaches generalize brain tumor segmentation and pay no particular attention to specific segmentation difficulties related to the biology of low-grade gliomas such as infiltrating growth and irregular contours. This is why, manual segmentation is still widely used as ground truth in automatic segmentation studies of brain tumor and why no software algorithms have yet been proved to adequately replace human expertise [183].

Because of the large number of low-grade gliomas in study I and II, we chose manual segmentation in order to avoid the uncertainties related to automatic segmentation, as mentioned above. Freehand ROI drawing requires the use of multi-modality MRI information together with anatomical and pathological knowledge. Our segmentation procedure involves manually drawn contours around the entire tumor volume on every representative image slice by the neuroradiologist. Tumor was defined as regions of hyperintense signal on T2-weighted images and on ADC maps. Areas of contrast enhancement on post contrast T1-weighted images were always included. This approach was used in previous studies and has demonstrated high discriminant ability between glioma types and WHO grades [165].

The most important limitation of manual segmentation is low intra- and inter-rater reliability that may affects results. However, the high intra-observer agreement of the histogram method suggests that small variations in ROI segmentation may not necessarily influence the results, given the large number of data points included in the histogram [184]. Several previous studies confirmed the inter-observer reproducibility of manual contouring [183, 185]. The intra-rater variability also decreases with higher radiologist experience and higher grade of border conspicuity [186]. As automatic segmentation algorithms do not yet offer a reliable solution for low-grade gliomas, manual contouring is still the preferred method.

Another limitation related to manual segmentation that is very labour intensive and requires a great deal of time. It is partly for this reason that we chose a semi-automatic method based on a region growing algorithm for segmentation of contrast-enhancing parts of the glioblastomas in study III. The region growing method is one of the simplest techniques of region based segmentation and is used to obtain bonded regions of pixels that are similar to the original image [187] . This method is part of the NordicICE software package which was used in our studies. Although ROIs for peritumoral zones in study III were generated automatically all results were carefully visually inspected in order to increase the accuracy of the segmentation.

Because of the infiltrative growth and irregular shape of gliomas, we believe that 3D-ROI segmentation is the most appropriate way to delineate pathologic neoplastic tissue from

normal appearing tissue in both low-grade and high-grade gliomas. We also used a compartment approach to measure diffusion separately in the contrast enhancing core and in three peritumoral ROIs (peri-enhancing zone, near zone and far zone) in study III. Compartment models highlight the heterogeneity within peritumoral brain zones and were used in several previous glioblastoma studies [188-190] .

To eliminate any potential observer bias during the segmentation routine related study endpoints, all image analysis was performed blinded to patient outcome.

5.1.3 Follow-up-imaging of glioma. RANO criteria (study I and III)

Traditionally, the success of new cancer treatments have been assessed by their ability to improve OS and/or surrogate endpoints for OS, such as PFS in large trials. OS and PFS defined by RANO criteria are also widely used to identify and validate prognostic imaging biomarkers for survival in order to navigate further treatment strategy. In order to have a standardized method for the evaluation of post treatment tumor growth, as well as for the comparison of our results with previous literature, we chose to use RANO criteria in study I and III [136].

All measurements and classifications of status of progression or non-progression were performed retrospectively for study I and prospectively in study III. While preoperative examinations were always performed with the same tumor protocol in our hospital, follow up examinations were often carried out in satelite institutions using different MRI routines. The main differences in the MR protocols were related to the use of 3D imaging versus 2D imaging and T1 gradient-echo (MPRAGE) versus spin-echo (SPACE) sequences, which may have had an impact on the accuracy and the reproducibility of our measurements.

Lack of standardization of initial and follow-up tumor protocols for high-grade gliomas were discussed broadly in our regional oncologic meeting of autumn 2019. Here specialists and researchers with an interest in neurooncology (radiotherapy and medical oncology), neurosurgery, neuropathology, neuroradiology were tasked with establishing minimum standards for imaging (preoperative, intraoperative, postoperative and follow-up controls), and multimodality therapy (surgical oncology for gliomas, radiotherapy, chemotherapy) in order to coordinate our academic brain tumor center with local institutions. Consensus was obtained that was also in agreement with the European recommendations for best clinical practice for glioma imaging [95]. This including the clear advantages of 3D volumetric imaging over 2D imaging whereby the ability of 3D imaging to make reconstruction in all planes, resulting in more accurate measurements was acknowledged. In addition, the higher resolution of 3D imaging reduces the risk of missing small foci of contrast enhancement due to partial volume effects [191]. A recent study also showed that bidimensional measurements was prone to underestimating progression in patients with glioblastoma [192].These findings emphasize importance to develop technics for volumetric assessment of glioblastoma growth in the future.

Another challenge was the estimation of PFS related to progression and pseudoprogression. We registered pseudoprogression in 18 % of glioblastoma patients in study III, by reviewing all available follow-up examinations and clinical information. None of the glioblastoma patients in study III received VEGF-targeted therapy and consequently the opposite phenomenon - pseudoresponse was not observed.

Ill-defined borders and uncertainties in differentiating tumors from other treatment-related changes (e.g.radiotherapy induced leukoencephalopathy) was an additional challenge in defining progression in non-contrast-enhanced low-grade gliomas in study I.

5.2 Specific considerations study I

5.2.1 The prediction of survival outcome in patients with diffuse glioma by perfusion and diffusion MRI

The use of MRI for prediction of recurrence and survival time in the clinical evaluation of gliomas, has received much attention. Grade of tumor cellularity and microvascularity associated with vascular neogenesis can be measured with diffusion and perfusion MRI techniques respectively. Those features of neoplastic tissue that reflect the aggressiveness of gliomas may assist in the stratification of patients into subgroups resulting in more uniform clinical outcomes. Considering the poor long-term survival in patients with diffuse glioma grade II and III, there is a pressing need to balance treatment and quality of life. Non-invasive imaging biomarkers can be used for monitoring disease and treatment decisions, particularly at the time of recurrence.

In study I, we identified the histogram derived perfusion and diffusion MR parameters that could most efficiently predict PFS and OS in patients with WHO grade II and III in a preoperative situation. We found that significantly longer PFS was associated with a more homogeneous rCBV distribution with higher $rCBV_{Peak}$ (median, 37 versus 26 months, HR=3.2, P=0.02) in patients with astrocytomas. Interestingly, in contrast to the astrocytoma subgroup, we identified longer PFS (median, 44 versus 39 months, HR=7.9, P=0.003) in the group of patients with oligodendrogliomas with heterogeneous microvascular anatomy (low $rCBV_{Peak}$) and higher vascularity (high $rCBV_{Mean}$). These results suggest, that high CBV in oligodendrogliomas, in contrast to astrocytomas, does not necessarily reflects aggressive behavior and consequently outcome. Previous studies showed that microvessel angiogenesis correlates more strongly with patient survival compared with microvessel density [193, 194]. High heterogeneous microvascularity in oligodendrogliomas may be explained by the presence of branching network of delicate capillaries, typically observed in oligodendrogliomas, rather than by presence of angioneogenesis [33]. Theoretically, the

presence of these vascular microstructures may also increase chemotherapy delivery of intravascularly administered drugs with benefit to response and consequently outcome. In contrast, vascular neogenesis in gliomas implicated resistance to TMZ treatment and was associated with shorter outcomes [195, 196]. The biological basis for increased chemosensitivity in patients with oligodendrogliomas, associated with the loss of chromosomes 1p19q, is still unclear [33].

Diffusion-based MRI metrics were not able to stratify survival in patients with WHO grade II and III in our study. These results were not in agreement with previous reports showing associations between diffusion parameters and survival in diffuse gliomas. Hilario et al in a study that included 126 diffuse gliomas found that lower ADC and higher rCBV values correlated with a worse prognosis. The median overall survival in patients with ADC < 0.799 $\times 10^{-3}$ mm^2/s was under 1 year. In addition, minimum ADC and maximum rCBV values predict overall survival regardless of histologic grade [197]. Cuccarini et al demonstrated in a cohort of 89 patients that significantly longer OS was observed in patients with minimum normalized ADC above cut-off ratio of 1.69 (80 versus 55 months, p = 0.01; 80 versus 51 months, p = 0.002, respectively) [198]. This result was also confirmed when cases were stratified according to pathology (low-grade gliomas versus high-grade gliomas). These conflicting results may be partially attributed to the differences in study populations. In addition to glioma grade II and III, Hilario and Cuccarini included patients with glioblastomas (grade IV) in their study cohord. Neill et al showed that median and 10% ADC was significantly associated with PFS in patients with recurrent gliomas grades II and III [199].

Generally, OS is the most definitive and objective endpoint in oncology. Nevertheless, the slow growth pattern of the majority of low-grade gliomas in association with a rare radiological true responses despite a favorable clinical response to treatment brings logistical challenges for using OS both for the purpose of research and in clinical trials [200]. In our study, we found differences in OS only for patients with astrocytoma grade III, but not in patients with diffuse astrocytoma grade II and oligodendrogliomas grade II/III. The most obvious reason is the long survival time among patients with oligodendrogliomas and grade II astrocytoma (up to 12-15 years), while OS censoring was performed after 5 years observation for practical reasons. Because of the long observation time of OS, PFS is instead considered the more reliable assessment of efficacy for investigational treatments in clinical trials. Prolonged PFS can be translated into a clinical benefit.

Determination of radiological progression in low-grade gliomas is a significant challenge because of their manifestation by small, incremental, and often asymptomatic increases in size on T2-weighted images. Low-grade gliomas most commonly present as ill-defined T2/FLAIR hyperintense lesions and display no contrast enhancement. Therefore, it can be difficult to differentiate tumor from other treatment-related changes, such as radiation-induced leukoencephalopathy. In addition, these tumors grow slowly. It may take a long time to achieve a 25% increase in lesion size (the threshold for radiographic progression in

high-grade gliomas by RANO criteria). For these reasons, in addition to determining changes in tumor size, other measures of clinical benefit such as changes in neurocognitive function, quality of life and seizures may be useful in assessing the utility of novel therapies. In particular seizure control has recently been proposed as an additional metric in disease response and as an endpoint in trials for low-grade gliomas [201].

5.3 Specific considerations study II

5.3.1. Identification of genetically defined oligodendroglioma by diffusion and perfusion MRI

The diagnostic criteria for astrocytoma and oligodendroglioma have been updated in 2016, where the genotype trumps the histological phenotype. In addition to the presence of the IDH mutation, 1p/19q codeletion is mandatory for the diagnosis of oligodendroglioma. All patients in studies I and II underwent genetic testing with determination of 1p/19q codeletion status and were reclassified to oligodendrogliomas or astrocytomas accordingly. Primary original diagnosis was based on histopathology and included mixed gliomas in addition to oligodendrogliomas and astrocytomas.

Prior to the WHO classification update of 2016, several studies evaluated the value of perfusion and diffusion-weighted MRI to differentiate between histopathological subtypes of gliomas [148, 202]. However, inclusion of mixed glioma (oligoastrocytomas) in these studies impedes a direct comparison of the results. For this reason, we reviewed our results in light of research based on the genotypic classification of glioma, published mainly after 2016.

Our main finding was higher microvascularity (high CBV_{Mean}) and higher cellular density (low ADC_{Mean}) in oligodendrogliomas compared with astrocytomas, regardless of histopathological grade. In particular the combined use of diffusion and perfusion histogram parameters ($CBV_{Mean,}$ $ADC_{Mean,}$ $CBV_{Peak,}$ ADC_{Peak}) included in logistic regression had superior diagnostic performance versus single parameters to identify oligodendroglial tumors. In agreement with our findings, Leu et al showed, that a separate multivariable logistic regression model was able to differentiate between 1p19q+ and 1p19q− WHO II–III gliomas with an AUC of 0.80 ($p = 0.0015$, 64% sensitivity, 82% specificity) [203].

Also similar to our results, Leu et al did not observe differences in vascular densities and cellularity between oligodendrogliomas and astrocytomas of WHO grade II with substantial overlap between rCBV and ADC measurement in these tumors [203]. Apparent intratumoral neoangiogenesis and cellularity are the main reason for elevated CBV and ADC in gliomas, respectively. The absence of apparent neoangiogenesis and high mitotic activity in low-grade tumors may be a possible explanation for these undetectable rCBV and ADC variations.

In contrast to our results, Yoon et al found that the rCBV values were not significantly different between the oligodendroglioma and astrocytoma groups grade II and III [204].

These conflicting results may be partially explained by different methodology (3D ROI analyzed of whole tumor volume in our study versus 2D ROI of the contrast enhanced part of tumor in the study by Yooh et al) and different study populations (WHO grade II and III in our study versus WHO grade II, III and IV in the study by Yooh et al).

In the last three years, an increased number of radiogenomics studies have attempted to predict gliomas with 1p19q mutation (oligodendrogliomas). Zhou et al used routine preoperative MRI of 165 patients from The Cancer Genome Atlas and The Cancer Imaging Archive to generate radiomic models based on automated texture analysis and predicted 1p19q status with an accuracy of 0.96 within the same data set [205]. Zhou et al also investigated a pre-operative cohort of 538 diffuse glioma patients from multi-institutional data. Based on the top 15 features (histogram, shape and texture, extracted from T1 contrast enhanced and T2-FLAIR sequences), a model achieved an AUC of 0.917 and 0.916 for the training and validation cohort, respectively [206]. Akkus et al identified 1p19q status of 159 low-grade gliomas from post-contrast T1- and T2-weighted MR images using convolutional neural networks (machine intelligence technique). The results of the best performing configuration on the unseen test set had sensitivity 93.3%, specificity 82.22% and diagnostic accuracy 87.7% [207].

There is an important limitation related to the patient cohorts in studies I and II. IDH1/2 status, which has become definitional for gliomas according to the updated classification, was only available in 57, 7% of cases. However, the Cancer Genome Atlas Research Network demonstrated that a strong correlation exists between the histologic class of oligodendroglioma and the presence of IDH mutation together with a combined whole-arm loss of 1p and 19q [208]. Furthermore, later data suggest that typical 1p19q loss is always associated with IDH mutations [209-215]. Finally, in the recently published work by Eckel-Passow JE a co-occurrence of 1p19q loss with IDH mutation was found [216]. In summary, although IDH mutation was not performed in all the cases, it seems reasonable to regard codeletion of 1p19q as a genetic hallmark defining oligodendrogliomas.

5.3.2 The discrimination between glioma WHO grades II and III using diffusion and perfusion MRI

Although genetic alteration, as *IDH*-mutation, 1p19q and MGMT-methylation provides prognostic data, the majority of available literature suggests that also WHO grading based on histopathological diagnosis is still important for the choice of therapeutic options and predicting clinical outcomes. In patients with low-grade gliomas, it may be beneficial to simply observe the patients' response after surgery, rather than immediate adjuvant therapy. Delaying radiotherapy in this setting does not have a negative impact on overall survival and may also postpone the potential adverse effects of the therapy. Immediate postoperative chemoradiotherapy is however appropriate in most patients with anaplastic astrocytoma [217].

Several studies have provided evidence of a clinically significant intraobserver variation in the histological diagnosis of glioma, that affect the grading of glial tumors, particularly the differentiation between grade II and grade III gliomas [218, 219]. Currently, both structural and functional imaging is well placed to contribute to improving the histopathologic diagnosis of gliomas.

Perfusion MR in patients with glioma has been studied with regard to pre-operative tumor grading [125, 220-222], and the CBV has been used to separate low-grade from high-grade astrocytomas [90, 119, 172, 222, 223]. However, the differentiation of glioma grade II from grade III is challenging, especially in oligodendrogliomas, due to overlapping features [222, 224, 225]. In our study histogram derived perfusion biomarkers ($rCBV_{Peak}$ and $rCBV_{Mean}$) were not able to separate between WHO glioma grade II and III in the univariate model. In contrast to our results, meta-analysis with inclusion of twenty-eight studies and evaluating a total of 727 individuals showed a significant difference of relative maximal CBV between glioma grades II and III with AUC 0.77 and an optimal cutoff of 2.02. Glioma grade III had higher relative maximal CBV compared with glioma grade II. When astrocytomas were analyzed separately, the AUC increased to 0.86 but decreased to 0.61 in the oligodendrogliomas cohort [226]. The concordance of results may be partly explained by preselection of patients with oligodendroglial histopathological features in our study.

Parameters from diffusion MRI (ADC_{Peak} and ADC_{Mean}) alone were not significantly different between grade II and grade III gliomas in either the entire patient population nor in separate subgroups of oligodendrogliomas and astrocytomas in our study. This finding is in agreement with other studies where a standard b-value (b=1000s/mm^2) was used [227-229]. Studies that used ADC derived parameters from diffusion MRI with high b-value (b=3000s/mm^2) showed ambiguous results. Han et al analyzed diffusion-weighted imaging (DWI) at 3T with standard and high b-values (b = 1000 and 3000 s/mm^2) of thirty-nine patients with non-enhancing high and low-grade oligodendrogliomas and astrocytomas. ADC values (minimum, maximum and mean) for the high-grade gliomas were lower than those for low-grade glioma. These differences were much larger when a high b-value was used (all $P < 0.0001$) compared to the use of a standard b-value. A cutoff value of 0.814×10^{-3} mm^2/s was significant to differentiate between low-grade and high-grade gliomas [89]. Kang et al used histogram analysis of ADC maps and reported that minimum ADC value was different between grades II and III gliomas for both standard and high b-value images [90]. In contrast, Cihangiroglu et al did not find any differences in ADC derived parameters between grade II and grade III gliomas using diffusion with standard b-value and high b-value [230]. However, differences in ADC values (minimum and maximum) within the tumor ROIs were found between grade III and grade IV only using high b-value. In the last mentioned study ADC parameters were derived only from the solid tumor region, while Han et al [89] and Kang et al [90] analyzed ADC of whole tumor volume including peritumoral edema.

In our study, the use of a multivariate regression model including all histogram parameters from both perfusion and diffusion($rCBV_{Peak}$, $rCBV_{Mean}$, ADC_{Peak} and ADC_{Mean}) showed superior diagnostic performance for the classification between histopathologic subgroups of astrocytoma (WHO II versus WHO III) (p=0.03). Anaplastic astrocytomas depicted higher and more heterogeneous vascular patterns in addition to higher cell densities compared to those of diffuse astrocytoma grade II. Qin et al demonstrated the same tendency. The combination of diagnostic methods, including diffusion and perfusion MRI, had the highest AUC 0.958, in distinguishing between grades II and III astrocytoma, followed by rCBV, AUC 0.913, and ADC AUC 0.885 [231].

Recently, promising results for grading of gliomas were achieved by means of radiogenomics. Kim et al extracted radiomics features (n = 6472) from multiparametric MRI including conventional MRI, ADC and CBV, acquired from 127 glioma patients with determined IDH mutation status and grade (WHO II or III). Radiomics models were constructed using machine learning-based feature selection and generalized linear model classifiers. In tumor grading, the multiparametric model with ADC features showed higher performance (AUC 0.932) than the conventional model (AUC 0.555) [232].

5.4 Specific considerations study III

5.4.1 RSI-cellularity index, FA and MD in different glioblastoma compartments

Aggressive invasiveness of glioblastoma cells into the surrounding brain is one of the biggest challenges for effective surgery and radiation therapy. However, today most surgical and adjuvant therapy efforts are concentrated on the contrast-enhancing part of glioblastoma, mainly guided by structural MR images. Even using modern microsurgical techniques, tumor recurrence is usual and typically occurs within 1–2 cm of the original tumor core boundary [233, 234]. There is henceforth a need to quantify cellular variability beyond the visible borders of the enhancing tissue on MRI, in order to help navigate the surgical process and to plan postoperative therapy.

We validated the ability of RSI to indicate cell-rich regions in the contrast-enhancing tumor core and in the peritumoral zones. We have also evaluated the prognostic value of RSI-cellularity index obtained from different tumoral zones in order to correlate with potential aggressive behavior and to define potential treatment targets. The prognostic value of RSI-cellularity index was compared with clinically established diffusion metrics such as FA and MD.

As expected, RSI-cellularity index was highest in the contrast-enhancing core and declined with increased distance from the tumor core to the peripheral borders of the tumor (abnormal T2/FLAIR signal). The correlation of cellularity with T1-shortening on gadolinium-enhanced sequences (contrast enhancing in tumor) has been reported before and may be explained by a dominant pattern of glioma cells invasion along perivascular spaces [235].

Invading glioma cells moves along vessel walls and disrupt connection between astrocytes and endotelium, leading to degradation of basement membrane by loss of tight junctions in the endothelial layer and leakage of contrast agent within the contrast-enhancing core [236-238]. The occurrence of contrast-enhancement in diffuse gliomas generally indicate a more malignant biological behavior [239].

The highest cellularity index was measured in the peri-enhancing zone compared to near infiltrating zone. In agreement with histopathologic findings, the decline of cellular density from tumor core to periphery reflects an extensively infiltrating pattern in glioblastomas with the highest concentration of invading cells around the primary tumor mass [8].

In contrast to RSI-cellularity index, we did not find significant differences in MD values between contrast-enhancing tumor core and peritumoral zones, which could reflect differences in cellularity. It may indicate affection of the MD value by extracellular edema, but less affection of RSI-cellularity index value, which maximize sensitivity to intracellular diffusion by excluding extracellular diffusion components. Because MD is mathematically equivalent to ADC, our results may be compared to previous DWI studies. Published reports of the association between ADC and cellularity in the peritumoral zone demonstrates conflicting results. Indeed, several studies demonstrated a strong negative correlation between the ADC and tumor cellularity. Tien et al have suggested that ADC may distinguish areas of predominantly non-enhancing tumor from areas of predominantly peritumoral edema, especially in tumor located in the white matter aligned in the direction of the diffusion-weighted gradient [240]. Negative correlation between ADC and cellularity was also shown by Chang et al with the use of multiparametric linear regression model at voxel level MR imaging that included ADC, T2-FLAIR and T1- weighted post contrast signal [235]. Barajas et al reported that in addition to cellularity, ADC in peritumoral zone inversely correlates with other histopathologic features of tumor aggressiveness such as microvascular expression, hypoxia and cellular mitosis [190]. In both Barajas' and Chang' studies, MRI findings have been approved histopathologically with stereotactic biopsy obtained from the peritumoral zone.

However, a weak to moderate inverse correlation between ADC and cellularity was demonstrated in studies including glioblastomas only [241, 242]. Several previous reports have also shown that ADC alone was not a significant predictor of either PFS or OS in patients with glioblastomas [173, 243].

These discrepancies may be explained by histopathologic heterogeneity of glioblastomas and a lack of full understanding of which tissue characteristics play a significant role in influencing the ADC. In fact, any structural variation of extracellular matrix can affect the ADC value. Glioma cells tend to produce large amount of extracellular matrix component (ECM), which serves as a substrate for cell invasion [14]. These structures theoretically may provide considerable restriction to diffusion. However, a previous study has also demonstrated that ECM is partly altered in gliomas and as a consequence, increased

extracellular water component and ADC. Thus, we can assume that variation in ECM composition may influence ADC in different directions. The heterogeneity of ECM were also demonstrated in the study of Virga et al, which determined that ECM components exhibit different genetic expression levels associated with poor and improved prognosis [244]. In addition, necrosis in different stages may have both increased and decreased ADC values. Low ADC in necrotic regions of glioblastomas was found in a post-mortem study by LaViolette et al [245], while Crawford et al reported elevated ADC values in necrotic areas, possibly due to protein degradation in the extracellular matrix [246].

We have also observed higher RSI-cellularity index and lower MD in normal-appearing tissue than in the contrast-enhancing tumor core and peritumoral zone. This finding is in line with previous rapports whereas ADC values of normal gray and white matter are exceeded by ADC values of tumor tissue measured over a normal b-factor range [78]. Thus, to compare ADC value between tumoral (both contrast-enhanced and non-contrast enhanced) zones is the most reliable and useful clinical approach to estimate cellular heterogeneity.

FA value reflects the directionality of diffusion and corresponds to the anisotropic component. There is an increasing use of DTI and tractography in neurosurgical planning and optimization of neuro-navigation in order to minimize neurologic morbidity [98, 247]. Our results showed lower FA in the contrast-enhanced zone than in peri-enhancing zone. In contrast, no significant differences between FA values were detected in the peri-enhancing zones and near tumoral zones that may indicate affection of FA value in the peritumoral zones by extracellular edema. DTI can demonstrate the local effects of tumor on white matter integrity. Four patterns have been typically described: (1) normal signal with changed position/direction suggesting tract displacement; (2) decreased but present signal with normal position/direction suggesting vasogenic edema; (3) decreased signal with disruption of fiber tracts suggesting tumor infiltration and (4) loss of anisotropic signal suggesting tract destruction [248]. Unfortunately FA value may not provide clear differentiating between those processes that make intraoperative detection of intact tracks challenging. McDonald et al have demonstrated the ability of RSI to address this limitation by removing the extracellular diffusion component [107]. FA values obtained from RSI and standard DTI were compared within regions of FLAIR hyperintensity. FA values increased when the FLAIR hyperintensity resolved by use of standard DTI, but remained stable with RSI. This result suggests that the microstructure of white matter was mainly intact in peritumoral tissue but was masked by edema.

5.4.2 Relationship between RSI-cellularity index, FA and MD in different glioblastoma compartments and survival outcome

In our study, we found that higher RSI-cellularity index in the CET, PEZ and NZ was a predictor of poor prognosis in glioblastoma patients and had superior diagnostic performance to stratify survival compared with ADC and FA. We observed a significant

association between lower MD in the CET and shorter survival, but MD in the peritumoral zones did not show predictive value to survival outcome. McDonald et al demonstrated the same results in a study of 40 patients with high-grade gliomas, treated with bevacizumab, where an increase in 90th percentile of RSI cellularity values in the FLAIR hyperintensity area was the strongest predictor of poor PFS and OS, whereas decreases in 10th percentile of ADC values in the FLAIR showed a weaker association with OS only [108].

The growth rate of glioma tissue with higher cellularity has been shown to be faster than that of tissue with lower cellularity [249]. Therefore, our results suggest that tumor parts with high RSI-cellularity index values may be predictive to tumor tissue with fast growth rates and consequently more aggressive behavior. The identification of these tumor compartments can be helpful to achieve representative biopsy, optimize the extent of surgical resection and radiation field mapping, with significant advantages for patient treatment.

In a future perspective study, detailed characterization of diffusion metrics within peri-enhancing-, near- and far zones may provide more accurate pre- and intraoperative information. The combination of diffusion with other functional quantitative metrics derived from perfusion and spectroscopy MRI may also improve characterization of different biological aspects of glioma.

5.4.3 Association between diffusion metrics and MGMT promoter methylation status in patients with glioblastoma

MGMT promoter methylation has strong correlation with IDH-mutation and is associated with a better response to temozolomide in patients with glioblastoma [39, 250, 251]. In our study the presence of MGMT promoter methylation was significantly associated with longer PFS (HR 3.3, P=0.006) and longer OS (HR 3.7, P=0.002), but we did not find any significant correlations between RCI-cellularity index, FA or ADC and MGMT promoter methylation status.

There is no consensus in the literature about the association between MGMT status and MRI-based diffusion metrics.

Indeed, several studies have reported that MGMT promotor methylated tumors display diffusion MRI features of lower cellularity (higher ADC) and severe disruption of white matter tracts (lower FA)[252-254]. Han et al in study of 77 patients with primary glioblastoma reported that significantly increased ADC value (P<0.001) was associated with MGMT promoter methylation with AUC, 0.860; sensitivity, 81.1%; specificity, 82.5% [253]. Rundle -Thiele et al have showed the same results in a study with 32 glioblastomas [254]. In both studies, 2D ROI with measures of minimum ADC were used, in contrast to whole-tumor 3D analysis by histogram method as in our study, which may be a possible explanation for result discrepancies. In line with our findings, Ahn et al, Gupta et al and Qin

et al did not find significant correlations between ADC or FA values and MGMT promoter methylation status [231, 255, 256].

6. CONCLUSIONS

We have investigated advanced imaging techniques, namely diffusion and perfusion MRI in order to characterize patients with low-grade and high-grade diffuse glioma. Our results suggest, that the methods proposed in this thesis may provide objective measures for tumor cellularity and vascularity. This can be implemented in combination with other structural and functional methods in clinical routine. Our methods may also be applied to other emerging MR imaging techniques in order to further development of reliable biomarkers.

Conclusions in study I and II

There is higher microvascularity and higher cellular density in oligodendrogliomas compared with astrocytomas, irrespective of histopathological grade. Combined use of diffusion and perfusion MR histogram parameters had the best diagnostic performance to identify oligodendroglial tumors.

We did not observe any differences in vascular densities and cellularity between oligodendrogliomas and astrocytomas WHO grade II, possibly due to the absence of apparent neoangiogenesis and high mitotic activity in low-grade gliomas.

Perfusion and diffusion MR histogram parameters alone were not useful to differentiate between glioma grade II and III. However, a multivariate regression model including parameters from both sequences was able to differentiate histopathologic grades in the astrocytoma subgroup.

Significant longer PFS was associated with more homogeneous rCBV distribution in patients with astrocytomas. In contrast, we identified longer PFS in oligodendrogliomas patients with heterogeneous microvascular anatomy and higher vascularity. Our results suggest that in oligodendrogliomas high CBV values are observed secondary to microvessel density and not necessarily angiogenesis.

Conclusions in study III

The highest RSI-cellularity index was measured in CET with a negative gradient from tumor core to the periphery of peritumoral zone (PEZ and NZ), which reflects an extensively infiltrating pattern in glioblastomas.

Shorter survival outcomes were significantly associated with higher RSI-cellularity index in the CET. This correlation was also persistent in the PEZ and NZ. These findings highlight the importance of the peritumoral areas (PEZ and NZ) to predict further tumor expansion.

In contrast to RSI-cellularity index, MD and FA in the near zone did not show predictive value to survival outcome. Our results suggest that RSI may overcome some limitations of the standard diffusion MRI metrics and may provide a more reliable measure of the increased cellularity associated with tumor progression.

Our results however, suggest that RSI, DWI and DTI cannot aid in the identification of MGMT promoter methylation status in patients with glioblastoma *IDH*-wild type.

7. FUTURE PERSPECTIVES

7.1 The pros and cons of radiologic multicenter studies

The studies presented in this thesis included patient data from a single institution (Oslo University Hospital, Rikshospitalet). This approach was chosen in an effort to obtain a controlled study in which all patients were examined with the same tumor protocol and with limited variation in the use of MRI scanners. This also reflects our attempt to avoid heterogeneity in clinical practice among institutions, which may be a major confounding factor in interpreting results.

However, in order to validate the stability of the proposed methods, reproducibility of measures and diagnostic efficacy, our results will need to be assessed via large, multi-institutional studies. Multicenter collaboration may also result in higher rates of patient enrolment than that of a single-center, thereby generating larger studies over a shorter time [257].

In the future, a cross-site study should include data from several medical centers in order to evaluate the reproducibility of our results across multiple vendor platforms.

7.2 Histopathologic validation of MRI findings.

Correlation of diffusion MRI metrics with survival outcome reflects indirectly histopathologic features of tumor aggressiveness such as tumoral cellular density, microvascular expression, hypoxia and cellular mitosis. In our RSI study, we have used OS and PFS as indicators to more infiltrative cell-rich regions with aggressive behavior. However, the lack of a histopathologic and molecular ground truth from the peritumoral infiltrating areas is an important limitation in our study. Rigorous histopathological validation of species obtained from the same tumoral zones as segmented on MRI is needed to assess the potential value of MRI techniques. In future work, we plan to perform targeted biopsies in several peritumoral regions and relate the imaging-based predictor-metrics to histopathology-proven density of neoplastic cells.

7.3 Future directions and applications of advanced MR imaging in neuro-oncology

The currently available advanced brain tumor MR imaging techniques, such as diffusion-weighted MR imaging and perfusion MR imaging, have been used for solving diagnostic challenges associated with conventional imaging. Further development of advanced MR imaging techniques and postprocessing methods as discussed below may contribute to more detailed histopathologic and molecular characterization of glioma, guiding surgical procedures and predicting the treatment response to a specific therapeutic regimen [258].

7.3.1 Emerging MRI techniques

Recent advances in MR technology including simultaneous multislice echoplanar imaging and the use of multiple receivers have accelerated acquisition times permitting diffusion spectrum imaging (DSI) to be used clinically. Many of these developments became possible due to the work being done on the Human Connectome Project, which is a collaborative 5-year effort to map human brain connections and their variability in healthy adults [259].

One of the latest achievements is Diffusional Kurtosis Imaging (DKI), a method that may assess non-Gaussian diffusion through high diffusion weighted imaging. DKI increase the sensitivity to tissue features and provides information associated with complex intratumoral cytoarchitectonic environment [260]. DKI has fewer systematic error than those from DWI/DTI and is qualitatively comparable to DSI. Kurtosis parameters demonstrate abilities to characterize microstructural differences between low-grade and high-grade gliomas [261]. In addition, kurtosis imaging allows assessment of isotropic structures, including the cortex and basal ganglia, which are important limitations of DTI [262]. Because diffusional kurtosis imaging has a shorter typical scan time than diffusion spectrum imaging, diffusional kurtosis imaging is potentially more suitable for a variety of clinical and research applications [263].

Intravoxel incoherent motion (IVIM) is entering the clinical field for evaluating tissue perfusion allowing separation of microcirculation from true water molecular diffusion. Simultaneous acquisition of diffusion and perfusion parameters by IVIM reflects tumor cellularity and vascularity, respectively, and does not require any co-registration process between diffusion and perfusion based images. IVIM is also independent of the arterial input function and does not require intravenous contrast agent injection for the data acquisition [264, 265]. Moreover, the combination of IVIM and ASL enables the estimation of water permeability across the BBB, suggesting a potential imaging biomarker for disrupted-BBB diseases, as brain tumor [266].

High Angular Resolution Diffusion Imaging (HARDI) produces more robust and accurate fiber orientation than standard DTI. HARDI q-ball fiber tractography successfully identified language tracts of glioma patients preoperatively and predicted postoperative functional recovery in its first clinical prospective study [267]. However, newer methods have not yet translated into the clinical arena due to complex post-processing algorithms and long acquisition times. We have yet to see which diffusion-weighted method, HARDI, DSI, or DKI, will achieve clinical predominance in the future.

Chemical Exchange Saturation Transfer (CEST) is a new contrast enhancement technique that enables the indirect detection of molecules with exchangeable protons and exchange-related properties [268] . CEST makes MRI sensitive to the concentrations of endogenous metabolites and their environments.

Amide proton transfer (APT) imaging is a variant of CEST imaging in which the magnetization of the "proton of interest" is detected indirectly through the chemical exchange with bulk-water protons [269, 270]. ATP is a noninvasive MR imaging technique, which is potentially useful to reflect tumor-cell proliferation and provides information regarding the pH of tissue by sensitive to endogenous mobile proteins and peptides [271]. Quantitative APT parameters have the potential to be sensitive indicators of treatment responses [272] and to function as a prognostic biomarker of brain gliomas by reflecting cellular proliferation levels that correlate with Ki-67[273]. Thus, APT imaging has the potential to provide completely different biologic information on molecular changes and the tumor proliferation index, compared with that shown by both DWI and perfusion MR imaging. Registration of changes in endogenous molecules caused by molecular events can provide valuable information relating to treatment response. For this reason, APT imaging could be a complementary imaging biomarker for glioma studies despite its inherent technical limitations, as low spatial resolution, long imaging time, and high operator dependency [258].

7.3.2 Artificial intelligence

Artificial intelligence (AI) algorithms, especially deep learning, have shown remarkable progress in image-recognition tasks. Methods ranging from convolutional neural networks to variation auto encoders have been applied for multiple medical radiological tasks, aiding in the detection, characterization and monitoring of diseases. AI methods generate automatically recognizable patterns in imaging data and providing quantitative, rather than qualitative assessments of radiographic characteristics and their interpretations [274].

There are two main approaches to AI for medical images in clinical use today. The first, machine learning, uses handcrafted engineered features, that are defined in terms of mathematical equations and can thus be quantified using computer programs [275]. The texture analysis, frequently used in brain tumor studies, is one of the examples of machine learning algorithms based on predefined engineered features.

The second method, deep learning, can automatically learn feature representations from data without prior definition by human experts. This data-driven approach allows for more abstract feature definitions, making it more informative and generalizable. Deep learning is also often robust against inter-reader variability due to its ability to learn complex data representations, and may be applied to a large variety of clinical conditions and parameters. [276].

In study II and III we used leave-one-out cross-validation, machine-learning techniques for statistical analysis. The goal of cross-validation is to test the ability of the model to predict new data that was not used in estimating it. This avoids issues such as overfitting and selection bias [277].

In a future perspective study, we will attempt to implement AI methods in our research algorithms. This will be especially useful for time-consuming tasks such as segmentation, volumetric estimation, statistical analysis and probably also could be used in characterization of tissue in order to increase efficiency and reduce errors.

REFERENCES

[1] Q.T. Ostrom, H. Gittleman, G. Truitt, A. Boscia, C. Kruchko, J.S. Barnholtz-Sloan, CBTRUS Statistical Report: Primary Brain and Other Central Nervous System Tumors Diagnosed in the United States in 2011-2015, Neuro-oncology, 20 (2018) iv1-iv86.
[2] E.H. Anette Storstein, Tom Børge Johannesen, Till Schellhorn, Sverre Mørk, René van Helvoirt Høygradige gliomer hos voksne, Tidskriftet for det norske legeforening, (2009).
[3] Q.T. Ostrom, H. Gittleman, L. Stetson, S. Virk, J.S. Barnholtz-Sloan, Epidemiology of Intracranial Gliomas, Progress in neurological surgery, 30 (2018) 1-11.
[4] C.R. Garcia, S.A. Slone, T. Pittman, W.H. St Clair, D.D. Lightner, J.L. Villano, Comprehensive evaluation of treatment and outcomes of low-grade diffuse gliomas, PloS one, 13 (2018) e0203639.
[5] P.A. Ronning, E. Helseth, T.R. Meling, T.B. Johannesen, A population-based study on the effect of temozolomide in the treatment of glioblastoma multiforme, Neuro-oncology, 14 (2012) 1178-1184.
[6] B.J. Theeler, M.R. Gilbert, Advances in the treatment of newly diagnosed glioblastoma, BMC medicine, 13 (2015) 293.
[7] D.N. Louis, H. Ohgaki, O.D. Wiestler, W.K. Cavenee, P.C. Burger, A. Jouvet, B.W. Scheithauer, P. Kleihues, The 2007 WHO classification of tumours of the central nervous system, Acta neuropathologica, 114 (2007) 97-109.
[8] A. Claes, A.J. Idema, P. Wesseling, Diffuse glioma growth: a guerilla war, Acta neuropathologica, 114 (2007) 443-458.
[9] M. Lacroix, D. Abi-Said, D.R. Fourney, Z.L. Gokaslan, W. Shi, F. DeMonte, F.F. Lang, I.E. McCutcheon, S.J. Hassenbusch, E. Holland, K. Hess, C. Michael, D. Miller, R. Sawaya, A multivariate analysis of 416 patients with glioblastoma multiforme: prognosis, extent of resection, and survival, Journal of neurosurgery, 95 (2001) 190-198.
[10] S.M. Raza, F.F. Lang, B.B. Aggarwal, G.N. Fuller, D.M. Wildrick, R. Sawaya, Necrosis and glioblastoma: a friend or a foe? A review and a hypothesis, Neurosurgery, 51 (2002) 2-12; discussion 12-13.
[11] S. Liu, Y. Wang, K. Xu, Z. Wang, X. Fan, C. Zhang, S. Li, X. Qiu, T. Jiang, Relationship between necrotic patterns in glioblastoma and patient survival: fractal dimension and lacunarity analyses using magnetic resonance imaging, Scientific reports, 7 (2017) 8302.
[12] Y. Rong, D.L. Durden, E.G. Van Meir, D.J. Brat, 'Pseudopalisading' necrosis in glioblastoma: a familiar morphologic feature that links vascular pathology, hypoxia, and angiogenesis, Journal of neuropathology and experimental neurology, 65 (2006) 529-539.
[13] S. Neves, P.R. Mazal, J. Wanschitz, A.C. Rudnay, M. Drlicek, T. Czech, C. Wustinger, H. Budka, Pseudogliomatous growth pattern of anaplastic small cell carcinomas metastatic to the brain, Clinical neuropathology, 20 (2001) 38-42.
[14] S. HJ, Structural development in gliomas, American journal of cancer research, (1938).
[15] A. Subramanian, A. Harris, K. Piggott, C. Shieff, R. Bradford, Metastasis to and from the central nervous system--the 'relatively protected site', The Lancet. Oncology, 3 (2002) 498-507.
[16] M. Alieva, V. Leidgens, M.J. Riemenschneider, C.A. Klein, P. Hau, J. van Rheenen, Intravital imaging of glioma border morphology reveals distinctive cellular dynamics and contribution to tumor cell invasion, Scientific reports, 9 (2019) 2054.
[17] D. Widera, I. Mikenberg, B. Kaltschmidt, C. Kaltschmidt, Potential role of NF-kappaB in adult neural stem cells: the underrated steersman?, International journal of developmental neuroscience : the official journal of the International Society for Developmental Neuroscience, 24 (2006) 91-102.
[18] A. Fayzullin, C.J. Sandberg, M. Spreadbury, B.M. Saberniak, Z. Grieg, E. Skaga, I.A. Langmoen, E.O. Vik-Mo, Phenotypic and Expressional Heterogeneity in the Invasive Glioma Cells, Translational oncology, 12 (2019) 122-133.
[19] S.H. Patel, L.M. Poisson, D.J. Brat, Y. Zhou, L. Cooper, M. Snuderl, C. Thomas, A.M. Franceschi, B. Griffith, A.E. Flanders, J.G. Golfinos, A.S. Chi, R. Jain, T2-FLAIR Mismatch, an Imaging Biomarker for IDH and 1p/19q

Status in Lower-grade Gliomas: A TCGA/TCIA Project, Clinical cancer research : an official journal of the American Association for Cancer Research, 23 (2017) 6078-6085.
[20] A. Sottoriva, I. Spiteri, S.G. Piccirillo, A. Touloumis, V.P. Collins, J.C. Marioni, C. Curtis, C. Watts, S. Tavare, Intratumor heterogeneity in human glioblastoma reflects cancer evolutionary dynamics, Proceedings of the National Academy of Sciences of the United States of America, 110 (2013) 4009-4014.
[21] A. Vartanian, S.K. Singh, S. Agnihotri, S. Jalali, K. Burrell, K.D. Aldape, G. Zadeh, GBM's multifaceted landscape: highlighting regional and microenvironmental heterogeneity, Neuro-oncology, 16 (2014) 1167-1175.
[22] A.P. Patel, I. Tirosh, J.J. Trombetta, A.K. Shalek, S.M. Gillespie, H. Wakimoto, D.P. Cahill, B.V. Nahed, W.T. Curry, R.L. Martuza, D.N. Louis, O. Rozenblatt-Rosen, M.L. Suva, A. Regev, B.E. Bernstein, Single-cell RNA-seq highlights intratumoral heterogeneity in primary glioblastoma, Science (New York, N.Y.), 344 (2014) 1396-1401.
[23] C. Neftel, J. Laffy, M.G. Filbin, T. Hara, M.E. Shore, G.J. Rahme, A.R. Richman, D. Silverbush, M.L. Shaw, C.M. Hebert, J. Dewitt, S. Gritsch, E.M. Perez, L.N. Gonzalez Castro, X. Lan, N. Druck, C. Rodman, D. Dionne, A. Kaplan, M.S. Bertalan, J. Small, K. Pelton, S. Becker, D. Bonal, Q.D. Nguyen, R.L. Servis, J.M. Fung, R. Mylvaganam, L. Mayr, J. Gojo, C. Haberler, R. Geyeregger, T. Czech, I. Slavc, B.V. Nahed, W.T. Curry, B.S. Carter, H. Wakimoto, P.K. Brastianos, T.T. Batchelor, A. Stemmer-Rachamimov, M. Martinez-Lage, M.P. Frosch, I. Stamenkovic, N. Riggi, E. Rheinbay, M. Monje, O. Rozenblatt-Rosen, D.P. Cahill, A.P. Patel, T. Hunter, I.M. Verma, K.L. Ligon, D.N. Louis, A. Regev, B.E. Bernstein, I. Tirosh, M.L. Suva, An Integrative Model of Cellular States, Plasticity, and Genetics for Glioblastoma, Cell, 178 (2019) 835-849.e821.
[24] H. Kim, S. Zheng, S.S. Amini, S.M. Virk, T. Mikkelsen, D.J. Brat, J. Grimsby, C. Sougnez, F. Muller, J. Hu, A.E. Sloan, M.L. Cohen, E.G. Van Meir, L. Scarpace, P.W. Laird, J.N. Weinstein, E.S. Lander, S. Gabriel, G. Getz, M. Meyerson, L. Chin, J.S. Barnholtz-Sloan, R.G. Verhaak, Whole-genome and multisector exome sequencing of primary and post-treatment glioblastoma reveals patterns of tumor evolution, Genome research, 25 (2015) 316-327.
[25] J. Wang, E. Cazzato, E. Ladewig, V. Frattini, D.I. Rosenbloom, S. Zairis, F. Abate, Z. Liu, O. Elliott, Y.J. Shin, J.K. Lee, I.H. Lee, W.Y. Park, M. Eoli, A.J. Blumberg, A. Lasorella, D.H. Nam, G. Finocchiaro, A. Iavarone, R. Rabadan, Clonal evolution of glioblastoma under therapy, Nature genetics, 48 (2016) 768-776.
[26] S. Osuka, E.G. Van Meir, Overcoming therapeutic resistance in glioblastoma: the way forward, The Journal of clinical investigation, 127 (2017) 415-426.
[27] M.L. Suva, Genetics and epigenetics of gliomas, Swiss medical weekly, 144 (2014) w14018.
[28] D.T. Di Carlo, H. Duffau, F. Cagnazzo, N. Benedetto, R. Morganti, P. Perrini, IDH wild-type WHO grade II diffuse low-grade gliomas. A heterogeneous family with different outcomes. Systematic review and meta-analysis, Neurosurgical review, (2018).
[29] A. Aibaidula, A.K. Chan, Z. Shi, Y. Li, R. Zhang, R. Yang, K.K. Li, N.Y. Chung, Y. Yao, L. Zhou, J. Wu, H. Chen, H.K. Ng, Adult IDH wild-type lower-grade gliomas should be further stratified, Neuro-oncology, 19 (2017) 1327-1337.
[30] G. Cairncross, M. Wang, E. Shaw, R. Jenkins, D. Brachman, J. Buckner, K. Fink, L. Souhami, N. Laperriere, W. Curran, M. Mehta, Phase III trial of chemoradiotherapy for anaplastic oligodendroglioma: long-term results of RTOG 9402, Journal of clinical oncology : official journal of the American Society of Clinical Oncology, 31 (2013) 337-343.
[31] M.J. van den Bent, A.A. Brandes, M.J. Taphoorn, J.M. Kros, M.C. Kouwenhoven, J.Y. Delattre, H.J. Bernsen, M. Frenay, C.C. Tijssen, W. Grisold, L. Sipos, R.H. Enting, P.J. French, W.N. Dinjens, C.J. Vecht, A. Allgeier, D. Lacombe, T. Gorlia, K. Hoang-Xuan, Adjuvant procarbazine, lomustine, and vincristine chemotherapy in newly diagnosed anaplastic oligodendroglioma: long-term follow-up of EORTC brain tumor group study 26951, Journal of clinical oncology : official journal of the American Society of Clinical Oncology, 31 (2013) 344-350.

[32] M.D. Jenkinson, C. Walker, A.R. Brodbelt, S. Wilkins, D. Husband, B. Haylock, Molecular genetics, imaging and treatment of oligodendroglial tumours, Acta neurochirurgica, 152 (2010) 1815-1825.
[33] P. Wesseling, M. van den Bent, A. Perry, Oligodendroglioma: pathology, molecular mechanisms and markers, Acta neuropathologica, 129 (2015) 809-827.
[34] M. Mizoguchi, K. Yoshimoto, X. Ma, Y. Guan, N. Hata, T. Amano, A. Nakamizo, S.O. Suzuki, T. Iwaki, T. Sasaki, Molecular characteristics of glioblastoma with 1p/19q co-deletion, Brain tumor pathology, 29 (2012) 148-153.
[35] P. Nandakumar, A. Mansouri, S. Das, The Role of ATRX in Glioma Biology, Frontiers in oncology, 7 (2017) 236.
[36] Y. Jiao, P.J. Killela, Z.J. Reitman, A.B. Rasheed, C.M. Heaphy, R.F. de Wilde, F.J. Rodriguez, S. Rosemberg, S.M. Oba-Shinjo, S.K. Nagahashi Marie, C. Bettegowda, N. Agrawal, E. Lipp, C. Pirozzi, G. Lopez, Y. He, H. Friedman, A.H. Friedman, G.J. Riggins, M. Holdhoff, P. Burger, R. McLendon, D.D. Bigner, B. Vogelstein, A.K. Meeker, K.W. Kinzler, N. Papadopoulos, L.A. Diaz, H. Yan, Frequent ATRX, CIC, FUBP1 and IDH1 mutations refine the classification of malignant gliomas, Oncotarget, 3 (2012) 709-722.
[37] W. Hanel, U.M. Moll, Links between mutant p53 and genomic instability, Journal of cellular biochemistry, 113 (2012) 433-439.
[38] D.N. Louis, A. Perry, G. Reifenberger, A. von Deimling, D. Figarella-Branger, W.K. Cavenee, H. Ohgaki, O.D. Wiestler, P. Kleihues, D.W. Ellison, The 2016 World Health Organization Classification of Tumors of the Central Nervous System: a summary, Acta neuropathologica, 131 (2016) 803-820.
[39] M.E. Hegi, A.C. Diserens, T. Gorlia, M.F. Hamou, N. de Tribolet, M. Weller, J.M. Kros, J.A. Hainfellner, W. Mason, L. Mariani, J.E. Bromberg, P. Hau, R.O. Mirimanoff, J.G. Cairncross, R.C. Janzer, R. Stupp, MGMT gene silencing and benefit from temozolomide in glioblastoma, The New England journal of medicine, 352 (2005) 997-1003.
[40] R. Stupp, M.E. Hegi, W.P. Mason, M.J. van den Bent, M.J. Taphoorn, R.C. Janzer, S.K. Ludwin, A. Allgeier, B. Fisher, K. Belanger, P. Hau, A.A. Brandes, J. Gijtenbeek, C. Marosi, C.J. Vecht, K. Mokhtari, P. Wesseling, S. Villa, E. Eisenhauer, T. Gorlia, M. Weller, D. Lacombe, J.G. Cairncross, R.O. Mirimanoff, Effects of radiotherapy with concomitant and adjuvant temozolomide versus radiotherapy alone on survival in glioblastoma in a randomised phase III study: 5-year analysis of the EORTC-NCIC trial, The Lancet. Oncology, 10 (2009) 459-466.
[41] D.R. Johnson, J.B. Guerin, C. Giannini, J.M. Morris, L.J. Eckel, T.J. Kaufmann, 2016 Updates to the WHO Brain Tumor Classification System: What the Radiologist Needs to Know, Radiographics : a review publication of the Radiological Society of North America, Inc, 37 (2017) 2164-2180.
[42] D.N. Louis, D.W. Ellison, D.J. Brat, K. Aldape, D. Capper, C. Hawkins, W. Paulus, A. Perry, G. Reifenberger, D. Figarella-Branger, A. von Deimling, P. Wesseling, cIMPACT-NOW: a practical summary of diagnostic points from Round 1 updates, Brain pathology (Zurich, Switzerland), 29 (2019) 469-472.
[43] M. Hasselblatt, M. Jaber, D. Reuss, O. Grauer, A. Bibo, S. Terwey, U. Schick, H. Ebel, T. Niederstadt, W. Stummer, A. von Deimling, W. Paulus, Diffuse Astrocytoma, IDH-Wildtype: A Dissolving Diagnosis, Journal of neuropathology and experimental neurology, 77 (2018) 422-425.
[44] M. Shirahata, T. Ono, D. Stichel, D. Schrimpf, D.E. Reuss, F. Sahm, C. Koelsche, A. Wefers, A. Reinhardt, K. Huang, P. Sievers, H. Shimizu, H. Nanjo, Y. Kobayashi, Y. Miyake, T. Suzuki, J.I. Adachi, K. Mishima, A. Sasaki, R. Nishikawa, M. Bewerunge-Hudler, M. Ryzhova, O. Absalyamova, A. Golanov, P. Sinn, M. Platten, C. Jungk, F. Winkler, A. Wick, D. Hanggi, A. Unterberg, S.M. Pfister, D.T.W. Jones, M. van den Bent, M. Hegi, P. French, B.G. Baumert, R. Stupp, T. Gorlia, M. Weller, D. Capper, A. Korshunov, C. Herold-Mende, W. Wick, D.N. Louis, A. von Deimling, Novel, improved grading system(s) for IDH-mutant astrocytic gliomas, Acta neuropathologica, 136 (2018) 153-166.
[45] G. Reifenberger, H.G. Wirsching, C.B. Knobbe-Thomsen, M. Weller, Advances in the molecular genetics of gliomas - implications for classification and therapy, Nature reviews. Clinical oncology, 14 (2017) 434-452.

[46] M. Castillo, History and evolution of brain tumor imaging: insights through radiology, Radiology, 273 (2014) S111-125.
[47] A. Schüller, Röntgen-diagnostik der Erkrankungen des Kopfes., Vienna:Holder, (1912).
[48] W.E. Dandy, VENTRICULOGRAPHY FOLLOWING THE INJECTION OF AIR INTO THE CEREBRAL VENTRICLES, Annals of surgery, 68 (1918) 5-11.
[49] W.E. Dandy, RONTGENOGRAPHY OF THE BRAIN AFTER THE INJECTION OF AIR INTO THE SPINAL CANAL, Annals of surgery, 70 (1919) 397-403.
[50] E. Moniz, Arterial Encephalography: Its importance in localization of cerebral tumors, Rev Neurol (Paris) 1927; 2:72-90, (1927).
[51] A.E. Rosenbaum, O.P. Eldevik, J.R. Mani, A.J. Pollock, R.L. Mani, T.O. Gabrielsen, In re: Amundsen P. Cerebral angiography via the femoral artery with particular reference to cerebrovascular disease. Acta Neurol Scand 1967; Suppl. 31:115, AJNR. American journal of neuroradiology, 22 (2001) 584-589.
[52] E.G. Hoeffner, S.K. Mukherji, A. Srinivasan, D.J. Quint, Neuroradiology back to the future: head and neck imaging, AJNR. American journal of neuroradiology, 33 (2012) 2026-2032.
[53] P.C. Lauterbur, Image formation by induced local interactions. Examples employing nuclear magnetic resonance. 1973, Clinical orthopaedics and related research, (1989) 3-6.
[54] P. Mansfield, Multi-planar image formation using NMR spin echoes, Journal of Physics C: Solid State Physics, Volume 10, Number 3, (14 February 1977).
[55] W. Kucharczyk, M. Brant-Zawadzki, D. Sobel, M.B. Edwards, W.M. Kelly, D. Norman, T.H. Newton, Central nervous system tumors in children: detection by magnetic resonance imaging, Radiology, 155 (1985) 131-136.
[56] R. Felix, W. Schorner, M. Laniado, H.P. Niendorf, C. Claussen, W. Fiegler, U. Speck, Brain tumors: MR imaging with gadolinium-DTPA, Radiology, 156 (1985) 681-688.
[57] E.J. Russell, G.K. Geremia, C.E. Johnson, M.S. Huckman, R.G. Ramsey, J. Washburn-Bleck, D.A. Turner, M. Norusis, Multiple cerebral metastases: detectability with Gd-DTPA-enhanced MR imaging, Radiology, 165 (1987) 609-617.
[58] P. Douek, R. Turner, J. Pekar, N. Patronas, D. Le Bihan, MR color mapping of myelin fiber orientation, Journal of computer assisted tomography, 15 (1991) 923-929.
[59] L. Axel, Cerebral blood flow determination by rapid-sequence computed tomography: theoretical analysis, Radiology, 137 (1980) 679-686.
[60] R.R. Edelman, H.P. Mattle, D.J. Atkinson, T. Hill, J.P. Finn, C. Mayman, M. Ronthal, H.M. Hoogewoud, J. Kleefield, Cerebral blood flow: assessment with dynamic contrast-enhanced T2*-weighted MR imaging at 1.5 T, Radiology, 176 (1990) 211-220.
[61] D. Bertholdo, A. Watcharakorn, M. Castillo, Brain proton magnetic resonance spectroscopy: introduction and overview, Neuroimaging clinics of North America, 23 (2013) 359-380.
[62] G.H. Glover, Overview of functional magnetic resonance imaging, Neurosurgery clinics of North America, 22 (2011) 133-139, vii.
[63] S. Ogawa, T.M. Lee, A.R. Kay, D.W. Tank, Brain magnetic resonance imaging with contrast dependent on blood oxygenation, Proceedings of the National Academy of Sciences of the United States of America, 87 (1990) 9868-9872.
[64] S. Ogawa, T.M. Lee, A.S. Nayak, P. Glynn, Oxygenation-sensitive contrast in magnetic resonance image of rodent brain at high magnetic fields, Magnetic resonance in medicine, 14 (1990) 68-78.
[65] S. Ogawa, R.S. Menon, D.W. Tank, S.G. Kim, H. Merkle, J.M. Ellermann, K. Ugurbil, Functional brain mapping by blood oxygenation level-dependent contrast magnetic resonance imaging. A comparison of signal characteristics with a biophysical model, Biophysical journal, 64 (1993) 803-812.
[66] J.S. Duncan, G.P. Winston, M.J. Koepp, S. Ourselin, Brain imaging in the assessment for epilepsy surgery, The Lancet. Neurology, 15 (2016) 420-433.
[67] C.T. Westbrook, J., MRI in Practice, 5th Edition, 5th Edition, ISBN: 978-1-119-39200-2|, (2018).

[68] R.A. Pooley, AAPM/RSNA physics tutorial for residents: fundamental physics of MR imaging, Radiographics : a review publication of the Radiological Society of North America, Inc, 25 (2005) 1087-1099.
[69] J.N. Scott, P.M. Brasher, R.J. Sevick, N.B. Rewcastle, P.A. Forsyth, How often are nonenhancing supratentorial gliomas malignant? A population study, Neurology, 59 (2002) 947-949.
[70] C.C. Hsu, T.W. Watkins, G.N. Kwan, E.M. Haacke, Susceptibility-Weighted Imaging of Glioma: Update on Current Imaging Status and Future Directions, Journal of neuroimaging : official journal of the American Society of Neuroimaging, 26 (2016) 383-390.
[71] A. Server, R. Josefsen, B. Kulle, J. Maehlen, T. Schellhorn, O. Gadmar, T. Kumar, M. Haakonsen, C.W. Langberg, P.H. Nakstad, Proton magnetic resonance spectroscopy in the distinction of high-grade cerebral gliomas from single metastatic brain tumors, Acta radiologica (Stockholm, Sweden : 1987), 51 (2010) 316-325.
[72] F. Durmo, A. Rydelius, S. Cuellar Baena, K. Askaner, J. Latt, J. Bengzon, E. Englund, T.L. Chenevert, I.M. Bjorkman-Burtscher, P.C. Sundgren, Multivoxel (1)H-MR Spectroscopy Biometrics for Preoprerative Differentiation Between Brain Tumors, Tomography (Ann Arbor, Mich.), 4 (2018) 172-181.
[73] A. Server, B.A. Graff, T.E. Orheim, T. Schellhorn, R. Josefsen, O.B. Gadmar, P.H. Nakstad, Measurements of diagnostic examination performance and correlation analysis using microvascular leakage, cerebral blood volume, and blood flow derived from 3T dynamic susceptibility-weighted contrast-enhanced perfusion MR imaging in glial tumor grading, Neuroradiology, 53 (2011) 435-447.
[74] J.H. Kim, K.H. Chang, D.G. Na, I.C. Song, B.J. Kwon, M.H. Han, K. Kim, 3T 1H-MR spectroscopy in grading of cerebral gliomas: comparison of short and intermediate echo time sequences, AJNR. American journal of neuroradiology, 27 (2006) 1412-1418.
[75] P.Y. Wen, D.R. Macdonald, D.A. Reardon, T.F. Cloughesy, A.G. Sorensen, E. Galanis, J. Degroot, W. Wick, M.R. Gilbert, A.B. Lassman, C. Tsien, T. Mikkelsen, E.T. Wong, M.C. Chamberlain, R. Stupp, K.R. Lamborn, M.A. Vogelbaum, M.J. van den Bent, S.M. Chang, Updated response assessment criteria for high-grade gliomas: response assessment in neuro-oncology working group, Journal of clinical oncology : official journal of the American Society of Clinical Oncology, 28 (2010) 1963-1972.
[76] B.M. Ellingson, M. Bendszus, J. Boxerman, D. Barboriak, B.J. Erickson, M. Smits, S.J. Nelson, E. Gerstner, B. Alexander, G. Goldmacher, W. Wick, M. Vogelbaum, M. Weller, E. Galanis, J. Kalpathy-Cramer, L. Shankar, P. Jacobs, W.B. Pope, D. Yang, C. Chung, M.V. Knopp, S. Cha, M.J. van den Bent, S. Chang, W.K. Yung, T.F. Cloughesy, P.Y. Wen, M.R. Gilbert, Consensus recommendations for a standardized Brain Tumor Imaging Protocol in clinical trials, Neuro-oncology, 17 (2015) 1188-1198.
[77] D. Le Bihan, E. Breton, D. Lallemand, P. Grenier, E. Cabanis, M. Laval-Jeantet, MR imaging of intravoxel incoherent motions: application to diffusion and perfusion in neurologic disorders, Radiology, 161 (1986) 401-407.
[78] S.E. Maier, Y. Sun, R.V. Mulkern, Diffusion imaging of brain tumors, NMR in biomedicine, 23 (2010) 849-864.
[79] P. Hagmann, L. Jonasson, P. Maeder, J.P. Thiran, V.J. Wedeen, R. Meuli, Understanding diffusion MR imaging techniques: from scalar diffusion-weighted imaging to diffusion tensor imaging and beyond, Radiographics : a review publication of the Radiological Society of North America, Inc, 26 Suppl 1 (2006) S205-223.
[80] R. Turner, D. Le Bihan, J. Maier, R. Vavrek, L.K. Hedges, J. Pekar, Echo-planar imaging of intravoxel incoherent motion, Radiology, 177 (1990) 407-414.
[81] T.G. Reese, O. Heid, R.M. Weisskoff, V.J. Wedeen, Reduction of eddy-current-induced distortion in diffusion MRI using a twice-refocused spin echo, Magnetic resonance in medicine, 49 (2003) 177-182.
[82] T. Feiweier, Bipolar Diffusion Encoding with Implicit Spoiling of Undesired Coherence Pathways, Place Published, 2011.
[83] P. Mukherjee, J.I. Berman, S.W. Chung, C.P. Hess, R.G. Henry, Diffusion tensor MR imaging and fiber tractography: theoretic underpinnings, AJNR. American journal of neuroradiology, 29 (2008) 632-641.

[84] A.R. Padhani, G. Liu, D.M. Koh, T.L. Chenevert, H.C. Thoeny, T. Takahara, A. Dzik-Jurasz, B.D. Ross, M. Van Cauteren, D. Collins, D.A. Hammoud, G.J. Rustin, B. Taouli, P.L. Choyke, Diffusion-weighted magnetic resonance imaging as a cancer biomarker: consensus and recommendations, Neoplasia (New York, N.Y.), 11 (2009) 102-125.
[85] K. Kono, Y. Inoue, K. Nakayama, M. Shakudo, M. Morino, K. Ohata, K. Wakasa, R. Yamada, The role of diffusion-weighted imaging in patients with brain tumors, AJNR. American journal of neuroradiology, 22 (2001) 1081-1088.
[86] A.C. Guo, T.J. Cummings, R.C. Dash, J.M. Provenzale, Lymphomas and high-grade astrocytomas: comparison of water diffusibility and histologic characteristics, Radiology, 224 (2002) 177-183.
[87] A. Server, B. Kulle, J. Maehlen, R. Josefsen, T. Schellhorn, T. Kumar, C.W. Langberg, P.H. Nakstad, Quantitative apparent diffusion coefficients in the characterization of brain tumors and associated peritumoral edema, Acta radiologica (Stockholm, Sweden : 1987), 50 (2009) 682-689.
[88] L. Zhang, Z. Min, M. Tang, S. Chen, X. Lei, X. Zhang, The utility of diffusion MRI with quantitative ADC measurements for differentiating high-grade from low-grade cerebral gliomas: Evidence from a meta-analysis, Journal of the neurological sciences, 373 (2017) 9-15.
[89] H. Han, C. Han, X. Wu, S. Zhong, X. Zhuang, G. Tan, H. Wu, Preoperative grading of supratentorial nonenhancing gliomas by high b-value diffusion-weighted 3 T magnetic resonance imaging, Journal of neuro-oncology, 133 (2017) 147-154.
[90] Y. Kang, S.H. Choi, Y.J. Kim, K.G. Kim, C.H. Sohn, J.H. Kim, T.J. Yun, K.H. Chang, Gliomas: Histogram analysis of apparent diffusion coefficient maps with standard- or high-b-value diffusion-weighted MR imaging--correlation with tumor grade, Radiology, 261 (2011) 882-890.
[91] M.D. Jenkinson, T.S. Smith, A.R. Brodbelt, K.A. Joyce, P.C. Warnke, C. Walker, Apparent diffusion coefficients in oligodendroglial tumors characterized by genotype, Journal of magnetic resonance imaging : JMRI, 26 (2007) 1405-1412.
[92] W.B. Pope, X.J. Qiao, H.J. Kim, A. Lai, P. Nghiemphu, X. Xue, B.M. Ellingson, D. Schiff, D. Aregawi, S. Cha, V.K. Puduvalli, J. Wu, W.K. Yung, G.S. Young, J. Vredenburgh, D. Barboriak, L.E. Abrey, T. Mikkelsen, R. Jain, N.A. Paleologos, P.L. Rn, M. Prados, J. Goldin, P.Y. Wen, T. Cloughesy, Apparent diffusion coefficient histogram analysis stratifies progression-free and overall survival in patients with recurrent GBM treated with bevacizumab: a multi-center study, Journal of neuro-oncology, 108 (2012) 491-498.
[93] K.M. Hasan, H. Ali, M.U. Shad, Atlas-based and DTI-guided quantification of human brain cerebral blood flow: feasibility, quality assurance, spatial heterogeneity and age effects, Magnetic resonance imaging, 31 (2013) 1445-1452.
[94] C. Beaulieu, The basis of anisotropic water diffusion in the nervous system - a technical review, NMR in biomedicine, 15 (2002) 435-455.
[95] S.C. Thust, S. Heiland, A. Falini, H.R. Jager, A.D. Waldman, P.C. Sundgren, C. Godi, V.K. Katsaros, A. Ramos, N. Bargallo, M.W. Vernooij, T. Yousry, M. Bendszus, M. Smits, Glioma imaging in Europe: A survey of 220 centres and recommendations for best clinical practice, European radiology, 28 (2018) 3306-3317.
[96] S. Pujol, W. Wells, C. Pierpaoli, C. Brun, J. Gee, G. Cheng, B. Vemuri, O. Commowick, S. Prima, A. Stamm, M. Goubran, A. Khan, T. Peters, P. Neher, K.H. Maier-Hein, Y. Shi, A. Tristan-Vega, G. Veni, R. Whitaker, M. Styner, C.F. Westin, S. Gouttard, I. Norton, L. Chauvin, H. Mamata, G. Gerig, A. Nabavi, A. Golby, R. Kikinis, The DTI Challenge: Toward Standardized Evaluation of Diffusion Tensor Imaging Tractography for Neurosurgery, Journal of neuroimaging : official journal of the American Society of Neuroimaging, 25 (2015) 875-882.
[97] A. Dubey, R. Kataria, V.D. Sinha, Role of Diffusion Tensor Imaging in Brain Tumor Surgery, Asian journal of neurosurgery, 13 (2018) 302-306.
[98] S.J. Price, R. Jena, N.G. Burnet, P.J. Hutchinson, A.F. Dean, A. Pena, J.D. Pickard, T.A. Carpenter, J.H. Gillard, Improved delineation of glioma margins and regions of infiltration with the use of diffusion tensor imaging: an image-guided biopsy study, AJNR. American journal of neuroradiology, 27 (2006) 1969-1974.

[99] A. Castellano, M. Donativi, R. Ruda, G. De Nunzio, M. Riva, A. Iadanza, L. Bertero, M. Rucco, L. Bello, R. Soffietti, A. Falini, Evaluation of low-grade glioma structural changes after chemotherapy using DTI-based histogram analysis and functional diffusion maps, European radiology, 26 (2016) 1263-1273.
[100] S. Mori, K. Frederiksen, P.C. van Zijl, B. Stieltjes, M.A. Kraut, M. Solaiyappan, M.G. Pomper, Brain white matter anatomy of tumor patients evaluated with diffusion tensor imaging, Annals of neurology, 51 (2002) 377-380.
[101] K. Yamada, O. Kizu, S. Mori, H. Ito, H. Nakamura, S. Yuen, T. Kubota, O. Tanaka, W. Akada, H. Sasajima, K. Mineura, T. Nishimura, Brain fiber tracking with clinically feasible diffusion-tensor MR imaging: initial experience, Radiology, 227 (2003) 295-301.
[102] W.H. Ng, D.L. Cheong, K.J. Khu, G. Venkatesh, Y.K. Ng, C.C. Lim, Diffusion tensor tractography: corticospinal tract fiber reduction is associated with temporary hemiparesis in benign extracerebral lesions, Neurosurgery, 63 (2008) 452-458; discussion 458-459.
[103] K.G. Schilling, V. Nath, C. Hansen, P. Parvathaneni, J. Blaber, Y. Gao, P. Neher, D.B. Aydogan, Y. Shi, M. Ocampo-Pineda, S. Schiavi, A. Daducci, G. Girard, M. Barakovic, J. Rafael-Patino, D. Romascano, G. Rensonnet, M. Pizzolato, A. Bates, E. Fischi, J.P. Thiran, E.J. Canales-Rodriguez, C. Huang, H. Zhu, L. Zhong, R. Cabeen, A.W. Toga, F. Rheault, G. Theaud, J.C. Houde, J. Sidhu, M. Chamberland, C.F. Westin, T.B. Dyrby, R. Verma, Y. Rathi, M.O. Irfanoglu, C. Thomas, C. Pierpaoli, M. Descoteaux, A.W. Anderson, B.A. Landman, Limits to anatomical accuracy of diffusion tractography using modern approaches, NeuroImage, 185 (2019) 1-11.
[104] N.S. White, C. McDonald, N. Farid, J. Kuperman, D. Karow, N.M. Schenker-Ahmed, H. Bartsch, R. Rakow-Penner, D. Holland, A. Shabaik, A. Bjornerud, T. Hope, J. Hattangadi-Gluth, M. Liss, J.K. Parsons, C.C. Chen, S. Raman, D. Margolis, R.E. Reiter, L. Marks, S. Kesari, A.J. Mundt, C.J. Kane, B.S. Carter, W.G. Bradley, A.M. Dale, Diffusion-weighted imaging in cancer: physical foundations and applications of restriction spectrum imaging, Cancer research, 74 (2014) 4638-4652.
[105] N.S. White, T.B. Leergaard, H. D'Arceuil, J.G. Bjaalie, A.M. Dale, Probing tissue microstructure with restriction spectrum imaging: Histological and theoretical validation, Human brain mapping, 34 (2013) 327-346.
[106] N.S. White, C.R. McDonald, N. Farid, J.M. Kuperman, S. Kesari, A.M. Dale, Improved conspicuity and delineation of high-grade primary and metastatic brain tumors using "restriction spectrum imaging": quantitative comparison with high B-value DWI and ADC, AJNR. American journal of neuroradiology, 34 (2013) 958-964, s951.
[107] C.R. McDonald, N.S. White, N. Farid, G. Lai, J.M. Kuperman, H. Bartsch, D.J. Hagler, S. Kesari, B.S. Carter, C.C. Chen, A.M. Dale, Recovery of white matter tracts in regions of peritumoral FLAIR hyperintensity with use of restriction spectrum imaging, AJNR. American journal of neuroradiology, 34 (2013) 1157-1163.
[108] C.R. McDonald, R.L. Delfanti, A.P. Krishnan, K.M. Leyden, J.A. Hattangadi-Gluth, T.M. Seibert, R. Karunamuni, P. Elbe, J.M. Kuperman, H. Bartsch, D.E. Piccioni, N.S. White, A.M. Dale, N. Farid, Restriction spectrum imaging predicts response to bevacizumab in patients with high-grade glioma, Neuro-oncology, 18 (2016) 1579-1590.
[109] N. Farid, D.B. Almeida-Freitas, N.S. White, C.R. McDonald, K.A. Muller, S.R. Vandenberg, S. Kesari, A.M. Dale, Restriction-Spectrum Imaging of Bevacizumab-Related Necrosis in a Patient with GBM, Frontiers in oncology, 3 (2013) 258.
[110] A. Villringer, B.R. Rosen, J.W. Belliveau, J.L. Ackerman, R.B. Lauffer, R.B. Buxton, Y.S. Chao, V.J. Wedeen, T.J. Brady, Dynamic imaging with lanthanide chelates in normal brain: contrast due to magnetic susceptibility effects, Magnetic resonance in medicine, 6 (1988) 164-174.
[111] G. Zaharchuk, Theoretical basis of hemodynamic MR imaging techniques to measure cerebral blood volume, cerebral blood flow, and permeability, AJNR. American journal of neuroradiology, 28 (2007) 1850-1858.

[112] M.S. Shiroishi, G. Castellazzi, J.L. Boxerman, F. D'Amore, M. Essig, T.B. Nguyen, J.M. Provenzale, D.S. Enterline, N. Anzalone, A. Dorfler, A. Rovira, M. Wintermark, M. Law, Principles of T2 *-weighted dynamic susceptibility contrast MRI technique in brain tumor imaging, Journal of magnetic resonance imaging : JMRI, 41 (2015) 296-313.
[113] D. Bedekar, T. Jensen, K.M. Schmainda, Standardization of relative cerebral blood volume (rCBV) image maps for ease of both inter- and intrapatient comparisons, Magnetic resonance in medicine, 64 (2010) 907-913.
[114] R.F. Barajas, Jr., S. Cha, Benefits of dynamic susceptibility-weighted contrast-enhanced perfusion MRI for glioma diagnosis and therapy, CNS oncology, 3 (2014) 407-419.
[115] P. Kickingereder, F. Sahm, B. Wiestler, M. Roethke, S. Heiland, H.P. Schlemmer, W. Wick, A. von Deimling, M. Bendszus, A. Radbruch, Evaluation of microvascular permeability with dynamic contrast-enhanced MRI for the differentiation of primary CNS lymphoma and glioblastoma: radiologic-pathologic correlation, AJNR. American journal of neuroradiology, 35 (2014) 1503-1508.
[116] C.H. Suh, H.S. Kim, S.C. Jung, J.E. Park, C.G. Choi, S.J. Kim, MRI as a diagnostic biomarker for differentiating primary central nervous system lymphoma from glioblastoma: A systematic review and meta-analysis, Journal of magnetic resonance imaging : JMRI, 50 (2019) 560-572.
[117] M. Neska-Matuszewska, J. Bladowska, M. Sasiadek, A. Zimny, Differentiation of glioblastoma multiforme, metastases and primary central nervous system lymphomas using multiparametric perfusion and diffusion MR imaging of a tumor core and a peritumoral zone-Searching for a practical approach, PloS one, 13 (2018) e0191341.
[118] A. Server, T.E. Orheim, B.A. Graff, R. Josefsen, T. Kumar, P.H. Nakstad, Diagnostic examination performance by using microvascular leakage, cerebral blood volume, and blood flow derived from 3-T dynamic susceptibility-weighted contrast-enhanced perfusion MR imaging in the differentiation of glioblastoma multiforme and brain metastasis, Neuroradiology, 53 (2011) 319-330.
[119] M. Law, S. Oh, J.S. Babb, E. Wang, M. Inglese, D. Zagzag, E.A. Knopp, G. Johnson, Low-grade gliomas: dynamic susceptibility-weighted contrast-enhanced perfusion MR imaging--prediction of patient clinical response, Radiology, 238 (2006) 658-667.
[120] A. Server, B. Kulle, O.B. Gadmar, R. Josefsen, T. Kumar, P.H. Nakstad, Measurements of diagnostic examination performance using quantitative apparent diffusion coefficient and proton MR spectroscopic imaging in the preoperative evaluation of tumor grade in cerebral gliomas, European journal of radiology, 80 (2011) 462-470.
[121] A.F. Delgado, A.F. Delgado, Discrimination between Glioma Grades II and III Using Dynamic Susceptibility Perfusion MRI: A Meta-Analysis, AJNR. American journal of neuroradiology, 38 (2017) 1348-1355.
[122] S. Bisdas, The role of dynamic susceptibility contrast perfusion- weighted MRI in the estimation of IDH mutation in gliomas., Journal of clinical oncology, (2018).
[123] I. Ryoo, S.H. Choi, J.H. Kim, C.H. Sohn, S.C. Kim, H.S. Shin, J.A. Yeom, S.C. Jung, A.L. Lee, T.J. Yun, C.K. Park, S.H. Park, Cerebral blood volume calculated by dynamic susceptibility contrast-enhanced perfusion MR imaging: preliminary correlation study with glioblastoma genetic profiles, PloS one, 8 (2013) e71704.
[124] K. Welker, J. Boxerman, A. Kalnin, T. Kaufmann, M. Shiroishi, M. Wintermark, ASFNR recommendations for clinical performance of MR dynamic susceptibility contrast perfusion imaging of the brain, AJNR. American journal of neuroradiology, 36 (2015) E41-51.
[125] A. Hilario, A. Hernandez-Lain, J.M. Sepulveda, A. Lagares, A. Perez-Nunez, A. Ramos, Perfusion MRI grading diffuse gliomas: Impact of permeability parameters on molecular biomarkers and survival, Neurocirugia (Asturias, Spain), 30 (2019) 11-18.
[126] B.L. Hou, S. Wen, G.A. Katsevman, H. Liu, O. Urhie, R.C. Turner, J. Carpenter, S. Bhatia, MRI Parameters and Their Impact on the Survival of Patients with Glioblastoma: Tumor Perfusion Predicts Survival, World neurosurgery, (2018).

[127] J.L. Boxerman, K.M. Schmainda, R.M. Weisskoff, Relative cerebral blood volume maps corrected for contrast agent extravasation significantly correlate with glioma tumor grade, whereas uncorrected maps do not, AJNR. American journal of neuroradiology, 27 (2006) 859-867.
[128] A. Bjornerud, A.G. Sorensen, K. Mouridsen, K.E. Emblem, T1- and T2*-dominant extravasation correction in DSC-MRI: part I--theoretical considerations and implications for assessment of tumor hemodynamic properties, Journal of cerebral blood flow and metabolism : official journal of the International Society of Cerebral Blood Flow and Metabolism, 31 (2011) 2041-2053.
[129] N. Zakhari, M.S. Taccone, C.H. Torres, S. Chakraborty, J. Sinclair, J. Woulfe, G.H. Jansen, G.O. Cron, R.E. Thornhill, M.D.F. McInnes, T.B. Nguyen, Prospective comparative diagnostic accuracy evaluation of dynamic contrast-enhanced (DCE) vs. dynamic susceptibility contrast (DSC) MR perfusion in differentiating tumor recurrence from radiation necrosis in treated high-grade gliomas, Journal of magnetic resonance imaging : JMRI, 50 (2019) 573-582.
[130] K. Nael, A.H. Bauer, A. Hormigo, M. Lemole, I.M. Germano, J. Puig, B. Stea, Multiparametric MRI for Differentiation of Radiation Necrosis From Recurrent Tumor in Patients With Treated Glioblastoma, AJR. American journal of roentgenology, 210 (2018) 18-23.
[131] S. Bisdas, T. Naegele, R. Ritz, A. Dimostheni, C. Pfannenberg, M. Reimold, T.S. Koh, U. Ernemann, Distinguishing recurrent high-grade gliomas from radiation injury: a pilot study using dynamic contrast-enhanced MR imaging, Academic radiology, 18 (2011) 575-583.
[132] A. Falk Delgado, F. De Luca, D. van Westen, A. Falk Delgado, Arterial spin labeling MR imaging for differentiation between high- and low-grade glioma-a meta-analysis, Neuro-oncology, 20 (2018) 1450-1461.
[133] J.P. O'Connor, P.S. Tofts, K.A. Miles, L.M. Parkes, G. Thompson, A. Jackson, Dynamic contrast-enhanced imaging techniques: CT and MRI, The British journal of radiology, 84 Spec No 2 (2011) S112-120.
[134] S.M. Chang, P.Y. Wen, M.A. Vogelbaum, D.R. Macdonald, M.J. van den Bent, Response Assessment in Neuro-Oncology (RANO): more than imaging criteria for malignant glioma, Neuro-oncology practice, 2 (2015) 205-209.
[135] O.L. Chinot, D.R. Macdonald, L.E. Abrey, G. Zahlmann, Y. Kerloeguen, T.F. Cloughesy, Response assessment criteria for glioblastoma: practical adaptation and implementation in clinical trials of antiangiogenic therapy, Current neurology and neuroscience reports, 13 (2013) 347.
[136] S.C. Eisele, P.Y. Wen, E.Q. Lee, Assessment of Brain Tumor Response: RANO and Its Offspring, Current treatment options in oncology, 17 (2016) 35.
[137] H. Okada, M. Weller, R. Huang, G. Finocchiaro, M.R. Gilbert, W. Wick, B.M. Ellingson, N. Hashimoto, I.F. Pollack, A.A. Brandes, E. Franceschi, C. Herold-Mende, L. Nayak, A. Panigrahy, W.B. Pope, R. Prins, J.H. Sampson, P.Y. Wen, D.A. Reardon, Immunotherapy response assessment in neuro-oncology: a report of the RANO working group, The Lancet. Oncology, 16 (2015) e534-e542.
[138] D. Aquino, A. Gioppo, G. Finocchiaro, M.G. Bruzzone, V. Cuccarini, MRI in Glioma Immunotherapy: Evidence, Pitfalls, and Perspectives, Journal of immunology research, 2017 (2017) 5813951.
[139] D. Brandsma, L. Stalpers, W. Taal, P. Sminia, M.J. van den Bent, Clinical features, mechanisms, and management of pseudoprogression in malignant gliomas, The Lancet. Oncology, 9 (2008) 453-461.
[140] E.R. Gerstner, M.B. McNamara, A.D. Norden, D. Lafrankie, P.Y. Wen, Effect of adding temozolomide to radiation therapy on the incidence of pseudo-progression, Journal of neuro-oncology, 94 (2009) 97-101.
[141] A.A. Brandes, E. Franceschi, A. Tosoni, V. Blatt, A. Pession, G. Tallini, R. Bertorelle, S. Bartolini, F. Calbucci, A. Andreoli, G. Frezza, M. Leonardi, F. Spagnolli, M. Ermani, MGMT promoter methylation status can predict the incidence and outcome of pseudoprogression after concomitant radiochemotherapy in newly diagnosed glioblastoma patients, Journal of clinical oncology : official journal of the American Society of Clinical Oncology, 26 (2008) 2192-2197.
[142] K. Han, M. Ren, W. Wick, L. Abrey, A. Das, J. Jin, D.A. Reardon, Progression-free survival as a surrogate endpoint for overall survival in glioblastoma: a literature-based meta-analysis from 91 trials, Neuro-oncology, 16 (2014) 696-706.

[143] G.D. Goss, D.M. Logan, T.E. Newman, W.K. Evans, Use of vinorelbine in non-small-cell lung cancer. Provincial Lung Disease Site Group, Cancer prevention & control : CPC = Prevention & controle en cancerologie : PCC, 1 (1997) 28-38.
[144] P.A. Tang, S.M. Bentzen, E.X. Chen, L.L. Siu, Surrogate end points for median overall survival in metastatic colorectal cancer: literature-based analysis from 39 randomized controlled trials of first-line chemotherapy, Journal of clinical oncology : official journal of the American Society of Clinical Oncology, 25 (2007) 4562-4568.
[145] R.A. Miksad, V. Zietemann, R. Gothe, R. Schwarzer, A. Conrads-Frank, P. Schnell-Inderst, B. Stollenwerk, U. Siebert, Progression-free survival as a surrogate endpoint in advanced breast cancer, International journal of technology assessment in health care, 24 (2008) 371-383.
[146] S.J. Price, A.M. Young, W.J. Scotton, J. Ching, L.A. Mohsen, N.R. Boonzaier, V.C. Lupson, J.R. Griffiths, M.A. McLean, T.J. Larkin, Multimodal MRI can identify perfusion and metabolic changes in the invasive margin of glioblastomas, Journal of magnetic resonance imaging : JMRI, 43 (2016) 487-494.
[147] J.L. Yan, C. Li, N.R. Boonzaier, D.M. Fountain, T.J. Larkin, T. Matys, A. van der Hoorn, S.J. Price, Multimodal MRI characteristics of the glioblastoma infiltration beyond contrast enhancement, Therapeutic advances in neurological disorders, 12 (2019) 1756286419844664.
[148] S. Fellah, D. Caudal, A.M. De Paula, P. Dory-Lautrec, D. Figarella-Branger, O. Chinot, P. Metellus, P.J. Cozzone, S. Confort-Gouny, B. Ghattas, V. Callot, N. Girard, Multimodal MR imaging (diffusion, perfusion, and spectroscopy): is it possible to distinguish oligodendroglial tumor grade and 1p/19q codeletion in the pretherapeutic diagnosis?, AJNR. American journal of neuroradiology, 34 (2013) 1326-1333.
[149] M. Zhou, J. Scott, B. Chaudhury, L. Hall, D. Goldgof, K.W. Yeom, M. Iv, Y. Ou, J. Kalpathy-Cramer, S. Napel, R. Gillies, O. Gevaert, R. Gatenby, Radiomics in Brain Tumor: Image Assessment, Quantitative Feature Descriptors, and Machine-Learning Approaches, AJNR. American journal of neuroradiology, 39 (2018) 208-216.
[150] P. Korfiatis, B. Erickson, Deep learning can see the unseeable: predicting molecular markers from MRI of brain gliomas, Clinical radiology, 74 (2019) 367-373.
[151] A. Zlochower, D.S. Chow, P. Chang, D. Khatri, J.A. Boockvar, C.G. Filippi, Deep Learning AI Applications in the Imaging of Glioma, Topics in magnetic resonance imaging : TMRI, 29 (2020) 115-110.
[152] R.A. Gatenby, O. Grove, R.J. Gillies, Quantitative imaging in cancer evolution and ecology, Radiology, 269 (2013) 8-15.
[153] R. Anil, R.R. Colen, Imaging Genomics in Glioblastoma Multiforme: A Predictive Tool for Patients Prognosis, Survival, and Outcome, Magnetic resonance imaging clinics of North America, 24 (2016) 731-740.
[154] P.O. Zinn, B. Mahajan, P. Sathyan, S.K. Singh, S. Majumder, F.A. Jolesz, R.R. Colen, Radiogenomic mapping of edema/cellular invasion MRI-phenotypes in glioblastoma multiforme, PloS one, 6 (2011) e25451.
[155] P. Kickingereder, O.C. Andronesi, Radiomics, Metabolic, and Molecular MRI for Brain Tumors, Seminars in neurology, 38 (2018) 32-40.
[156] L. Macyszyn, H. Akbari, J.M. Pisapia, X. Da, M. Attiah, V. Pigrish, Y. Bi, S. Pal, R.V. Davuluri, L. Roccograndi, N. Dahmane, M. Martinez-Lage, G. Biros, R.L. Wolf, M. Bilello, D.M. O'Rourke, C. Davatzikos, Imaging patterns predict patient survival and molecular subtype in glioblastoma via machine learning techniques, Neuro-oncology, 18 (2016) 417-425.
[157] A.F.I. Osman, A Multi-parametric MRI-Based Radiomics Signature and a Practical ML Model for Stratifying Glioblastoma Patients Based on Survival Toward Precision Oncology, Frontiers in computational neuroscience, 13 (2019) 58.
[158] M.M. Shaver, P.A. Kohanteb, C. Chiou, M.D. Bardis, C. Chantaduly, D. Bota, C.G. Filippi, B. Weinberg, J. Grinband, D.S. Chow, P.D. Chang, Optimizing Neuro-Oncology Imaging: A Review of Deep Learning Approaches for Glioma Imaging, Cancers, 11 (2019).
[159] BEST, BEST (Biomarkers, EndpointS, and other Tools) Resource. Maryland

(2016).
[160] A. Saenz-Antonanzas, J. Auzmendi-Iriarte, E. Carrasco-Garcia, L. Moreno-Cugnon, I. Ruiz, J. Villanua, L. Egana, D. Otaegui, N. Sampron, A. Matheu, Liquid Biopsy in Glioblastoma: Opportunities, Applications and Challenges, Cancers, 11 (2019).
[161] G.M. Shankar, L. Balaj, S.L. Stott, B. Nahed, B.S. Carter, Liquid biopsy for brain tumors, Expert review of molecular diagnostics, 17 (2017) 943-947.
[162] R.M. Califf, Biomarker definitions and their applications, Experimental biology and medicine (Maywood, N.J.), 243 (2018) 213-221.
[163] J. Deng, Y. Wang, Quantitative magnetic resonance imaging biomarkers in oncological clinical trials: Current techniques and standardization challenges, Chronic diseases and translational medicine, 3 (2017) 8-20.
[164] J.P. O'Connor, E.O. Aboagye, J.E. Adams, H.J. Aerts, S.F. Barrington, A.J. Beer, R. Boellaard, S.E. Bohndiek, M. Brady, G. Brown, D.L. Buckley, T.L. Chenevert, L.P. Clarke, S. Collette, G.J. Cook, N.M. deSouza, J.C. Dickson, C. Dive, J.L. Evelhoch, C. Faivre-Finn, F.A. Gallagher, F.J. Gilbert, R.J. Gillies, V. Goh, J.R. Griffiths, A.M. Groves, S. Halligan, A.L. Harris, D.J. Hawkes, O.S. Hoekstra, E.P. Huang, B.F. Hutton, E.F. Jackson, G.C. Jayson, A. Jones, D.M. Koh, D. Lacombe, P. Lambin, N. Lassau, M.O. Leach, T.Y. Lee, E.L. Leen, J.S. Lewis, Y. Liu, M.F. Lythgoe, P. Manoharan, R.J. Maxwell, K.A. Miles, B. Morgan, S. Morris, T. Ng, A.R. Padhani, G.J. Parker, M. Partridge, A.P. Pathak, A.C. Peet, S. Punwani, A.R. Reynolds, S.P. Robinson, L.K. Shankar, R.A. Sharma, D. Soloviev, S. Stroobants, D.C. Sullivan, S.A. Taylor, P.S. Tofts, G.M. Tozer, M. van Herk, S. Walker-Samuel, J. Wason, K.J. Williams, P. Workman, T.E. Yankeelov, K.M. Brindle, L.M. McShane, A. Jackson, J.C. Waterton, Imaging biomarker roadmap for cancer studies, Nature reviews. Clinical oncology, 14 (2017) 169-186.
[165] K.E. Emblem, B. Nedregaard, T. Nome, P. Due-Tonnessen, J.K. Hald, D. Scheie, O.C. Borota, M. Cvancarova, A. Bjornerud, Glioma grading by using histogram analysis of blood volume heterogeneity from MR-derived cerebral blood volume maps, Radiology, 247 (2008) 808-817.
[166] M.D. Jenkinson, D.G. du Plessis, T.S. Smith, A.R. Brodbelt, K.A. Joyce, C. Walker, Cellularity and apparent diffusion coefficient in oligodendroglial tumours characterized by genotype, Journal of neuro-oncology, 96 (2010) 385-392.
[167] D. Scheie, P.A. Andresen, M. Cvancarova, A.S. Bo, E. Helseth, K. Skullerud, K. Beiske, Fluorescence in situ hybridization (FISH) on touch preparations: a reliable method for detecting loss of heterozygosity at 1p and 19q in oligodendroglial tumors, The American journal of surgical pathology, 30 (2006) 828-837.
[168] R. Natte, R. van Eijk, P. Eilers, A.M. Cleton-Jansen, J. Oosting, M. Kouwenhove, J.M. Kros, S. van Duinen, Multiplex ligation-dependent probe amplification for the detection of 1p and 19q chromosomal loss in oligodendroglial tumors, Brain pathology (Zurich, Switzerland), 15 (2005) 192-197.
[169] A. Agostini, I. Panagopoulos, H.K. Andersen, L.E. Johannesen, B. Davidson, C.G. Trope, S. Heim, F. Micci, HMGA2 expression pattern and TERT mutations in tumors of the vulva, Oncology reports, 33 (2015) 2675-2680.
[170] M.S. Ahluwalia, H. Xie, S. Dahiya, N. Hashemi-Sadraei, D. Schiff, P.G. Fisher, M.C. Chamberlain, S. Pannullo, H.B. Newton, C. Brewer, L. Wood, R. Prayson, P. Elson, D.M. Peereboom, Efficacy and patient-reported outcomes with dose-intense temozolomide in patients with newly diagnosed pure and mixed anaplastic oligodendroglioma: a phase II multicenter study, Journal of neuro-oncology, 122 (2015) 111-119.
[171] W.B. Pope, A. Lai, R. Mehta, H.J. Kim, J. Qiao, J.R. Young, X. Xue, J. Goldin, M.S. Brown, P.L. Nghiemphu, A. Tran, T.F. Cloughesy, Apparent diffusion coefficient histogram analysis stratifies progression-free survival in newly diagnosed bevacizumab-treated glioblastoma, AJNR. American journal of neuroradiology, 32 (2011) 882-889.
[172] A. Falk, M. Fahlstrom, E. Rostrup, S. Berntsson, M. Zetterling, A. Morell, H.B. Larsson, A. Smits, E.M. Larsson, Discrimination between glioma grades II and III in suspected low-grade gliomas using dynamic

contrast-enhanced and dynamic susceptibility contrast perfusion MR imaging: a histogram analysis approach, Neuroradiology, 56 (2014) 1031-1038.
[173] M. Kondo, Y. Uchiyama, Apparent diffusion coefficient histogram analysis for prediction of prognosis in glioblastoma, Journal of neuroradiology. Journal de neuroradiologie, 45 (2018) 236-241.
[174] Y.S. Choi, S.S. Ahn, D.W. Kim, J.H. Chang, S.G. Kang, E.H. Kim, S.H. Kim, T.H. Rim, S.K. Lee, Incremental Prognostic Value of ADC Histogram Analysis over MGMT Promoter Methylation Status in Patients with Glioblastoma, Radiology, 281 (2016) 175-184.
[175] C.R. McDonald, R.L. Delfanti, A.P. Krishnan, K.M. Leyden, J.A. Hattangadi-Gluth, T.M. Seibert, R. Karunamuni, P. Elbe, J.M. Kuperman, H. Bartsch, D.E. Piccioni, N.S. White, A.M. Dale, N. Farid, Restriction spectrum imaging predicts response to bevacizumab in patients with high-grade glioma, Neuro-oncology, (2016).
[176] T. Huber, S. Bette, B. Wiestler, J. Gempt, J. Gerhardt, C. Delbridge, M. Barz, B. Meyer, C. Zimmer, J.S. Kirschke, Fractional Anisotropy Correlates with Overall Survival in Glioblastoma, World neurosurgery, 95 (2016) 525-534.e521.
[177] C.D. Ali Işin, Melike Şah, Review of MRI-based Brain Tumor Image Segmentation Using Deep Learning Methods.
[178] S. Bauer, L.P. Nolte, M. Reyes, Fully automatic segmentation of brain tumor images using support vector machine classification in combination with hierarchical conditional random field regularization, Medical image computing and computer-assisted intervention : MICCAI ... International Conference on Medical Image Computing and Computer-Assisted Intervention, 14 (2011) 354-361.
[179] K. Xie, J. Yang, Z.G. Zhang, Y.M. Zhu, Semi-automated brain tumor and edema segmentation using MRI, European journal of radiology, 56 (2005) 12-19.
[180] M.R. Kaus, S.K. Warfield, A. Nabavi, P.M. Black, F.A. Jolesz, R. Kikinis, Automated segmentation of MR images of brain tumors, Radiology, 218 (2001) 586-591.
[181] P. Chang, J. Grinband, B.D. Weinberg, M. Bardis, M. Khy, G. Cadena, M.Y. Su, S. Cha, C.G. Filippi, D. Bota, P. Baldi, L.M. Poisson, R. Jain, D. Chow, Deep-Learning Convolutional Neural Networks Accurately Classify Genetic Mutations in Gliomas, AJNR. American journal of neuroradiology, 39 (2018) 1201-1207.
[182] S. Cui, L. Mao, J. Jiang, C. Liu, S. Xiong, Automatic Semantic Segmentation of Brain Gliomas from MRI Images Using a Deep Cascaded Neural Network, Journal of healthcare engineering, 2018 (2018) 4940593.
[183] M. Ben Abdallah, M. Blonski, S. Wantz-Mezieres, Y. Gaudeau, L. Taillandier, J.M. Moureaux, Relevance of two manual tumour volume estimation methods for diffuse low-grade gliomas, Healthcare technology letters, 5 (2018) 13-17.
[184] K.E. Emblem, B. Nedregaard, J.K. Hald, T. Nome, P. Due-Tonnessen, A. Bjornerud, Automatic glioma characterization from dynamic susceptibility contrast imaging: brain tumor segmentation using knowledge-based fuzzy clustering, Journal of magnetic resonance imaging : JMRI, 30 (2009) 1-10.
[185] M. Ben Abdallah, M. Blonski, S. Wantz-Mezieres, Y. Gaudeau, L. Taillandier, J.M. Moureaux, Statistical evaluation of manual segmentation of a diffuse low-grade glioma MRI dataset, Conference proceedings : ... Annual International Conference of the IEEE Engineering in Medicine and Biology Society. IEEE Engineering in Medicine and Biology Society. Annual Conference, 2016 (2016) 4403-4406.
[186] H.K. Bo, O. Solheim, A.S. Jakola, K.A. Kvistad, I. Reinertsen, E.M. Berntsen, Intra-rater variability in low-grade glioma segmentation, Journal of neuro-oncology, 131 (2017) 393-402.
[187] B.L. Adams R, Seeded region growing. IEEE Transactions on Pattern Analysis and Machine Intelligence., (1994; 16(6):641–647).

[188] N. Sadeghi, N. D'Haene, C. Decaestecker, M. Levivier, T. Metens, C. Maris, D. Wikler, D. Baleriaux, I. Salmon, S. Goldman, Apparent diffusion coefficient and cerebral blood volume in brain gliomas: relation to tumor cell density and tumor microvessel density based on stereotactic biopsies, AJNR. American journal of neuroradiology, 29 (2008) 476-482.

[189] H. Akbari, L. Macyszyn, X. Da, R.L. Wolf, M. Bilello, R. Verma, D.M. O'Rourke, C. Davatzikos, Pattern analysis of dynamic susceptibility contrast-enhanced MR imaging demonstrates peritumoral tissue heterogeneity, Radiology, 273 (2014) 502-510.
[190] R.F. Barajas, Jr., J.J. Phillips, R. Parvataneni, A. Molinaro, E. Essock-Burns, G. Bourne, A.T. Parsa, M.K. Aghi, M.W. McDermott, M.S. Berger, S. Cha, S.M. Chang, S.J. Nelson, Regional variation in histopathologic features of tumor specimens from treatment-naive glioblastoma correlates with anatomic and physiologic MR Imaging, Neuro-oncology, 14 (2012) 942-954.
[191] H.S. Kwak, S. Hwang, G.H. Chung, J.S. Song, E.J. Choi, Detection of small brain metastases at 3 T: comparing the diagnostic performances of contrast-enhanced T1-weighted SPACE, MPRAGE, and 2D FLASH imaging, Clinical imaging, 39 (2015) 571-575.
[192] E.M. Berntsen, A.L. Stensjøen, M.S. Langlo, S.Q. Simonsen, P. Christensen, V.A. Moholdt, O. Solheim, Volumetric segmentation of glioblastoma progression compared to bidimensional products and clinical radiological reports, Acta neurochirurgica, 162 (2020) 379-387.
[193] P. Korkolopoulou, E. Patsouris, N. Kavantzas, A.E. Konstantinidou, P. Christodoulou, E. Thomas-Tsagli, A. Pananikolaou, C. Eftychiadis, P.M. Pavlopoulos, D. Angelidakis, D. Rologis, P. Davaris, Prognostic implications of microvessel morphometry in diffuse astrocytic neoplasms, Neuropathology and applied neurobiology, 28 (2002) 57-66.
[194] P. Wesseling, J.A. van der Laak, M. Link, H.L. Teepen, D.J. Ruiter, Quantitative analysis of microvascular changes in diffuse astrocytic neoplasms with increasing grade of malignancy, Human pathology, 29 (1998) 352-358.
[195] Z. Shi, Q. Chen, C. Li, L. Wang, X. Qian, C. Jiang, X. Liu, X. Wang, H. Li, C. Kang, T. Jiang, L.Z. Liu, Y. You, N. Liu, B.H. Jiang, MiR-124 governs glioma growth and angiogenesis and enhances chemosensitivity by targeting R-Ras and N-Ras, Neuro-oncology, 16 (2014) 1341-1353.
[196] A. Griveau, G. Seano, S.J. Shelton, R. Kupp, A. Jahangiri, K. Obernier, S. Krishnan, O.R. Lindberg, T.J. Yuen, A.C. Tien, J.K. Sabo, N. Wang, I. Chen, J. Kloepper, L. Larrouquere, M. Ghosh, I. Tirosh, E. Huillard, A. Alvarez-Buylla, M.C. Oldham, A.I. Persson, W.A. Weiss, T.T. Batchelor, A. Stemmer-Rachamimov, M.L. Suva, J.J. Phillips, M.K. Aghi, S. Mehta, R.K. Jain, D.H. Rowitch, A Glial Signature and Wnt7 Signaling Regulate Glioma-Vascular Interactions and Tumor Microenvironment, Cancer cell, 33 (2018) 874-889.e877.
[197] A. Hilario, J.M. Sepulveda, A. Perez-Nunez, E. Salvador, J.M. Millan, A. Hernandez-Lain, V. Rodriguez-Gonzalez, A. Lagares, A. Ramos, A prognostic model based on preoperative MRI predicts overall survival in patients with diffuse gliomas, AJNR. American journal of neuroradiology, 35 (2014) 1096-1102.
[198] V. Cuccarini, A. Erbetta, M. Farinotti, L. Cuppini, F. Ghielmetti, B. Pollo, F. Di Meco, M. Grisoli, G. Filippini, G. Finocchiaro, M.G. Bruzzone, M. Eoli, Advanced MRI may complement histological diagnosis of lower grade gliomas and help in predicting survival, Journal of neuro-oncology, 126 (2016) 279-288.
[199] E. Neill, T. Luks, M. Dayal, J.J. Phillips, A. Perry, L.E. Jalbert, S. Cha, A. Molinaro, S.M. Chang, S.J. Nelson, Quantitative multi-modal MR imaging as a non-invasive prognostic tool for patients with recurrent low-grade glioma, Journal of neuro-oncology, 132 (2017) 171-179.
[200] M.J. van den Bent, J.S. Wefel, D. Schiff, M.J. Taphoorn, K. Jaeckle, L. Junck, T. Armstrong, A. Choucair, A.D. Waldman, T. Gorlia, M. Chamberlain, B.G. Baumert, M.A. Vogelbaum, D.R. Macdonald, D.A. Reardon, P.Y. Wen, S.M. Chang, A.H. Jacobs, Response assessment in neuro-oncology (a report of the RANO group): assessment of outcome in trials of diffuse low-grade gliomas, The Lancet. Oncology, 12 (2011) 583-593.
[201] E.K. Avila, M. Chamberlain, D. Schiff, J.C. Reijneveld, T.S. Armstrong, R. Ruda, P.Y. Wen, M. Weller, J.A. Koekkoek, S. Mittal, Y. Arakawa, A. Choucair, J. Gonzalez-Martinez, D.R. MacDonald, R. Nishikawa, A. Shah, C.J. Vecht, P. Warren, M.J. van den Bent, L.M. DeAngelis, Seizure control as a new metric in assessing efficacy of tumor treatment in low-grade glioma trials, Neuro-oncology, 19 (2017) 12-21.
[202] M.D. Jenkinson, T.S. Smith, K.A. Joyce, D. Fildes, J. Broome, D.G. du Plessis, B. Haylock, D.J. Husband, P.C. Warnke, C. Walker, Cerebral blood volume, genotype and chemosensitivity in oligodendroglial tumours, Neuroradiology, 48 (2006) 703-713.

[203] K. Leu, G.A. Ott, A. Lai, P.L. Nghiemphu, W.B. Pope, W.H. Yong, L.M. Liau, T.F. Cloughesy, B.M. Ellingson, Perfusion and diffusion MRI signatures in histologic and genetic subtypes of WHO grade II-III diffuse gliomas, Journal of neuro-oncology, (2017).
[204] H.J. Yoon, K.J. Ahn, S. Lee, J.H. Jang, H.S. Choi, S.L. Jung, B.S. Kim, S.S. Jeun, Y.K. Hong, Differential diagnosis of oligodendroglial and astrocytic tumors using imaging results: the added value of perfusion MR imaging, Neuroradiology, 59 (2017) 665-675.
[205] H. Zhou, M. Vallieres, H.X. Bai, C. Su, H. Tang, D. Oldridge, Z. Zhang, B. Xiao, W. Liao, Y. Tao, J. Zhou, P. Zhang, L. Yang, MRI features predict survival and molecular markers in diffuse lower-grade gliomas, Neuro-oncology, 19 (2017) 862-870.
[206] H. Zhou, K. Chang, H.X. Bai, B. Xiao, C. Su, W.L. Bi, P.J. Zhang, J.T. Senders, M. Vallieres, V.K. Kavouridis, A. Boaro, O. Arnaout, L. Yang, R.Y. Huang, Machine learning reveals multimodal MRI patterns predictive of isocitrate dehydrogenase and 1p/19q status in diffuse low- and high-grade gliomas, Journal of neuro-oncology, 142 (2019) 299-307.
[207] Z. Akkus, I. Ali, J. Sedlar, J.P. Agrawal, I.F. Parney, C. Giannini, B.J. Erickson, Predicting Deletion of Chromosomal Arms 1p/19q in Low-Grade Gliomas from MR Images Using Machine Intelligence, Journal of digital imaging, 30 (2017) 469-476.
[208] D.J. Brat, R.G. Verhaak, K.D. Aldape, W.K. Yung, S.R. Salama, L.A. Cooper, E. Rheinbay, C.R. Miller, M. Vitucci, O. Morozova, A.G. Robertson, H. Noushmehr, P.W. Laird, A.D. Cherniack, R. Akbani, J.T. Huse, G. Ciriello, L.M. Poisson, J.S. Barnholtz-Sloan, M.S. Berger, C. Brennan, R.R. Colen, H. Colman, A.E. Flanders, C. Giannini, M. Grifford, A. Iavarone, R. Jain, I. Joseph, J. Kim, K. Kasaian, T. Mikkelsen, B.A. Murray, B.P. O'Neill, L. Pachter, D.W. Parsons, C. Sougnez, E.P. Sulman, S.R. Vandenberg, E.G. Van Meir, A. von Deimling, H. Zhang, D. Crain, K. Lau, D. Mallery, S. Morris, J. Paulauskis, R. Penny, T. Shelton, M. Sherman, P. Yena, A. Black, J. Bowen, K. Dicostanzo, J. Gastier-Foster, K.M. Leraas, T.M. Lichtenberg, C.R. Pierson, N.C. Ramirez, C. Taylor, S. Weaver, L. Wise, E. Zmuda, T. Davidsen, J.A. Demchok, G. Eley, M.L. Ferguson, C.M. Hutter, K.R. Mills Shaw, B.A. Ozenberger, M. Sheth, H.J. Sofia, R. Tarnuzzer, Z. Wang, L. Yang, J.C. Zenklusen, B. Ayala, J. Baboud, S. Chudamani, M.A. Jensen, J. Liu, T. Pihl, R. Raman, Y. Wan, Y. Wu, A. Ally, J.T. Auman, M. Balasundaram, S. Balu, S.B. Baylin, R. Beroukhim, M.S. Bootwalla, R. Bowlby, C.A. Bristow, D. Brooks, Y. Butterfield, R. Carlsen, S. Carter, L. Chin, A. Chu, E. Chuah, K. Cibulskis, A. Clarke, S.G. Coetzee, N. Dhalla, T. Fennell, S. Fisher, S. Gabriel, G. Getz, R. Gibbs, R. Guin, A. Hadjipanayis, D.N. Hayes, T. Hinoue, K. Hoadley, R.A. Holt, A.P. Hoyle, S.R. Jefferys, S. Jones, C.D. Jones, R. Kucherlapati, P.H. Lai, E. Lander, S. Lee, L. Lichtenstein, Y. Ma, D.T. Maglinte, H.S. Mahadeshwar, M.A. Marra, M. Mayo, S. Meng, M.L. Meyerson, P.A. Mieczkowski, R.A. Moore, L.E. Mose, A.J. Mungall, A. Pantazi, M. Parfenov, P.J. Park, J.S. Parker, C.M. Perou, A. Protopopov, X. Ren, J. Roach, T.S. Sabedot, J. Schein, S.E. Schumacher, J.G. Seidman, S. Seth, H. Shen, J.V. Simons, P. Sipahimalani, M.G. Soloway, X. Song, H. Sun, B. Tabak, A. Tam, D. Tan, J. Tang, N. Thiessen, T. Triche, Jr., D.J. Van Den Berg, U. Veluvolu, S. Waring, D.J. Weisenberger, M.D. Wilkerson, T. Wong, J. Wu, L. Xi, A.W. Xu, L. Yang, T.I. Zack, J. Zhang, B.A. Aksoy, H. Arachchi, C. Benz, B. Bernard, D. Carlin, J. Cho, D. DiCara, S. Frazer, G.N. Fuller, J. Gao, N. Gehlenborg, D. Haussler, D.I. Heiman, L. Iype, A. Jacobsen, Z. Ju, S. Katzman, H. Kim, T. Knijnenburg, R.B. Kreisberg, M.S. Lawrence, W. Lee, K. Leinonen, P. Lin, S. Ling, W. Liu, Y. Liu, Y. Liu, Y. Lu, G. Mills, S. Ng, M.S. Noble, E. Paull, A. Rao, S. Reynolds, G. Saksena, Z. Sanborn, C. Sander, N. Schultz, Y. Senbabaoglu, R. Shen, I. Shmulevich, R. Sinha, J. Stuart, S.O. Sumer, Y. Sun, N. Tasman, B.S. Taylor, D. Voet, N. Weinhold, J.N. Weinstein, D. Yang, K. Yoshihara, S. Zheng, W. Zhang, L. Zou, T. Abel, S. Sadeghi, M.L. Cohen, J. Eschbacher, E.M. Hattab, A. Raghunathan, M.J. Schniederjan, D. Aziz, G. Barnett, W. Barrett, D.D. Bigner, L. Boice, C. Brewer, C. Calatozzolo, B. Campos, C.G. Carlotti, Jr., T.A. Chan, L. Cuppini, E. Curley, S. Cuzzubbo, K. Devine, F. DiMeco, R. Duell, J.B. Elder, A. Fehrenbach, G. Finocchiaro, W. Friedman, J. Fulop, J. Gardner, B. Hermes, C. Herold-Mende, C. Jungk, A. Kendler, N.L. Lehman, E. Lipp, O. Liu, R. Mandt, M. McGraw, R. McLendon, C. McPherson, L. Neder, P. Nguyen, A. Noss, R. Nunziata, Q.T. Ostrom, C. Palmer, A. Perin, B. Pollo, A. Potapov, O. Potapova, W.K. Rathmell, D. Rotin, L. Scarpace, C. Schilero, K. Senecal, K. Shimmel, V. Shurkhay, S. Sifri, R. Singh, A.E. Sloan, K. Smolenski, S.M. Staugaitis, R. Steele, L. Thorne, D.P.

Tirapelli, A. Unterberg, M. Vallurupalli, Y. Wang, R. Warnick, F. Williams, Y. Wolinsky, S. Bell, M. Rosenberg, C. Stewart, F. Huang, J.L. Grimsby, A.J. Radenbaugh, J. Zhang, Comprehensive, Integrative Genomic Analysis of Diffuse Lower-Grade Gliomas, The New England journal of medicine, 372 (2015) 2481-2498.
[209] L.Y. Ballester, J.T. Huse, G. Tang, G.N. Fuller, Molecular Classification of Adult Diffuse Gliomas: Conflicting IDH1/IDH2, ATRX and 1p/19q Results, Human pathology, (2017).
[210] F. Sahm, D. Reuss, C. Koelsche, D. Capper, J. Schittenhelm, S. Heim, D.T. Jones, S.M. Pfister, C. Herold-Mende, W. Wick, W. Mueller, C. Hartmann, W. Paulus, A. von Deimling, Farewell to oligoastrocytoma: in situ molecular genetics favor classification as either oligodendroglioma or astrocytoma, Acta neuropathologica, 128 (2014) 551-559.
[211] M. Valera-Mele, O. Mateo Sierra, E. Sola Vendrell, L.J. Guzman de Villoria, L. Carvajal Diaz, O.L. Gil de Sagredo Del Corral, R. Garcia Leal, Assessment of the impact of glioma diagnostic reclassification following the new 2016 WHO classification on a series of cases, Neurocirugia (Asturias, Spain), (2018).
[212] H.J. Yoon, K.J. Ahn, S. Lee, J.H. Jang, H.S. Choi, S.L. Jung, B.S. Kim, S.S. Jeun, Y.K. Hong, Differential diagnosis of oligodendroglial and astrocytic tumors using imaging results: the added value of perfusion MR imaging, Neuroradiology, (2017).
[213] M.J. van den Bent, M. Smits, J.M. Kros, S.M. Chang, Diffuse Infiltrating Oligodendroglioma and Astrocytoma, Journal of clinical oncology : official journal of the American Society of Clinical Oncology, 35 (2017) 2394-2401.
[214] S.I. Kim, Y. Lee, J.K. Won, C.K. Park, S.H. Choi, S.H. Park, Reclassification of Mixed Oligoastrocytic Tumors Using a Genetically Integrated Diagnostic Approach, Journal of pathology and translational medicine, (2017).
[215] M. Mellai, L. Annovazzi, R. Senetta, C. Dell'Aglio, M. Mazzucco, P. Cassoni, D. Schiffer, Diagnostic revision of 206 adult gliomas (including 40 oligoastrocytomas) based on ATRX, IDH1/2 and 1p/19q status, Journal of neuro-oncology, 131 (2017) 213-222.
[216] J.E. Eckel-Passow, D.H. Lachance, A.M. Molinaro, K.M. Walsh, P.A. Decker, H. Sicotte, M. Pekmezci, T. Rice, M.L. Kosel, I.V. Smirnov, G. Sarkar, A.A. Caron, T.M. Kollmeyer, C.E. Praska, A.R. Chada, C. Halder, H.M. Hansen, L.S. McCoy, P.M. Bracci, R. Marshall, S. Zheng, G.F. Reis, A.R. Pico, B.P. O'Neill, J.C. Buckner, C. Giannini, J.T. Huse, A. Perry, T. Tihan, M.S. Berger, S.M. Chang, M.D. Prados, J. Wiemels, J.K. Wiencke, M.R. Wrensch, R.B. Jenkins, Glioma Groups Based on 1p/19q, IDH, and TERT Promoter Mutations in Tumors, The New England journal of medicine, 372 (2015) 2499-2508.
[217] M. Weller, M. van den Bent, J.C. Tonn, R. Stupp, M. Preusser, E. Cohen-Jonathan-Moyal, R. Henriksson, E.L. Rhun, C. Balana, O. Chinot, M. Bendszus, J.C. Reijneveld, F. Dhermain, P. French, C. Marosi, C. Watts, I. Oberg, G. Pilkington, B.G. Baumert, M.J.B. Taphoorn, M. Hegi, M. Westphal, G. Reifenberger, R. Soffietti, W. Wick, European Association for Neuro-Oncology (EANO) guideline on the diagnosis and treatment of adult astrocytic and oligodendroglial gliomas, The Lancet. Oncology, 18 (2017) e315-e329.
[218] Y. Muragaki, M. Chernov, T. Maruyama, T. Ochiai, T. Taira, O. Kubo, R. Nakamura, H. Iseki, T. Hori, K. Takakura, Low-grade glioma on stereotactic biopsy: how often is the diagnosis accurate?, Minimally invasive neurosurgery : MIN, 51 (2008) 275-279.
[219] M.J. van den Bent, Interobserver variation of the histopathological diagnosis in clinical trials on glioma: a clinician's perspective, Acta neuropathologica, 120 (2010) 297-304.
[220] E.A. Knopp, S. Cha, G. Johnson, A. Mazumdar, J.G. Golfinos, D. Zagzag, D.C. Miller, P.J. Kelly, Kricheff, II, Glial neoplasms: dynamic contrast-enhanced T2*-weighted MR imaging, Radiology, 211 (1999) 791-798.
[221] B. Hakyemez, C. Erdogan, I. Ercan, N. Ergin, S. Uysal, S. Atahan, High-grade and low-grade gliomas: differentiation by using perfusion MR imaging, Clinical radiology, 60 (2005) 493-502.
[222] J.M. Abrigo, D.M. Fountain, J.M. Provenzale, E.K. Law, J.S. Kwong, M.G. Hart, W.W.S. Tam, Magnetic resonance perfusion for differentiating low-grade from high-grade gliomas at first presentation, The Cochrane database of systematic reviews, 1 (2018) Cd011551.

[223] N. Morita, S. Wang, S. Chawla, H. Poptani, E.R. Melhem, Dynamic susceptibility contrast perfusion weighted imaging in grading of nonenhancing astrocytomas, Journal of magnetic resonance imaging : JMRI, 32 (2010) 803-808.
[224] X. Liu, W. Tian, B. Kolar, G.A. Yeaney, X. Qiu, M.D. Johnson, S. Ekholm, MR diffusion tensor and perfusion-weighted imaging in preoperative grading of supratentorial nonenhancing gliomas, Neuro-oncology, 13 (2011) 447-455.
[225] M.H. Lev, Y. Ozsunar, J.W. Henson, A.A. Rasheed, G.D. Barest, G.R.t. Harsh, M.M. Fitzek, E.A. Chiocca, J.D. Rabinov, A.N. Csavoy, B.R. Rosen, F.H. Hochberg, P.W. Schaefer, R.G. Gonzalez, Glial tumor grading and outcome prediction using dynamic spin-echo MR susceptibility mapping compared with conventional contrast-enhanced MR: confounding effect of elevated rCBV of oligodendrogliomas [corrected], AJNR. American journal of neuroradiology, 25 (2004) 214-221.
[226] A.F. Delgado, A.F. Delgado, Discrimination between Glioma Grades II and III Using Dynamic Susceptibility Perfusion MRI: A Meta-Analysis, AJNR. American journal of neuroradiology, (2017).
[227] P. Zonari, P. Baraldi, G. Crisi, Multimodal MRI in the characterization of glial neoplasms: the combined role of single-voxel MR spectroscopy, diffusion imaging and echo-planar perfusion imaging, Neuroradiology, 49 (2007) 795-803.
[228] I. Catalaa, R. Henry, W.P. Dillon, E.E. Graves, T.R. McKnight, Y. Lu, D.B. Vigneron, S.J. Nelson, Perfusion, diffusion and spectroscopy values in newly diagnosed cerebral gliomas, NMR in biomedicine, 19 (2006) 463-475.
[229] M.A. Naveed, P. Goyal, A. Malhotra, X. Liu, S. Gupta, M. Mangla, R. Mangla, Grading of oligodendroglial tumors of the brain with apparent diffusion coefficient, magnetic resonance spectroscopy, and dynamic susceptibility contrast imaging, The neuroradiology journal, 31 (2018) 379-385.
[230] M.M. Cihangiroglu, E. Ozturk-Isik, Z. Firat, O. Kilickesmez, A.M. Ulug, U. Ture, Preoperative grading of supratentorial gliomas using high or standard b-value diffusion-weighted MR imaging at 3T, Diagnostic and interventional imaging, 98 (2017) 261-268.
[231] J.B. Qin, H. Zhang, X.C. Wang, Y. Tan, X.F. Wu, Combination value of diffusion-weighted imaging and dynamic susceptibility contrast-enhanced MRI in astrocytoma grading and correlation with GFAP, Topoisomerase IIalpha and MGMT, Oncology letters, 18 (2019) 2763-2770.
[232] M. Kim, S.Y. Jung, J.E. Park, Y. Jo, S.Y. Park, S.J. Nam, J.H. Kim, H.S. Kim, Diffusion- and perfusion-weighted MRI radiomics model may predict isocitrate dehydrogenase (IDH) mutation and tumor aggressiveness in diffuse lower grade glioma, European radiology, (2019).
[233] J.A. Neira, T.H. Ung, J.S. Sims, H.R. Malone, D.S. Chow, J.L. Samanamud, G.J. Zanazzi, X. Guo, S.G. Bowden, B. Zhao, S.A. Sheth, G.M. McKhann, 2nd, M.B. Sisti, P. Canoll, R.S. D'Amico, J.N. Bruce, Aggressive resection at the infiltrative margins of glioblastoma facilitated by intraoperative fluorescein guidance, Journal of neurosurgery, 127 (2017) 111-122.
[234] M. Lara-Velazquez, R. Al-Kharboosh, S. Jeanneret, C. Vazquez-Ramos, D. Mahato, D. Tavanaiepour, G. Rahmathulla, A. Quinones-Hinojosa, Advances in Brain Tumor Surgery for Glioblastoma in Adults, Brain sciences, 7 (2017).
[235] P.D. Chang, H.R. Malone, S.G. Bowden, D.S. Chow, B.J.A. Gill, T.H. Ung, J. Samanamud, Z.K. Englander, A.M. Sonabend, S.A. Sheth, G.M. McKhann, 2nd, M.B. Sisti, L.H. Schwartz, A. Lignelli, J. Grinband, J.N. Bruce, P. Canoll, A Multiparametric Model for Mapping Cellularity in Glioblastoma Using Radiographically Localized Biopsies, AJNR. American journal of neuroradiology, 38 (2017) 890-898.
[236] S. Watkins, S. Robel, I.F. Kimbrough, S.M. Robert, G. Ellis-Davies, H. Sontheimer, Disruption of astrocyte-vascular coupling and the blood-brain barrier by invading glioma cells, Nature communications, 5 (2014) 4196.
[237] V.A. Cuddapah, S. Robel, S. Watkins, H. Sontheimer, A neurocentric perspective on glioma invasion, Nature reviews. Neuroscience, 15 (2014) 455-465.

[238] M. Diksin, S.J. Smith, R. Rahman, The Molecular and Phenotypic Basis of the Glioma Invasive Perivascular Niche, International journal of molecular sciences, 18 (2017).
[239] F.G. Barker, 2nd, S.M. Chang, S.L. Huhn, R.L. Davis, P.H. Gutin, M.W. McDermott, C.B. Wilson, M.D. Prados, Age and the risk of anaplasia in magnetic resonance-nonenhancing supratentorial cerebral tumors, Cancer, 80 (1997) 936-941.
[240] R.D. Tien, G.J. Felsberg, H. Friedman, M. Brown, J. MacFall, MR imaging of high-grade cerebral gliomas: value of diffusion-weighted echoplanar pulse sequences, AJR. American journal of roentgenology, 162 (1994) 671-677.
[241] O. Eidel, J.O. Neumann, S. Burth, P.J. Kieslich, C. Jungk, F. Sahm, P. Kickingereder, K. Kiening, A. Unterberg, W. Wick, H.P. Schlemmer, M. Bendszus, A. Radbruch, Automatic Analysis of Cellularity in Glioblastoma and Correlation with ADC Using Trajectory Analysis and Automatic Nuclei Counting, PloS one, 11 (2016) e0160250.
[242] A. Stecco, C. Pisani, R. Quarta, M. Brambilla, L. Masini, D. Beldi, S. Zizzari, R. Fossaceca, M. Krengli, A. Carriero, DTI and PWI analysis of peri-enhancing tumoral brain tissue in patients treated for glioblastoma, Journal of neuro-oncology, 102 (2011) 261-271.
[243] Q. Wen, L. Jalilian, J.M. Lupo, A.M. Molinaro, S.M. Chang, J. Clarke, M. Prados, S.J. Nelson, Comparison of ADC metrics and their association with outcome for patients with newly diagnosed glioblastoma being treated with radiation therapy, temozolomide, erlotinib and bevacizumab, Journal of neuro-oncology, 121 (2015) 331-339.
[244] J. Virga, L. Szivos, T. Hortobagyi, M.K. Chalsaraei, G. Zahuczky, L. Steiner, J. Toth, J. Remenyi-Puskar, L. Bognar, A. Klekner, Extracellular matrix differences in glioblastoma patients with different prognoses, Oncology letters, 17 (2019) 797-806.
[245] P.S. LaViolette, N.J. Mickevicius, E.J. Cochran, S.D. Rand, J. Connelly, J.A. Bovi, M.G. Malkin, W.M. Mueller, K.M. Schmainda, Precise ex vivo histological validation of heightened cellularity and diffusion-restricted necrosis in regions of dark apparent diffusion coefficient in 7 cases of high-grade glioma, Neuro-oncology, 16 (2014) 1599-1606.
[246] F.W. Crawford, I.S. Khayal, C. McGue, S. Saraswathy, A. Pirzkall, S. Cha, K.R. Lamborn, S.M. Chang, M.S. Berger, S.J. Nelson, Relationship of pre-surgery metabolic and physiological MR imaging parameters to survival for patients with untreated GBM, Journal of neuro-oncology, 91 (2009) 337-351.
[247] A. Stadlbauer, O. Ganslandt, R. Buslei, T. Hammen, S. Gruber, E. Moser, M. Buchfelder, E. Salomonowitz, C. Nimsky, Gliomas: histopathologic evaluation of changes in directionality and magnitude of water diffusion at diffusion-tensor MR imaging, Radiology, 240 (2006) 803-810.
[248] B.J. Jellison, A.S. Field, J. Medow, M. Lazar, M.S. Salamat, A.L. Alexander, Diffusion tensor imaging of cerebral white matter: a pictorial review of physics, fiber tract anatomy, and tumor imaging patterns, AJNR. American journal of neuroradiology, 25 (2004) 356-369.
[249] P. McConville, D. Hambardzumyan, J.B. Moody, W.R. Leopold, A.R. Kreger, M.J. Woolliscroft, A. Rehemtulla, B.D. Ross, E.C. Holland, Magnetic resonance imaging determination of tumor grade and early response to temozolomide in a genetically engineered mouse model of glioma, Clinical cancer research : an official journal of the American Association for Cancer Research, 13 (2007) 2897-2904.
[250] W. Wick, C. Meisner, B. Hentschel, M. Platten, A. Schilling, B. Wiestler, M.C. Sabel, S. Koeppen, R. Ketter, M. Weiler, G. Tabatabai, A. von Deimling, D. Gramatzki, M. Westphal, G. Schackert, M. Loeffler, M. Simon, G. Reifenberger, M. Weller, Prognostic or predictive value of MGMT promoter methylation in gliomas depends on IDH1 mutation, Neurology, 81 (2013) 1515-1522.
[251] M.J. van den Bent, L. Erdem-Eraslan, A. Idbaih, J. de Rooi, P.H. Eilers, W.G. Spliet, W.F. den Dunnen, C. Tijssen, P. Wesseling, P.A. Sillevis Smitt, J.M. Kros, T. Gorlia, P.J. French, MGMT-STP27 methylation status as predictive marker for response to PCV in anaplastic Oligodendrogliomas and Oligoastrocytomas. A report from EORTC study 26951, Clinical cancer research : an official journal of the American Association for Cancer Research, 19 (2013) 5513-5522.

[252] W.J. Moon, J.W. Choi, H.G. Roh, S.D. Lim, Y.C. Koh, Imaging parameters of high grade gliomas in relation to the MGMT promoter methylation status: the CT, diffusion tensor imaging, and perfusion MR imaging, Neuroradiology, 54 (2012) 555-563.
[253] Y. Han, L.F. Yan, X.B. Wang, Y.Z. Sun, X. Zhang, Z.C. Liu, H.Y. Nan, Y.C. Hu, Y. Yang, J. Zhang, Y. Yu, Q. Sun, Q. Tian, B. Hu, G. Xiao, W. Wang, G.B. Cui, Structural and advanced imaging in predicting MGMT promoter methylation of primary glioblastoma: a region of interest based analysis, BMC cancer, 18 (2018) 215.
[254] D. Rundle-Thiele, B. Day, B. Stringer, M. Fay, J. Martin, R.L. Jeffree, P. Thomas, C. Bell, O. Salvado, Y. Gal, A. Coulthard, S. Crozier, S. Rose, Using the apparent diffusion coefficient to identifying MGMT promoter methylation status early in glioblastoma: importance of analytical method, Journal of medical radiation sciences, 62 (2015) 92-98.
[255] S.S. Ahn, N.Y. Shin, J.H. Chang, S.H. Kim, E.H. Kim, D.W. Kim, S.K. Lee, Prediction of methylguanine methyltransferase promoter methylation in glioblastoma using dynamic contrast-enhanced magnetic resonance and diffusion tensor imaging, Journal of neurosurgery, 121 (2014) 367-373.
[256] A. Gupta, A. Prager, R.J. Young, W. Shi, A.M. Omuro, J.J. Graber, Diffusion-weighted MR imaging and MGMT methylation status in glioblastoma: a reappraisal of the role of preoperative quantitative ADC measurements, AJNR. American journal of neuroradiology, 34 (2013) E10-11.
[257] K.R. NCM Youssef1, Y Sakr1, The pros and cons of multicentre studies, Neth j crit care • volume 12 • no 3 • june 2008.
[258] M. Kim, H.S. Kim, Emerging Techniques in Brain Tumor Imaging: What Radiologists Need to Know, Korean journal of radiology, 17 (2016) 598-619.
[259] S.N. Sotiropoulos, S. Jbabdi, J. Xu, J.L. Andersson, S. Moeller, E.J. Auerbach, M.F. Glasser, M. Hernandez, G. Sapiro, M. Jenkinson, D.A. Feinberg, E. Yacoub, C. Lenglet, D.C. Van Essen, K. Ugurbil, T.E. Behrens, Advances in diffusion MRI acquisition and processing in the Human Connectome Project, NeuroImage, 80 (2013) 125-143.
[260] J.H. Jensen, J.A. Helpern, A. Ramani, H. Lu, K. Kaczynski, Diffusional kurtosis imaging: the quantification of non-gaussian water diffusion by means of magnetic resonance imaging, Magnetic resonance in medicine, 53 (2005) 1432-1440.
[261] S. Van Cauter, F. De Keyzer, D.M. Sima, A.C. Sava, F. D'Arco, J. Veraart, R.R. Peeters, A. Leemans, S. Van Gool, G. Wilms, P. Demaerel, S. Van Huffel, S. Sunaert, U. Himmelreich, Integrating diffusion kurtosis imaging, dynamic susceptibility-weighted contrast-enhanced MRI, and short echo time chemical shift imaging for grading gliomas, Neuro-oncology, 16 (2014) 1010-1021.
[262] A.J. Steven, J. Zhuo, E.R. Melhem, Diffusion kurtosis imaging: an emerging technique for evaluating the microstructural environment of the brain, AJR. American journal of roentgenology, 202 (2014) W26-33.
[263] G.R. Glenn, L.W. Kuo, Y.P. Chao, C.Y. Lee, J.A. Helpern, J.H. Jensen, Mapping the Orientation of White Matter Fiber Bundles: A Comparative Study of Diffusion Tensor Imaging, Diffusional Kurtosis Imaging, and Diffusion Spectrum Imaging, AJNR. American journal of neuroradiology, 37 (2016) 1216-1222.
[264] D.Y. Kim, H.S. Kim, M.J. Goh, C.G. Choi, S.J. Kim, Utility of intravoxel incoherent motion MR imaging for distinguishing recurrent metastatic tumor from treatment effect following gamma knife radiosurgery: initial experience, AJNR. American journal of neuroradiology, 35 (2014) 2082-2090.
[265] H.S. Kim, C.H. Suh, N. Kim, C.G. Choi, S.J. Kim, Histogram analysis of intravoxel incoherent motion for differentiating recurrent tumor from treatment effect in patients with glioblastoma: initial clinical experience, AJNR. American journal of neuroradiology, 35 (2014) 490-497.
[266] A.M. Paschoal, R.F. Leoni, A.C. Dos Santos, F.F. Paiva, Intravoxel incoherent motion MRI in neurological and cerebrovascular diseases, NeuroImage. Clinical, 20 (2018) 705-714.
[267] E. Caverzasi, S.L. Hervey-Jumper, K.M. Jordan, I.V. Lobach, J. Li, V. Panara, C.A. Racine, V. Sankaranarayanan, B. Amirbekian, N. Papinutto, M.S. Berger, R.G. Henry, Identifying preoperative language

tracts and predicting postoperative functional recovery using HARDI q-ball fiber tractography in patients with gliomas, Journal of neurosurgery, 125 (2016) 33-45.
[268] F. Kogan, H. Hariharan, R. Reddy, Chemical Exchange Saturation Transfer (CEST) Imaging: Description of Technique and Potential Clinical Applications, Current radiology reports, 1 (2013) 102-114.
[269] C.K. Jones, M.J. Schlosser, P.C. van Zijl, M.G. Pomper, X. Golay, J. Zhou, Amide proton transfer imaging of human brain tumors at 3T, Magnetic resonance in medicine, 56 (2006) 585-592.
[270] R.M. Henkelman, G.J. Stanisz, S.J. Graham, Magnetization transfer in MRI: a review, NMR in biomedicine, 14 (2001) 57-64.
[271] J. Zhou, H. Zhu, M. Lim, L. Blair, A. Quinones-Hinojosa, S.A. Messina, C.G. Eberhart, M.G. Pomper, J. Laterra, P.B. Barker, P.C. van Zijl, J.O. Blakeley, Three-dimensional amide proton transfer MR imaging of gliomas: Initial experience and comparison with gadolinium enhancement, Journal of magnetic resonance imaging : JMRI, 38 (2013) 1119-1128.
[272] K. Sagiyama, T. Mashimo, O. Togao, V. Vemireddy, K.J. Hatanpaa, E.A. Maher, B.E. Mickey, E. Pan, A.D. Sherry, R.M. Bachoo, M. Takahashi, In vivo chemical exchange saturation transfer imaging allows early detection of a therapeutic response in glioblastoma, Proceedings of the National Academy of Sciences of the United States of America, 111 (2014) 4542-4547.
[273] O. Togao, T. Yoshiura, J. Keupp, A. Hiwatashi, K. Yamashita, K. Kikuchi, Y. Suzuki, S.O. Suzuki, T. Iwaki, N. Hata, M. Mizoguchi, K. Yoshimoto, K. Sagiyama, M. Takahashi, H. Honda, Amide proton transfer imaging of adult diffuse gliomas: correlation with histopathological grades, Neuro-oncology, 16 (2014) 441-448.
[274] A. Hosny, C. Parmar, J. Quackenbush, L.H. Schwartz, H. Aerts, Artificial intelligence in radiology, Nature reviews. Cancer, 18 (2018) 500-510.
[275] R.A. Castellino, Computer aided detection (CAD): an overview, Cancer imaging : the official publication of the International Cancer Imaging Society, 5 (2005) 17-19.
[276] D. Shen, G. Wu, H.I. Suk, Deep Learning in Medical Image Analysis, Annual review of biomedical engineering, 19 (2017) 221-248.
[277] G.C.T. Cawley, Nicola L. C. , On Over-fitting in Model Selection and Subsequent Selection Bias in Performance Evaluation, Journal of Machine Learning Research: 2079–2107., (2010).

PAPERS

PAPER I

PAPER II

Neuroradiology (2019) 61:545–555
https://doi.org/10.1007/s00234-019-02173-5

DIAGNOSTIC NEURORADIOLOGY

Dynamic susceptibility contrast and diffusion MR imaging identify oligodendroglioma as defined by the 2016 WHO classification for brain tumors: histogram analysis approach

Anna Latysheva[1] · Kyrre Eeg Emblem[2] · Petter Brandal[3] · Einar Osland Vik-Mo[4,5] · Jens Pahnke[6,7] · Kjetil Røysland[8] · John K. Hald[1] · Andrés Server[1]

Received: 15 November 2018 / Accepted: 16 January 2019 / Published online: 2 February 2019

Abstract

Purpose According to the revised World Health Organization (WHO) Classification of Tumors of the Central Nervous System (CNS) of 2016, oligodendrogliomas are now defined primarily by a specific molecular signature (presence of IDH mutation and 1p19q codeletion). The purpose of our study was to assess the value of dynamic susceptibility contrast MR imaging (DSC-MRI) and diffusion-weighted imaging (DWI) to characterize oligodendrogliomas and to distinguish them from astrocytomas.

Methods Seventy-one adult patients with untreated WHO grade II and grade III diffuse infiltrating gliomas and known 1p/19q codeletion status were retrospectively identified and analyzed using relative cerebral blood volume (rCBV) and apparent diffusion coefficient (ADC) maps based on whole-tumor volume histograms. The Mann-Whitney *U* test and logistic regression were used to assess the ability of rCBV and ADC to differentiate between oligodendrogliomas and astrocytomas both independently, but also related to the WHO grade. Prediction performance was evaluated in leave-one-out cross-validation (LOOCV).

Results Oligodendrogliomas showed significantly higher microvascularity (higher $rCBV_{Mean} \geq 0.80$, $p = 0.013$) and higher vascular heterogeneity (lower $rCBV_{Peak} \leq 0.044$, $p = 0.015$) than astrocytomas. Diffuse gliomas with higher cellular density (lower $ADC_{Mean} \leq 1094 \times 10^{-6}$ mm^2/s, $p = 0.009$) were more likely to be oligodendrogliomas than astrocytomas. Histogram analysis of rCBV and ADC was able to differentiate between diffuse astrocytomas (WHO grade II) and anaplastic astrocytomas (WHO grade III).

Conclusion Histogram-derived rCBV and ADC parameter may be used as biomarkers for identification of oligodendrogliomas and may help characterize diffuse gliomas based upon their genetic characteristics.

Keywords Diffuse glioma · Perfusion MRI · Diffusion MRI

Electronic supplementary material The online version of this article (https://doi.org/10.1007/s00234-019-02173-5) contains supplementary material, which is available to authorized users.

✉ Anna Latysheva
alatysheva@ous-hf.no

[1] Department of Radiology, Oslo University Hospital—Rikshospitalet, 4950 Nydalen, 0424 Oslo, Norway

[2] Department of Diagnostic Physics, Oslo University Hospital—Rikshospitalet, Oslo, Norway

[3] Department of Oncology, Oslo University Hospital—Radiumhospitalet, Oslo, Norway

[4] Department of Neurosurgery, Oslo University Hospital—Rikshospitalet, Oslo, Norway

[5] Faculty of Medicine, University of Oslo, Oslo, Norway

[6] Department of Neuro-/Pathology, Translational Neurodegeneration Research and Neuropathology Lab, University of Oslo and Oslo University Hospital, Oslo, Norway

[7] University of Lübeck, LIED, Lübeck, Germany

[8] Department of Biostatistics, Institute of Basic Medical Sciences, University of Oslo, Oslo, Norway

Introduction

Increasing evidence suggests that the presence of certain genetic aberrations in diffuse gliomas significantly improves prognostic accuracy compared to a diagnosis based exclusively on histology. Several large clinical trials have demonstrated more benefit from chemotherapy and better overall survival in patients with the presence of an IDH mutation and 1p19q codeleted gliomas (oligodendrogliomas) as compared to their genetic counterparts (astrocytomas). Differentiation between these two entities affects treatment strategy [1–4].

The revised fourth edition of the 2016 World Health Organization (WHO) Classification of Tumors of the Central Nervous System (CNS) incorporates genetic markers as the basis for classification [5]. For tumors harboring astrocytic and oligodendroglial elements, the genetic constitution will define it as an astrocytoma or oligodendroglioma [6, 7]. Specifically, diffuse gliomas with mutations in isocitrate dehydrogenase 1 or 2 (*IDH1* and *IDH2*) and whole-arm losses of 1p and 19q (1p/19q codeletion) will be classified as oligodendrogliomas, while those without 1p/19q codeletion will be classified as astrocytomas with or without *IDH1/2* mutation [5].

The current diagnostic standard for grading of diffuse glioma is histopathological evaluation of tissue specimens and molecular testing for the identification of genetic alteration (IDH1/2, IDH wild type, and 1p19q codeletion status). In cases with possible non-representative biopsy sampling and/or conflicting molecular results, it is important to identify robust non-invasive biomarkers that may help guide clinical decision making [6, 8].

Dynamic susceptibility contrast MR imaging (DSC-MRI) and diffusion-weighted imaging (DWI) are widely used techniques in brain tumor diagnostics. They allow characterization of specific tumor components, as well as functional signatures of the entire tumor and surrounding tissue. Relative cerebral blood volume (rCBV) from perfusion MRI is a reliable biomarker used to assess tissue vascularity and, what is most important for glioma grading, to estimate the apparent grade of neoangiogenesis [9–11]. Apparent diffusion coefficient (ADC) from DWI is used as a quantitative parameter to assess the grade of restrictive diffusion and to provide information about tissue structure and cellularity [12, 13].

Previous studies have demonstrated the ability of DSC and DWI to differentiate oligodendroglioma from astrocytoma, diffuse glioma WHO grade II from grade III, and 1p19q codeleted tumors from 1p19q non-codeleted tumors [14–19]. But in most studies which were performed prior to the updated WHO CNS tumor classification [20], oligoastrocytomas were included in oligodendroglioma's subgroup and were analyzed together. For this reason, non-invasive in vivo functional tissue information to compliment the new genetic entities oligodendroglioma (IDH mutant, 1p19q codeleted) and astrocytoma (IDH mutant, non-1p19q codeleted) is necessary.

The purposes of this retrospective study were to determine whether the rCBV and ADC values analyzed by histogram methods could help to classify oligodendrogliomas from astrocytic tumors and to distinguish diffuse gliomas WHO grade II from grade III.

Material and methods

Patient selection

From November 2006 until May 2013, a total of 352 consecutive adult patients with a histopathologic diagnosis of diffuse glioma were identified based on our clinical database. Of these, 87 diffuse glioma grades II and III were diagnosed histopathologically as oligodendroglioma, oligoastrocytoma, or astrocytoma, classified according to the 2007 WHO Classification of Tumors of the CNS, were selected. Molecular genetic status with respect to 1p19q codeletion was available for all patients and met the following inclusion criteria: (1) a baseline pretreatment MRI examination from our institution including DSC-MRI and DWI in addition to T1-weighted and T2-weighted images, (2) age > 18 years, and (3) a signed consent. From this group, 71 were included in the final study cohort. The following patients were excluded: (1) incomplete imaging sequences ($n = 8$), (2) insufficient image quality ($n = 6$), and (3) previously performed biopsy ($n = 2$). The patient inclusion and exclusion process is shown in Fig. 1.

Histopathologic, molecular genetic analysis and classification

Tumor tissue obtained from needle biopsy or surgical excision, routinely formalin-fixed and paraffin-embedded (FFPE), was reviewed and diagnosed by experienced neuropathologists. All tumors were initially classified as oligodendroglioma, astrocytoma, or oligoastrocytoma according to WHO 2007. They were, thereafter, divided into genetically defined subtypes according to WHO 2016 criteria: (1) oligodendroglioma-grade II with 1p/19q codeletion, (2) anaplastic oligodendroglioma-grade III with 1p/19q codeletion, (3) diffuse astrocytoma-grade II without 1p/19q codeletion, and (4) anaplastic astrocytoma-grade III without 1p19q codeletion. Astrocytoma subtypes were also stratified as IDH1/2 mutant or IDH1/2 wild type when IDH1/2 status was known.

In the period from 2006 to 2009, routine 1p19q codeletion status analysis was performed by polymerase chain reaction (PCR) using at least four of six microsatellite markers on 1p35–36 and 19q13 [21]. From 2009 on, multiplex ligation-dependent probe amplification (MLPA) was performed for

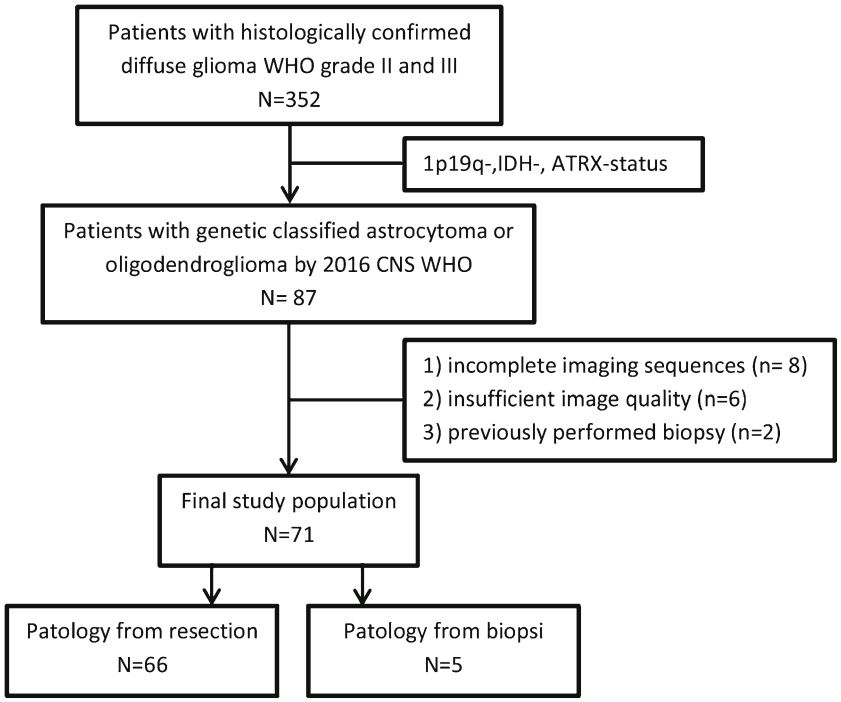

Fig. 1 Patient flow diagram

detection of 1p19q codeletion (SALSA MLPA probemix P088-C2), ATRX (SALSA MLPA P013 ATRX), TP53 (SALSA MLPA P056 TP53), IDH1 (isocitrate dehydrogenase 1 gene NM_005896.3), or IDH2 (isocitrate dehydrogenase 2 gene NM_005896.3) (SALSA MLPA P370 BRAF-IDH1-IDH2). MLPA is based on the ligation of two DNA oligonucleotides that hybridize adjacently to DNA target sequence and has previously been described [22]. The MLPA kit was assembled by MRC-Holland (Amsterdam, The Netherlands).

MR imaging

MRI was performed with a 1.5-T scanner (Sonata, Symphony, or Avanto; Siemens, Erlangen, Germany) equipped with an 8-channel (Sonata and Symphony imagers) or 12-channel (Avanto imager) phased-array head coil. The pretherapeutic MRI protocol included the following sequences: axial T2-weighted fast spin-echo (repetition time, TR 4000 ms; echo time, TE 104 ms; slice thickness, 5 mm; flip angel 146°), coronal fluid-attenuated inversion recovery (TR, 9000; TE, 108 ms; slice thickness, 5 mm; flip angel 120°), and axial T1-weighted spin-echo (TR, 500 ms; TE 77 ms; section thickness, 5 mm; flip angel 120°).

DWI was obtained using an axial echo-planar spin-echo sequence (TR, 2900 ms; TE 84 ms; section thickness 5 mm) before the injection of contrast agent. Diffusion was measured in three orthogonal directions using *b* values 0, 500, and 1000 s/mm^2.

Echo-planar gradient-echo DSC-MRI was acquired during contrast agent administration with TR, 1430 ms; TE 46 ms (12 axial sections) to TR, 1590 ms; TE 52 ms (14 axial sections); bandwidth, 1345 Hz/pixel; voxel size, 1.80 × 1.80 × 5 mm^3; intersection gap, 1.5 mm; 50 time points; flip angel 90°. After approximately eight time points, 0.2 mmol/kg of gadobutrol (Gadovist; Bayer Pharma AG, Berlin, Germany) was injected at a rate of 5 mL/s, immediately followed by a 20-mL bolus of NaCl (9 mg/mL) injected at a rate of at 5 mL/s. Post-contrast T1-weighted images were acquired after completion of the DSC-MRI [15].

Image processing

Data analysis was performed independently by two neuroradiologists and blinded to the histopathological and genetic/molecular characteristics. Tumor outlining and processing of ADC and rCBV maps were performed using nordicICE (NordicNeuroLab AS, Bergen, Norway). A series of ROIs were manually drawn on every representative slice for the entire tumor volume separately on ADC maps and T2-weighted images (Fig. 2). The borders were drawn at the transition between abnormal hyperintensity and normal parenchymal signal intensity based on visual evaluation with preferably avoidance of cystic components. The entire tumor volume includes both enhanced and non-enhanced components [23, 24]. Discrepancies were resolved by consensus reading.

Standard tracer kinetic models were used for creating CBV maps from DSC-MRI, corrected for potential contrast agent leakage from blood-brain barrier breakdown and normalized with respect to blood volume values from normal-appearing tissue to obtain relative CBV [24]. ADC maps from DWI were created using standard Stejskal-Tanner diffusion approximation [17, 25]. Whole-tumor normalized histogram

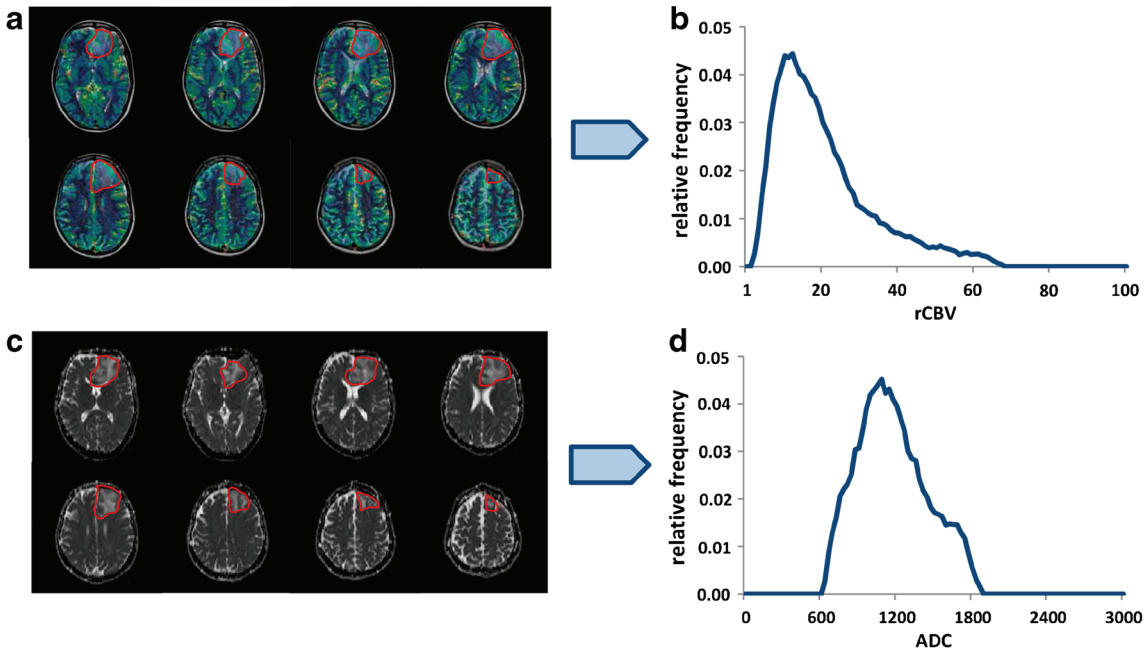

Fig. 2 Generation of rCBV and ADC histograms. Regions with signal hyperintensities were segmented on axial T2 images, coregistrated with rCBV maps and corresponding rCBV histogram in a 44-year-old woman with anaplastic oligodendroglioma (**a**, **b**). Total tumor volume was segmented on ADC maps in the same patient with corresponding ADC histogram (**c**, **d**)

distributions of the ADC and rCBV maps were created as described elsewhere [24]. In short, using MATLAB 2013 (MathWorks, Natick, Mass), 100 bin histograms were created over an ADC range of 0–300 and an rCBV range of 0–7.5 (ratios; arbitrary units), respectively. The histograms were normalized by making all areas under the curves equal to one to correct for varying tumor sizes [23]. To reduce the effect of outliers, all ADC and rCBV values below the 5% percentile and over the 95% percentile were excluded. The maximum peak heights of the normalized histogram (ADC_{Peak} and $rCBV_{Peak}$), as well as means of the tumor regions of interests (ADC_{Mean}, $rCBV_{Mean}$), were calculated. $rCBV_{Peak}$ and ADC_{Peak} were statistically used as measures of vascular and cellular tumor heterogeneity, respectively [17, 23].

Statistical analysis

The Mann-Whitney *U* test was used to assess ability of histogram-derived parameters to identify patients suggestive of an oligodendroglioma independent of histopathologic grade, but also in subgroups related to the WHO grade (II and III). The overall diagnostic performance was analyzed by the receiver operating characteristic curve (ROC), including values of sensitivity, specificity, and area under the curve (AUC). Optimal cutoff points based on the Youden index were also estimated. Association between genetically defined subtypes, WHO grade, and ADC and rCBV parameters was evaluated by both univariate and multivariate logistic regressions The leave-one-out cross-validation (LOOCV) algorithm was used to estimate how accurately a predictive model differentiates between glioma subtypes. For all cases, an analysis value of less than 0.05 was considered to indicate a significant difference. The Holm-Bonferroni correction was used to control for multiple comparisons. Statistical analysis was performed using SPSS version 18 software (SPSS, Chicago, USA) and R version 3.3.3 (R Project for Statistical Computing; http://www.r-project.org).

Ethical consideration

Institutional and regional medical ethics committees approved this study (REC-number 2013/81 2.2006.541).

Results

Study population

Seventy-one patients (37 women, 34 men; median age, 48 years; range, 18–82 years) with diffuse infiltrating glioma grade II and III met all inclusion criteria and made up the study population. 1p19q status was considered for all patients, and IDH profile (IDH1 mutated, IDH2 mutated, or IDH wild type) was determined for 57.7% of the cases. We found that 28% of previously diagnosed oligodendrogliomas and almost 85% of oligoastrocytomas were reclassified as astrocytomas.

Table 1 summarizes patient demographics, histopathology, and molecular genetic status.

Table 1 Patient demographics, histopathology, and molecular genetic status

	Total ($n = 71$)	Oligodendroglioma ($n = 33$)	Astrocytoma ($n = 38$)
Age, mean (SD) (years)	48 (11.2)	49 (11.3)	38 (12.1)
Female sex (no.)	36 (52.2%)	19 (57.6%)	17 (47.2%)
Tumor grade			
WHO II	42 (59.1%)	23 (54.7%)	19 (45.3%)
WHO III	29 (40.9%)	10 (34.4%)	19 (65.6%)
Known IDH mutation status	43 (57.7%)	18 (41.9%)	25 (58.1%)
IDH—mutant	41 (95.3%)	18 (100%)	23 (92%)
IDH—wild type	2 (4.6%)		2 (8%)

DSC-MRI and DWI histogram parameters for differentiation between oligodendrogliomas and astrocytomas

Detailed results for DSC-MRI and DWI parameters based on histogram analysis to distinguish oligodendrogliomas from astrocytomas are summarized in Table S1. ROC analysis with suggested optimal cutoff value and estimated positive and negative predictive values for each of parameters with significant probability values is given in Table 2.

Oligodendrogliomas showed a significantly higher $rCBV_{Mean}$ and lower $rCBV_{Peak}$ compared to diffuse astrocytomas ($p = 0.013$; $p = 0.015$, respectively). ROC analysis yielded AUC values of 77% using the parameter $rCBV_{Mean}$ and 80% for the parameter $rCBV_{Peak}$, respectively, for discrimination of oligodendrogliomas from diffuse astrocytomas. Figure 3 illustrates average $rCBV_{Peak}$ histograms for all oligodendrogliomas and astrocytomas regardless of grade.

Diffuse gliomas with lower ADC_{Mean} were more likely to be oligodendroglioma rather than astrocytoma ($p = 0.009$). Higher ADC_{Peak} and lower ADC_{Mean} indicated oligodendroglioma when the glioma grade II subgroup was analyzed separately ($p = 0.042$; $p = 0.001$, respectively).

Figure 4 demonstrates boxplots with distribution range of $rCBV_{Peak}$, $rCBV_{Mean}$, and ADC_{Mean} values in different subgroups of diffuse gliomas.

In our study, the linear combination of most significant variables ($rCBV_{Peak}$, $rCBV_{Mean}$, and ADC_{Mean}) based on logistic regression had the superior diagnostic performance in differentiating oligodendrogliomas from diffuse astrocytomas. ROC analysis yielded AUC value of 84% (Table 2, Fig. 5). In LOOCV, this combined predictive model have 28% error rate when all gliomas were included and 21% in grade II gliomas subtype; however, misclassification rate was increased to 42% when just grade III gliomas were analyzed.

Table 2 Results of ROC curve analysis and error rate estimated using leave-one-out cross-validation of DWI and DSC-MRI histogram-derived parameters in patients with diffuse glioma grade II and III

	Cutoff points	Sensitivity % (95% CI)	Specificity % (95% CI)	Positive predictive value % (95% CI)	Negative predictive value % (95% CI)	AUC	Error rate (%)**
Oligodendroglioma vs astrocytoma (WHO grade II and III)							
ADC_{Mean}	$\leq 1094 \times 10^{-6}$ mm^2/s	63 (54; 82)	61 (51; 83)	65 (52; 81)	73 (61; 87)	76	32
$rCBV_{Peak}$	≤ 0.044	78 (56; 82)	78 (54; 93)	76 (63; 88)	76 (63; 88)	80	30
$rCBV_{Mean}$	≥ 0.80 mL/100 g	68 (52; 90)	93 (69; 99)	65 (48; 83)	92 (70; 98)	77	32
Linear combination based on logistic regression*		92 (62; 96)	81 (69; 99)	88 (62; 96)	80 (70; 98)	84	28
Oligodendroglioma vs astrocytoma (WHO grade II)							
ADC_{Peak}	≥ 0.043	57 (37; 75)	95 (68; 99)	54 (36; 75)	94 (70; 98)	69	36
ADC_{Mean}	$\leq 1101 \times 10^{-6}$ mm^2/s	84 (70; 93)	65 (47; 82)	85 (70; 93)	67 (49; 82)	75	33
Oligodendroglioma vs astrocytoma (WHO grade III)							
$rCBV_{Peak}$	≤ 0.046	68 (49; 85)	73 (61; 87)	65 (46; 81)	72 (61; 87)	73	34

CI confidence interval, *AUC* area under the curve

*Linear combination included most significant variables: ADC_{Mean}, $rCBV_{Mean}$, and $rCBV_{Peak}$

**Error rate was estimated using leave-one-out cross-validation

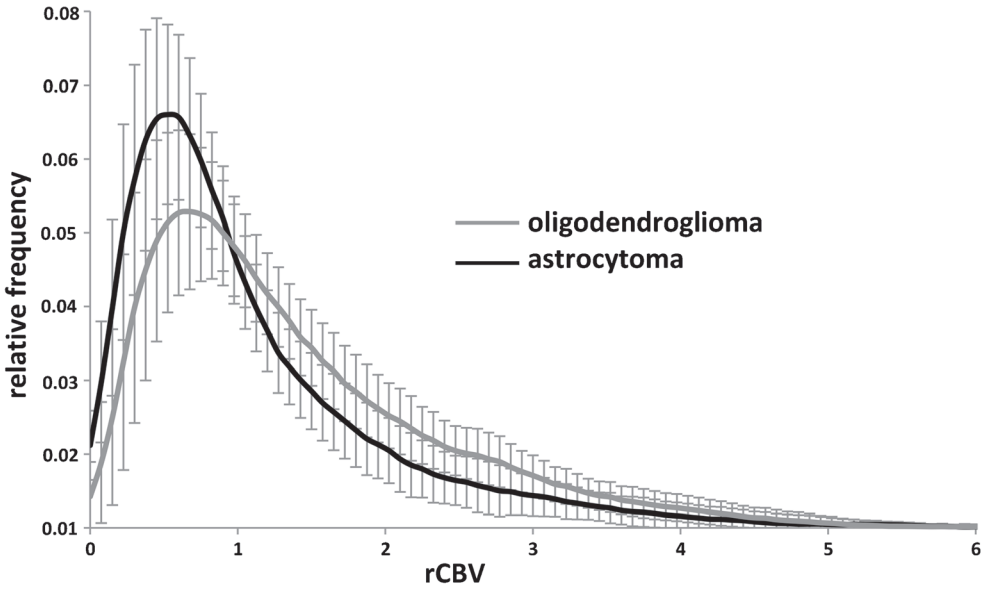

Fig. 3 Whole-volume average $rCBV_{Peak}$ histograms (± 1.96 standard error of mean (SEM)) of all oligodendroglioma and astrocytomas WHO grades II and III

DSC-MRI and DWI histogram parameters for differentiation between WHO grade II and grade III

The correlations between $rCBV_{Peak}$, $rCBV_{Mean}$, ADC_{Peak}, and ADC_{Mean} and WHO grade are demonstrated in Table S2. There was a substantial overlap in rCBV and ADC histogram-derived biomarkers between WHO glioma grade II and III, and no significant differences were observed in the univariate model. LOOCV performed with inclusion of these four parameters showed also high error rate (49%). In the multivariate regression model, the value of ADC_{Mean} was an independent variable for discriminating between astrocytoma WHO grades II and III ($p = 0.03$). The odds of astrocytoma WHO grade III increased in low ADC_{Mean} lesions (OR, 0.92 for each unit decrease in ADC_{Mean} with 95% CI, 0.82–0.98).

Discussion

In our study, we identified microvascularity parameters suggesting a denser and more heterogeneous vascular distribution in oligodendrogliomas compared to those of astrocytomas. Measures of rCBV parameters showed fair diagnostic performance and further improved diagnostic value in combination with ADC parameters for discriminating oligodendroglioma from astrocytoma.

Our results imply that histogram-derived rCBV and ADC values could be useful imaging biomarkers for differentiating these two types of diffuse glioma. Non-invasive biomarkers are of special relevance in cases with ambiguous biopsy results, deep-seated inoperable tumors, and in patients with primary or recurrent tumors where a "wait-and-see" management is pursued. Moreover, identification of oligodendroglioma is also

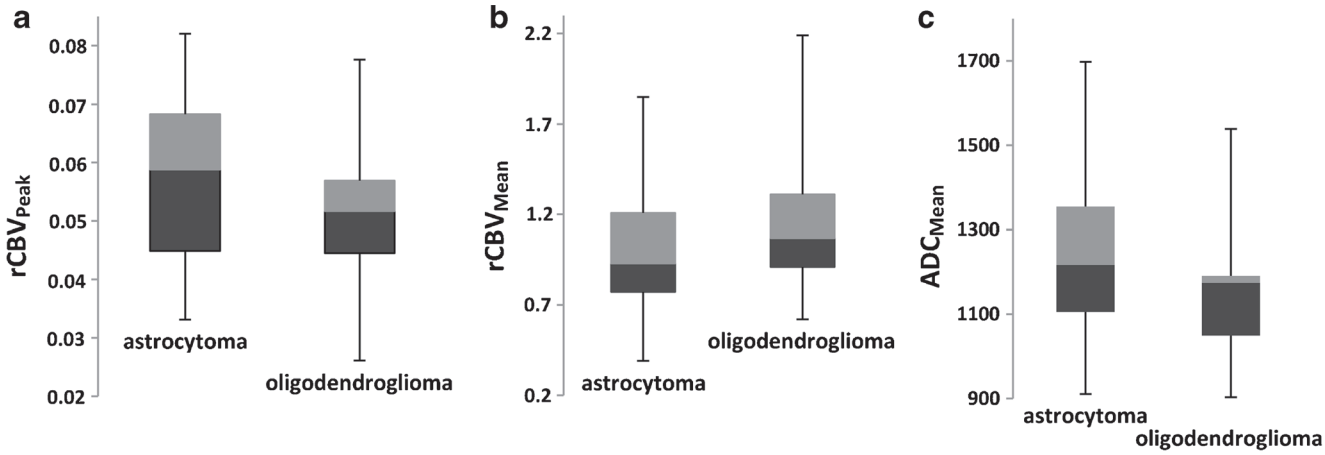

Fig. 4 Boxplots with distribution range of **a** $rCBV_{Peak}$, **b** $rCBV_{Mean}$, and **c** ADC_{Mean} values in different subgroups of diffuse gliomas

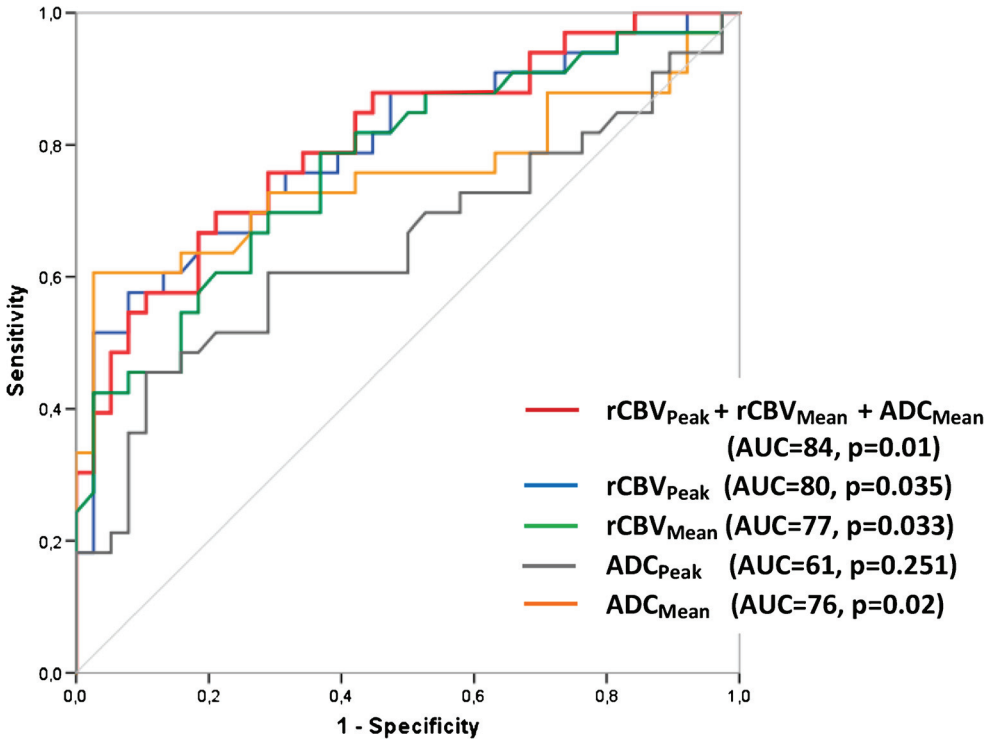

Fig. 5 Receiver operating characteristic (ROC) curves for imaging derived histogram biomarkers ($rCBV_{Peak}$, $rCBV_{Mean}$, ADC_{Mean}, ADC_{Peak}) used to identify oligodendroglioma

of importance for the choice of therapeutic strategy. Patients with oligodendroglial tumor grade III have been shown to benefit from procarbazine, lomustine, and vincristine (PCV), whereas in patients with astrocytoma grade III, temozolomide has been shown to be beneficial [1, 2].

The key finding in our study is higher vascularity (high $rCBV_{Mean}$) in oligodendrogliomas as compared to astrocytomas, regardless of histopathological grade. A few retrospective studies have attempted to correlate 1p19q codeletion with rCBV and have demonstrated findings similar to ours [19, 26]. Jenkinson et al. showed that rCBV > 1.59 predicted 1p/19q status with 92% sensitivity and 76% specificity [18]. In contrast to our results, Yoon et al. found that the volume transfer coefficient (K^{trans}), extravascular extracellular distribution volume (V_e), and rCBV values were not significantly different between the oligodendroglioma group and grade II/III astrocytoma group [27]. Increased blood volumes in oligodendrogliomas could be explained by higher metabolic demands associated with 1p/19q codeletion [28]. Increased F-FDG uptake was demonstrated in positron emission tomography and single-photon emission computed tomography studies [28, 29]. Moreover, high intratumoral metabolism may also explain increased sensitivity to chemotherapy. It was suggested that alkylating agents exert a more beneficial effect in tumors with higher cell turnover and DNA synthesis rates, which are known to correlate with higher glucose utilization and metabolism [30, 31]. We did not observe differences in vascular densities between oligodendroglioma and astrocytoma in grade II tumors. While this result is based on the new WHO classification, our finding corroborates previous work and suggests that 1p/19q codeletion alone is not categorically linked to vascular status and apparent neoangiogenesis in low-grade tumors. Instead, our data also suggest higher vascular heterogeneity (low $rCBV_{Peak}$) in oligodendrogliomas compared to astrocytomas regardless of tumor grade. This idea is also consistent with previous findings from our group [15], as well as that of Cha et al. who also showed that rCBVmax measurements varied greatly within each individual oligodendroglioma (1.29 to 9.24), whereas astrocytomas tended to have little relative variation (0.48 to 1.34) [32].

Another important finding in our study was the higher cellular density (low ADC_{Mean}) in patients with oligodendroglioma compared to astrocytoma. These results parallel those of previous studies reporting lower maximum ADC, and a lower mean histogram ADC, in tumors with 1p/19q loss compared to those without [16, 17, 33]. There are several possible explanations for the increase of restrictive diffusion in oligodendroglioma. One of them is the presence of calcification which is common in oligodendroglioma and may limit water content as well as and hinder water movement [34]. Classical oligodendroglial tumors are often highly cellular lesions with closely packed, relatively small cells in central regions and prominent secondary structure formation, such as clustering of tumor cells around the

perikarya of preexisting neurons (satellitosis) and surrounding cortical small vessels (perivascular aggregates) [35]. These formations may also delay passage of small molecules as they need to navigate around cellular obstacles.

In our study, ADC_{Peak} and ADC_{Mean} values were not significantly different between oligodendroglioma grade II and oligodendroglioma grade III. Our findings therefore do not seem to corroborate those of Lin et al. who reported a significantly lower normalized ADC in high-grade oligodendrogliomas compared to low-grade oligodendrogliomas [36]. These differences, however, may be explained through differences in methodology (hotspot method vs histogram approach).

Other authors have demonstrated that tumors with 1p/19q codeletion tend to have a narrow histogram peak (higher ADC_{Peak}) indicating greater homogeneity, compared to tumors with intact 1p/19q [17]. In our study, this association was observed just for grade II tumors, a finding that most likely may be explained by higher numbers of edematous areas, hemorrhage, and cystic or mucinous degeneration in anaplastic tumors compared to low-grade tumors.

Moreover, we found that combined use of ADC and rCBV histogram parameters also improved the ability to identify oligodendroglial from astrocytic tumors. This result is in line with those of a recently published study that found that ADC in combination with rCBV, T2 volume enhancement, and contrast enhancement distinguished IDH mutant/1p19q codeleted from IDH mutant/1p19q non-codeleted gliomas [37]. In contradiction, neither rCBV nor ADC parameters could distinguish between histopathologic grades in diffuse gliomas as previously suggested [38].

Our study has limitations. First, two different assays (FISH and MLPA) were used for detection of 1p and 19q deletions in tumoral tissue. 1p/19q codeletion as detected by FISH could in principle be loss of alleles and not the whole arms, thereby yielding false positive results. Although MLPA in principle is more sensitive and less dependent on individual interpretation than FISH, both technologies have showed concordant results in validation studies [6, 39]. Second, there is a risk of classification errors in histopathological diagnoses of tumor samples derived from biopsies, particularly with regard to the differentiation between grade II and grade III gliomas [8, 40]. Third, our study may also be limited by the preselection of patients with histological oligodendroglial features only. Fourth, IDH1/2 status was not available in all the patients (57.7% of patients cohort). However, a large number of studies show that IDH1/2 mutation occurs in all 1p19q-codeleted tumors and the great majority of diffuse glioma grade II/III also falls into the IDH mutant category [6, 7, 41–45]. Finally, as is true across all imaging modalities, the manual tumor outlining performed in our study is subjective and reproducibility may be challenged when used in combination with advanced imaging techniques. However, the high intraobserver agreement of the histogram method suggests that subtle changes in ROI editing are relatively unimportant, given the large number of data points included in the histogram [23].

In conclusion, non-invasive glioma assessment is an important supplement to neuropathological evaluation in newly diagnosed disease and longitudinal follow-up. Histograms derived DSC-MRI, and DWI parameters may be used as non-invasive imaging biomarkers for identification of oligodendroglioma as defined by the new WHO 2016 classification criteria.

Funding This work was funded by the Southeastern Norway Regional Health Authority Extended Career Grants 2017073, 2013069 (KEE), the Research Council of Norway Grant ES435705 (KEE), Deutsche Forschungsgemeinschaft/Germany (DFG PA930/9, DFG PA930/12) (JP), the Leibniz Society/Germany (SAW-2015-IPB-2) (JP), HelseSØ/Norway (2016062) (JP), Norsk forskningsrådet/Norway (247179 NeuroGeM, 251290 FRIMEDIO, 260786 PROP-AD) (JP) and Horizon 2020/European Union (643417 (PROP-AD) (JP).

Compliance with ethical standards

Conflict of interest KEE has intellectual property rights with NordicNeuroLaB, Bergen Oslo.

Ethical approval All procedures performed in the studies involving human participants were in accordance with the ethical standards of the institutional and/or national research committee and with the 1964 Helsinki Declaration and its later amendments or comparable ethical standards.

Informed consent Informed consent was obtained from all individual participants included in the study.

References

1. van den Bent MJ, Brandes AA, Taphoorn MJ, Kros JM, Kouwenhoven MC, Delattre JY, Bernsen HJ, Frenay M, Tijssen CC, Grisold W, Sipos L, Enting RH, French PJ, Dinjens WN, Vecht CJ, Allgeier A, Lacombe D, Gorlia T, Hoang-Xuan K (2013) Adjuvant procarbazine, lomustine, and vincristine chemotherapy in newly diagnosed anaplastic oligodendroglioma: long-term follow-up of EORTC brain tumor group study 26951. J Clin Oncol 31(3):344–350. https://doi.org/10.1200/jco.2012.43.2229
2. Cairncross G, Wang M, Shaw E, Jenkins R, Brachman D, Buckner J, Fink K, Souhami L, Laperriere N, Curran W, Mehta M (2013) Phase III trial of chemoradiotherapy for anaplastic oligodendroglioma: long-term results of RTOG 9402. J Clin Oncol 31(3):337–343. https://doi.org/10.1200/jco.2012.43.2674
3. Buckner JC, Shaw EG, Pugh SL, Chakravarti A, Gilbert MR, Barger GR, Coons S, Ricci P, Bullard D, Brown PD, Stelzer K, Brachman D, Suh JH, Schultz CJ, Bahary JP, Fisher BJ, Kim H, Murtha AD, Bell EH, Won M, Mehta MP, Curran WJ Jr (2016) Radiation plus procarbazine, CCNU, and vincristine in low-grade

glioma. N Engl J Med 374(14):1344–1355. https://doi.org/10.1056/NEJMoa1500925
4. Sanson M, Marie Y, Paris S, Idbaih A, Laffaire J, Ducray F, El Hallani S, Boisselier B, Mokhtari K, Hoang-Xuan K, Delattre JY (2009) Isocitrate dehydrogenase 1 codon 132 mutation is an important prognostic biomarker in gliomas. J Clin Oncol 27(25):4150–4154. https://doi.org/10.1200/jco.2009.21.9832
5. Louis DN, Perry A, Reifenberger G, von Deimling A, Figarella-Branger D, Cavenee WK, Ohgaki H, Wiestler OD, Kleihues P, Ellison DW (2016) The 2016 World Health Organization Classification of Tumors of the Central Nervous System: a summary. Acta Neuropathol 131(6):803–820. https://doi.org/10.1007/s00401-016-1545-1
6. Ballester LY, Huse JT, Tang G, Fuller GN (2017) Molecular classification of adult diffuse gliomas: conflicting IDH1/IDH2, ATRX and 1p/19q results. Hum Pathol 69:15–22. https://doi.org/10.1016/j.humpath.2017.05.005
7. Sahm F, Reuss D, Koelsche C, Capper D, Schittenhelm J, Heim S, Jones DT, Pfister SM, Herold-Mende C, Wick W, Mueller W, Hartmann C, Paulus W, von Deimling A (2014) Farewell to oligoastrocytoma: in situ molecular genetics favor classification as either oligodendroglioma or astrocytoma. Acta Neuropathol 128(4):551–559. https://doi.org/10.1007/s00401-014-1326-7
8. Giannini C, Scheithauer BW, Weaver AL, Burger PC, Kros JM, Mork S, Graeber MB, Bauserman S, Buckner JC, Burton J, Riepe R, Tazelaar HD, Nascimento AG, Crotty T, Keeney GL, Pernicone P, Altermatt H (2001) Oligodendrogliomas: reproducibility and prognostic value of histologic diagnosis and grading. J Neuropathol Exp Neurol 60(3):248–262
9. Lev MH, Ozsunar Y, Henson JW, Rasheed AA, Barest GD, Harsh GR, Fitzek MM, Chiocca EA, Rabinov JD, Csavoy AN, Rosen BR, Hochberg FH, Schaefer PW, Gonzalez RG (2004) Glial tumor grading and outcome prediction using dynamic spin-echo MR susceptibility mapping compared with conventional contrast-enhanced MR: confounding effect of elevated rCBV of oligodendrogliomas [corrected]. AJNR Am J Neuroradiol 25(2):214–221
10. Law M, Oh S, Babb JS, Wang E, Inglese M, Zagzag D, Knopp EA, Johnson G (2006) Low-grade gliomas: dynamic susceptibility-weighted contrast-enhanced perfusion MR imaging–prediction of patient clinical response. Radiology 238(2):658–667. https://doi.org/10.1148/radiol.2382042180
11. Knopp EA, Cha S, Johnson G, Mazumdar A, Golfinos JG, Zagzag D, Miller DC, Kelly PJ, Kricheff II (1999) Glial neoplasms: dynamic contrast-enhanced T2*-weighted MR imaging. Radiology 211(3):791–798. https://doi.org/10.1148/radiology.211.3.r99jn46791
12. Le Bihan D (1991) Molecular diffusion nuclear magnetic resonance imaging. Magn Reson Q 7(1):1–30
13. Kono K, Inoue Y, Nakayama K, Shakudo M, Morino M, Ohata K, Wakasa K, Yamada R (2001) The role of diffusion-weighted imaging in patients with brain tumors. AJNR Am J Neuroradiol 22(6):1081–1088
14. Chawla S, Krejza J, Vossough A, Zhang Y, Kapoor GS, Wang S, O'Rourke DM, Melhem ER, Poptani H (2013) Differentiation between oligodendroglioma genotypes using dynamic susceptibility contrast perfusion-weighted imaging and proton MR spectroscopy. AJNR Am J Neuroradiol 34(8):1542–1549. https://doi.org/10.3174/ajnr.A3384
15. Emblem KE, Scheie D, Due-Tonnessen P, Nedregaard B, Nome T, Hald JK, Beiske K, Meling TR, Bjornerud A (2008) Histogram analysis of MR imaging-derived cerebral blood volume maps: combined glioma grading and identification of low-grade oligodendroglial subtypes. AJNR Am J Neuroradiol 29(9):1664–1670. https://doi.org/10.3174/ajnr.A1182
16. Fellah S, Caudal D, De Paula AM, Dory-Lautrec P, Figarella-Branger D, Chinot O, Metellus P, Cozzone PJ, Confort-Gouny S, Ghattas B, Callot V, Girard N (2013) Multimodal MR imaging (diffusion, perfusion, and spectroscopy): is it possible to distinguish oligodendroglial tumor grade and 1p/19q codeletion in the pretherapeutic diagnosis? AJNR Am J Neuroradiol 34(7):1326–1333. https://doi.org/10.3174/ajnr.A3352
17. Jenkinson MD, du Plessis DG, Smith TS, Brodbelt AR, Joyce KA, Walker C (2010) Cellularity and apparent diffusion coefficient in oligodendroglial tumours characterized by genotype. J Neuro-Oncol 96(3):385–392. https://doi.org/10.1007/s11060-009-9970-9
18. Jenkinson MD, Smith TS, Joyce KA, Fildes D, Broome J, du Plessis DG, Haylock B, Husband DJ, Warnke PC, Walker C (2006) Cerebral blood volume, genotype and chemosensitivity in oligodendroglial tumours. Neuroradiology 48(10):703–713. https://doi.org/10.1007/s00234-006-0122-z
19. Whitmore RG, Krejza J, Kapoor GS, Huse J, Woo JH, Bloom S, Lopinto J, Wolf RL, Judy K, Rosenfeld MR, Biegel JA, Melhem ER, O'Rourke DM (2007) Prediction of oligodendroglial tumor subtype and grade using perfusion weighted magnetic resonance imaging. J Neurosurg 107(3):600–609. https://doi.org/10.3171/jns-07/09/0600
20. Louis DN, Ohgaki H, Wiestler OD, Cavenee WK, Burger PC, Jouvet A, Scheithauer BW, Kleihues P (2007) The 2007 WHO classification of tumours of the central nervous system. Acta Neuropathol 114(2):97–109. https://doi.org/10.1007/s00401-007-0243-4
21. Scheie D, Andresen PA, Cvancarova M, Bo AS, Helseth E, Skullerud K, Beiske K (2006) Fluorescence in situ hybridization (FISH) on touch preparations: a reliable method for detecting loss of heterozygosity at 1p and 19q in oligodendroglial tumors. Am J Surg Pathol 30(7):828–837. https://doi.org/10.1097/01.pas.0000213250.44822.2e
22. Natte R, van Eijk R, Eilers P, Cleton-Jansen AM, Oosting J, Kouwenhove M, Kros JM, van Duinen S (2005) Multiplex ligation-dependent probe amplification for the detection of 1p and 19q chromosomal loss in oligodendroglial tumors. Brain Pathol (Zurich, Switzerland) 15(3):192–197
23. Emblem KE, Nedregaard B, Nome T, Due-Tonnessen P, Hald JK, Scheie D, Borota OC, Cvancarova M, Bjornerud A (2008) Glioma grading by using histogram analysis of blood volume heterogeneity from MR-derived cerebral blood volume maps. Radiology 247(3):808–817. https://doi.org/10.1148/radiol.2473070571
24. Emblem KE, Pinho MC, Zollner FG, Due-Tonnessen P, Hald JK, Schad LR, Meling TR, Rapalino O, Bjornerud A (2015) A generic support vector machine model for preoperative glioma survival associations. Radiology 275(1):228–234. https://doi.org/10.1148/radiol.14140770
25. Pope WB, Kim HJ, Huo J, Alger J, Brown MS, Gjertson D, Sai V, Young JR, Tekchandani L, Cloughesy T, Mischel PS, Lai A, Nghiemphu P, Rahmanuddin S, Goldin J (2009) Recurrent glioblastoma multiforme: ADC histogram analysis predicts response to bevacizumab treatment. Radiology 252(1):182–189. https://doi.org/10.1148/radiol.2521081534
26. Kapoor GS, Gocke TA, Chawla S, Whitmore RG, Nabavizadeh A, Krejza J, Lopinto J, Plaum J, Maloney-Wilensky E, Poptani H, Melhem ER, Judy KD, O'Rourke DM (2009) Magnetic resonance perfusion-weighted imaging defines angiogenic subtypes of oligodendroglioma according to 1p19q and EGFR status. J Neuro-Oncol 92(3):373–386. https://doi.org/10.1007/s11060-009-9880-x
27. Yoon HJ, Ahn KJ, Lee S, Jang JH, Choi HS, Jung SL, Kim BS, Jeun SS, Hong YK (2017) Differential diagnosis of oligodendroglial and astrocytic tumors using imaging results: the added value of perfusion MR imaging. Neuroradiology 59:665–675. https://doi.org/10.1007/s00234-017-1851-x
28. Walker C, Haylock B, Husband D, Joyce KA, Fildes D, Jenkinson MD, Smith T, Broome J, Kopitzki K, du Plessis DG, Prosser J,

Vinjamuri S, Warnke PC (2006) Genetic and metabolic predictors of chemosensitivity in oligodendroglial neoplasms. Br J Cancer 95(10):1424–1431. https://doi.org/10.1038/sj.bjc.6603390

29. Shinozaki N, Uchino Y, Yoshikawa K, Matsutani T, Hasegawa A, Saeki N, Iwadate Y (2011) Discrimination between low-grade oligodendrogliomas and diffuse astrocytoma with the aid of 11C-methionine positron emission tomography. J Neurosurg 114(6): 1640–1647. https://doi.org/10.3171/2010.11.jns10553
30. Herholz K, Pietrzyk U, Voges J, Schroder R, Halber M, Treuer H, Sturm V, Heiss WD (1993) Correlation of glucose consumption and tumor cell density in astrocytomas. A stereotactic PET study. J Neurosurg 79(6):853–858. https://doi.org/10.3171/jns.1993.79.6.0853
31. Brock CS, Young H, O'Reilly SM, Matthews J, Osman S, Evans H, Newlands ES, Price PM (2000) Early evaluation of tumour metabolic response using [18F]fluorodeoxyglucose and positron emission tomography: a pilot study following the phase II chemotherapy schedule for temozolomide in recurrent high-grade gliomas. Br J Cancer 82(3):608–615. https://doi.org/10.1054/bjoc.1999.0971
32. Cha S, Tihan T, Crawford F, Fischbein NJ, Chang S, Bollen A, Nelson SJ, Prados M, Berger MS, Dillon WP (2005) Differentiation of low-grade oligodendrogliomas from low-grade astrocytomas by using quantitative blood-volume measurements derived from dynamic susceptibility contrast-enhanced MR imaging. AJNR Am J Neuroradiol 26(2):266–273
33. Johnson DR, Diehn FE, Giannini C, Jenkins RB, Jenkins SM, Parney IF, Kaufmann TJ (2017) Genetically defined oligodendroglioma is characterized by indistinct tumor borders at MRI. AJNR Am J Neuroradiol 38:678–684. https://doi.org/10.3174/ajnr.A5070
34. Smits M (2016) Imaging of oligodendroglioma. Br J Radiol 89(1060):20150857. https://doi.org/10.1259/bjr.20150857
35. Wesseling P, van den Bent M, Perry A (2015) Oligodendroglioma: pathology, molecular mechanisms and markers. Acta Neuropathol 129(6):809–827. https://doi.org/10.1007/s00401-015-1424-1
36. Lin Y, Xing Z, She D, Yang X, Zheng Y, Xiao Z, Wang X, Cao D (2017) IDH mutant and 1p/19q co-deleted oligodendrogliomas: tumor grade stratification using diffusion-, susceptibility-, and perfusion-weighted MRI. Neuroradiology 59(6):555–562. https://doi.org/10.1007/s00234-017-1839-6
37. Leu K, Ott GA, Lai A, Nghiemphu PL, Pope WB, Yong WH, Liau LM, Cloughesy TF, Ellingson BM (2017) Perfusion and diffusion MRI signatures in histologic and genetic subtypes of WHO grade II-III diffuse gliomas. J Neuro-Oncol 134:177–188. https://doi.org/10.1007/s11060-017-2506-9
38. Delgado AF, Delgado AF (2017) Discrimination between glioma grades II and III using dynamic susceptibility perfusion MRI: a meta-analysis. AJNR Am J Neuroradiol 38(7):1348–1355. https://doi.org/10.3174/ajnr.A5218
39. Franco-Hernandez C, Martinez-Glez V, de Campos JM, Isla A, Vaquero J, Gutierrez M, Casartelli C, Rey JA (2009) Allelic status of 1p and 19q in oligodendrogliomas and glioblastomas: multiplex ligation-dependent probe amplification versus loss of heterozygosity. Cancer Genet Cytogenet 190(2):93–96. https://doi.org/10.1016/j.cancergencyto.2008.09.017
40. van den Bent MJ (2010) Interobserver variation of the histopathological diagnosis in clinical trials on glioma: a clinician's perspective. Acta Neuropathol 120(3):297–304. https://doi.org/10.1007/s00401-010-0725-7
41. Kim SI, Lee Y, Won JK, Park CK, Choi SH, Park SH (2017) Reclassification of mixed oligoastrocytic tumors using a genetically integrated diagnostic approach. J Pathol Transl Med 52:28–36. https://doi.org/10.4132/jptm.2017.09.25
42. Brat DJ, Verhaak RG, Aldape KD, Yung WK, Salama SR, Cooper LA, Rheinbay E, Miller CR, Vitucci M, Morozova O, Robertson AG, Noushmehr H, Laird PW, Cherniack AD, Akbani R, Huse JT, Ciriello G, Poisson LM, Barnholtz-Sloan JS, Berger MS, Brennan C, Colen RR, Colman H, Flanders AE, Giannini C, Grifford M, Iavarone A, Jain R, Joseph I, Kim J, Kasaian K, Mikkelsen T, Murray BA, O'Neill BP, Pachter L, Parsons DW, Sougnez C, Sulman EP, Vandenberg SR, Van Meir EG, von Deimling A, Zhang H, Crain D, Lau K, Mallery D, Morris S, Paulauskis J, Penny R, Shelton T, Sherman M, Yena P, Black A, Bowen J, Dicostanzo K, Gastier-Foster J, Leraas KM, Lichtenberg TM, Pierson CR, Ramirez NC, Taylor C, Weaver S, Wise L, Zmuda E, Davidsen T, Demchok JA, Eley G, Ferguson ML, Hutter CM, Mills Shaw KR, Ozenberger BA, Sheth M, Sofia HJ, Tarnuzzer R, Wang Z, Yang L, Zenklusen JC, Ayala B, Baboud J, Chudamani S, Jensen MA, Liu J, Pihl T, Raman R, Wan Y, Wu Y, Ally A, Auman JT, Balasundaram M, Balu S, Baylin SB, Beroukhim R, Bootwalla MS, Bowlby R, Bristow CA, Brooks D, Butterfield Y, Carlsen R, Carter S, Chin L, Chu A, Chuah E, Cibulskis K, Clarke A, Coetzee SG, Dhalla N, Fennell T, Fisher S, Gabriel S, Getz G, Gibbs R, Guin R, Hadjipanayis A, Hayes DN, Hinoue T, Hoadley K, Holt RA, Hoyle AP, Jefferys SR, Jones S, Jones CD, Kucherlapati R, Lai PH, Lander E, Lee S, Lichtenstein L, Ma Y, Maglinte DT, Mahadeshwar HS, Marra MA, Mayo M, Meng S, Meyerson ML, Mieczkowski PA, Moore RA, Mose LE, Mungall AJ, Pantazi A, Parfenov M, Park PJ, Parker JS, Perou CM, Protopopov A, Ren X, Roach J, Sabedot TS, Schein J, Schumacher SE, Seidman JG, Seth S, Shen H, Simons JV, Sipahimalani P, Soloway MG, Song X, Sun H, Tabak B, Tam A, Tan D, Tang J, Thiessen N, Triche T Jr, Van Den Berg DJ, Veluvolu U, Waring S, Weisenberger DJ, Wilkerson MD, Wong T, Wu J, Xi L, Xu AW, Yang L, Zack TI, Zhang J, Aksoy BA, Arachchi H, Benz C, Bernard B, Carlin D, Cho J, DiCara D, Frazer S, Fuller GN, Gao J, Gehlenborg N, Haussler D, Heiman DI, Iype L, Jacobsen A, Ju Z, Katzman S, Kim H, Knijnenburg T, Kreisberg RB, Lawrence MS, Lee W, Leinonen K, Lin P, Ling S, Liu W, Liu Y, Liu Y, Lu Y, Mills G, Ng S, Noble MS, Paull E, Rao A, Reynolds S, Saksena G, Sanborn Z, Sander C, Schultz N, Senbabaoglu Y, Shen R, Shmulevich I, Sinha R, Stuart J, Sumer SO, Sun Y, Tasman N, Taylor BS, Voet D, Weinhold N, Weinstein JN, Yang D, Yoshihara K, Zheng S, Zhang W, Zou L, Abel T, Sadeghi S, Cohen ML, Eschbacher J, Hattab EM, Raghunathan A, Schniederjan MJ, Aziz D, Barnett G, Barrett W, Bigner DD, Boice L, Brewer C, Calatozzolo C, Campos B, Carlotti CG Jr, Chan TA, Cuppini L, Curley E, Cuzzubbo S, Devine K, DiMeco F, Duell R, Elder JB, Fehrenbach A, Finocchiaro G, Friedman W, Fulop J, Gardner J, Hermes B, Herold-Mende C, Jungk C, Kendler A, Lehman NL, Lipp E, Liu O, Mandt R, McGraw M, McLendon R, McPherson C, Neder L, Nguyen P, Noss A, Nunziata R, Ostrom QT, Palmer C, Perin A, Pollo B, Potapov A, Potapova O, Rathmell WK, Rotin D, Scarpace L, Schilero C, Senecal K, Shimmel K, Shurkhay V, Sifri S, Singh R, Sloan AE, Smolenski K, Staugaitis SM, Steele R, Thorne L, Tirapelli DP, Unterberg A, Vallurupalli M, Wang Y, Warnick R, Williams F, Wolinsky Y, Bell S, Rosenberg M, Stewart C, Huang F, Grimsby JL, Radenbaugh AJ, Zhang J (2015) Comprehensive, integrative genomic analysis of diffuse lower-grade gliomas. N Engl J Med 372(26):2481–2498. https://doi.org/10.1056/NEJMoa1402121
43. Valera-Mele M, Mateo Sierra O, Sola Vendrell E, Guzman de Villoria LJ, Carvajal Diaz L, Gil de Sagredo Del Corral OL, Garcia Leal R (2018) Evaluación del impacto del cambio diagnóstico de los gliomas aplicando la nueva clasificación de la OMS de 2016 sobre una serie de casos. In: Assessment of the impact of glioma diagnostic reclassification following the new 2016 WHO classification on a series of cases. Neurocirugia. https://doi.org/10.1016/j.neucir.2018.09.002
44. van den Bent MJ, Smits M, Kros JM, Chang SM (2017) Diffuse infiltrating oligodendroglioma and astrocytoma. J Clin Oncol 35(21):2394–2401. https://doi.org/10.1200/jco.2017.72.6737

45. Eckel-Passow JE, Lachance DH, Molinaro AM, Walsh KM, Decker PA, Sicotte H, Pekmezci M, Rice T, Kosel ML, Smirnov IV, Sarkar G, Caron AA, Kollmeyer TM, Praska CE, Chada AR, Halder C, Hansen HM, McCoy LS, Bracci PM, Marshall R, Zheng S, Reis GF, Pico AR, O'Neill BP, Buckner JC, Giannini C, Huse JT, Perry A, Tihan T, Berger MS, Chang SM, Prados MD, Wiemels J, Wiencke JK, Wrensch MR, Jenkins RB (2015) Glioma groups based on 1p/19q, IDH, and TERT promoter mutations in tumors. N Engl J Med 372(26):2499–2508. https://doi.org/10.1056/NEJMoa1407279

46. Gadji M, Fortin D, Tsanaclis AM, Drouin R (2009) Is the 1p/19q deletion a diagnostic marker of oligodendrogliomas? Cancer Genet Cytogenet 194(1):12–22. https://doi.org/10.1016/j.cancergencyto.2009.05.004

47. Waitkus MS, Diplas BH, Yan H (2016) Isocitrate dehydrogenase mutations in gliomas. Neuro-Oncology 18(1):16–26. https://doi.org/10.1093/neuonc/nov136

PAPER III

Diagnostic utility of Restriction Spectrum Imaging in the characterization of the peritumoral brain zone in glioblastoma: Analysis of overall and progression-free survival.

Anna Latysheva, MD[1,5] ID 0000-0002-0061-5609, *Oliver Marcel Geier, PhD[2], Tuva R. Hope, PhD[2],* Marta Brunetti, PhD[3], Francesca Micci, PhD[3], Einar Osland Vik-Mo, MD, PhD[4,5] Kyrre E. Emblem, PhD[2], Andrés Server, MD, PhD[1].

[1]Section of Neuroradiology, Department of Radiology, Oslo University Hospital – Rikshospitalet, Oslo, Norway.
[2]Department of Diagnostic Physics, Oslo University Hospital – Rikshospitalet, Oslo, Norway.
[3]Section for Cancer Cytogenetics, Institute for Cancer Genetics and Informatics, Oslo University Hospital.
[4]Department of Neurosurgery, Oslo University Hospital – Rikshospitalet, Oslo, Norway.
[5]Faculty of Medicine, University of Oslo, Oslo, Norway.

Corresponding author:

Anna Latysheva

Section of Neuroradiology, Dept. of Radiology , Oslo University Hospital - Rikshospitalet, Postbox 4950 Nydalen, 0424 OSLO, Norway
Telephone number: +47 91598432. Fax number: +47 23072610.
E-mail address: alatysheva@ous-hf.no

Abbreviations

RSI = Restriction Spectrum Imaging, FA = fractional anisotropy, MD = mean diffusivity, OS = overall survival, PFS = progression free survival, CET= contrast-enhancing tumor core, PBZ = peritumoral brain zone, PEZ = peri-enhancing zone, NZ = near zone, FZ = far zone.

Abstract

Background and Purpose.

Standard surgical and adjuvant therapy of glioblastoma are mainly guided by structural MRI which is insufficient for identification and delineation of the non-enhanced infiltrating part of the tumor. We studied the ability of Restriction Spectrum Imaging (RSI), a novel advanced diffusion imaging technique, to estimate levels of cellularity in different glioblastoma regions and evaluated their prognostic value.

Methods

Forty-two patients with untreated glioblastoma, were examined with an advanced MRI tumor protocol. ROI was obtained from the contrast-enhancing part of tumor and the peritumoral brain zones and then co-registered with RSI-cellularity index, fractional anisotropy (FA) and mean diffusivity (MD) maps. The ability of diffusion metrics to stratify survival were assessed by Cox proportional hazard regression analysis (CPH), adjusted for significant clinical predictors.

Results

The highest RSI-cellularity index values were measured in the contrast-enhancing tumor core with negative gradient towards to the tumor edge ($P<0.001$). Shorter OS was significant associated with higher RSI-cellularity index (Hazard ratio (HR) 3.6, $P=0.002$) with synchronal decrease in FA (HR 5.72, $P=0.006$) and MD (HR 0.31, $P=0.008$) in the contrast-enhanced tumor core. This association was also consistent for RSI-cellularity index value measured in the peri-enhancing zone (HR 3.6, $P=0.041$).

Conclusion

Unlike conventional diffusion metrics, RSI-cellularity index was robust and stable measurement for tumor tissue cellularity. Pretreatment RSI may be used as biomarker to improve risk stratification in patients with glioblastoma.

Introduction

Glioblastomas are the most common and invasive primary tumors of the brain in adults. Despite recent advents in treatment options, the prognosis of glioblastoma remains nearly uniformly fatal. Among other prognostic predictors, surgical treatment related to its extension is the only one that can be directly influenced in the initial stage of disease.[1]Complete macroscopic tumor removal (gross total resection) in patients with glioblastoma is a primary surgical goal and in comparison to subtotal resection prolongs overall survival (OS) and progression free survival (PFS).[2]

Glioblastoma growth is characterized by diffuse infiltration of normal brain tissue, with tumor cells moving through the hyaluronic acid-rich parenchyma towards microvasculature and then migrating rapidly along vascular tracks.[3] Intraoperative navigation based mainly on postcontrast MRI is the standard of care for glioma surgery in an effort to achieve maximal safety resection. Still, this technique is based on visual identification of regions with disrupted blood-brain barrier that cannot accurately detect tumor infiltration beyond the apparent borders of the enhancing region. Similarly, the current radiation treatment regimen involves exposure of a margin around the resection cavity, which normally receives a spatially uniform radiation dose.[4, 5]Non-invasive and robust diagnostic biomarkers are therefore warranted for identification of high-cellularity components in efforts to increase cytoreductive treatment with real benefits to prognosis.

ADC derived from DWI is inversely related to tissue cellularity, the number of tissue cells, and has been proposed to be a noninvasive imaging biomarker for detection of intratumoral high cell density areas[6]. However, edema associated with inflammation, infiltration and necrosis increases extracellular diffusion and thus ADC values[7].

In this work we attempted to evaluate the role of Restriction Spectrum Imaging (RSI), a novel diffusion-weighted MRI technique, that separates the relative contributions of hindered and restricted signals originating from extracellular and intracellular water compartments, respectively, by using a multi-shell acquisition, together with an advanced linear mixture model to resolve a spectrum of length scales and incorporating geometric information [8, 9]. Use of RSI has previously demonstrated to improve tumor delineation and also to help stratify survival in patients with glioblastoma [10, 11].

In the current study, we tested the hypothesis that the cellularity in the peritumoral brain zone declines with increased distance to the tumor core and RSI is able to provide information that highlights heterogeneity with the peritumoral brain zone. Therefore, the aims of this study were threefold: (1) to evaluate the ability of RSI for improved delineation of tumor core from peritumoral brain zone and perilesional normal-appearing zone; (2) to evaluate the association between RSI metrics and O^6-methylguanine-DNA methyltransferase promoter methylation (MGMT) status; (3) to investigate the association of RSI parameters with OS and PFS in patients with glioblastoma and whether the RSI-cellularity index value would be a more robust imaging biomarker than DTI derived parameters.

Materials and Methods

Study design and ethics

The study is a prospective cross-sectional analysis of data acquired from Oslo University Hospital from June 2016 to December 2018. All patients provided written informed consent for use of clinical data and imaging surveys for research purpose. Institutional and regional medical ethics committees approved this study, REC-number 2018/2464.

Patient population

The prospective cohort included ninety-two patients who required an image-guided stereotactic biopsy or surgery for presumed high-grade gliomas referred from local hospitals. ***Supplementary figure 1*** shows the patient selection and dichotomization in a flow diagram with inclusion and exclusion criteria. Advanced tumor MRI examination (anatomic, diffusion MRI, perfusion MRI, spectroscopy and RSI imaging modalities) was obtained before surgical treatment. The diagnosis was based on histological and molecular examination of specimens obtained by stereotactic navigated biopsy or from tumor resection. In the final study cohort, forty-two patients with glioblastoma, *IDH-wildtype,* classified according 2016 World Health Organization (WHO) classification of tumors of the Central Nervous System (CNS) were included[12]. Maximum safe resection was performed by using neuronavigation (BrainLab) and 5-aminolevulinic acid (5-ALA) fluorescence guidance. The extension of resection was considered either gross total resection or subtotal resection. Standard treatment, consisting of radiotherapy (a total of 60 Gy in fractions of 2 Gy per day over 6 weeks) and concomitant/adjuvant chemotherapy (Temozolomide) was initiated 3-4 weeks after surgery. Patients and tumors characteristics including age, Karnofsky performance status, MGMT promoter methylation status and degree of surgical extent of resection are shown in ***Table 1.***

Table 1. Molecular profile and clinical characteristics of the patients sample.

Gender[a]	Karnofsky performance status scale[b]	Surgical extension[c]	*MGMT* promoter methylation status[d]
26/16(62.8/37.2%)	20/22 (47.6/52.4 %)	18/24(42.9/57.1%)	26/16(61.9/38.1%)

[a] *No. of male/female (%)*

[b] *No. of patients with Karnofsky performance scale ≥ 70/ No. of patients with Karnofsky performance scale < 70.*

[c] *No. of subtotal resections/ No. of gross total resections*

[d] *No. of patients with MGMT methylated tumors/No. of patients with non-MGMT methylated tumors*

Data acquisition/MRI protocol

All examinations were performed on a 3T MR scanners (Skyra, Siemens Healthcare, Erlangen Germany) using a 20 channel head/neck coil. The following tumor protocol was carried out before gadolinium-based contrast agent (Clariscan 279.3 mg/mL, 0.2 mL/kg bodyweight, GE Healthcare, USA) administration: RSI, DTI, 3D MPRAGE images, FLAIR and axial T2-weighted images. After contrast agent injection: DSC MRI with a bolus injection (3ml/s) of the Gadolinium-based contrast agent, followed by 30 ml of physiologic saline solution; susceptibility weighted imaging (SWI); 3D MPRAGE images. Specific sequence parameters are summarized in ***Supplementary table 1***. RSI was performed using spin echo planar imaging with 5 b-values of 0, 200, 800, 1500 and 3000 s/mm ^{2} and with 12 directions at each respective nonzero b-value.

DNA extraction and molecular analyses

The DNA was extracted using the Maxwell 16 extractor (Promega, Madison, WI, USA) and the Maxwell 16 Tissue DNA Purification kit (Promega) according to the manufacturer's recommendations. The mutational analyses were performed using M13-linked Polymerase chain reaction (PCR) primers designed to flank and amplify targeted sequences. All PCR were run on a Bio-Rad C100 Thermal Cycler (Bio-Rad Laboratories, Hercules, CA, USA). Direct sequencing was performed using a 3500 Genetic Analyser (Applied Biosystems, Foster City, CA, USA). The BLAST (http://blast.ncbi.nlm.nih.gov/blast.cgi) and BLAT (http://genome.ucsc.edu/cgi-bin/hgblat) programs were used for computer analysis of sequence data. Detailed information about analysis of *IDH1*, *IDH2, TERT* and *MGMT* using PCR is outlined in ***Supplementary table 2*** and were described previously [13].

Image processing and model estimation

All image post processing was carried out using the FMRIB Software Library v6.0 (FSL) [14] and Matlab R2018b (MathWorks, Natick, Massachusetts). First, the DWI were denoised using local Principal Component Analysis (LPCA) filter [15] and Gibbs ringing artifacts were removed [16]. Brain extraction, EPI-distortion, eddy-current and movement corrections were then applied using the *bet*, *topup* and *eddy* toolboxes from FSL. The quality of all corrected output data was evaluated by visual inspection. A standard tensor model was fit to the DW-data using weighted linear least-squares fit [17]and the b-values of 0, 200, 800 s/mm^2. The descriptive diffusion parameters fractional anisotropy (FA) and mean diffusivity (MD) were derived based on the tensor information [17]. Furthermore, RSI was estimated from the high-angular DW data based on the parameterization of the fiber orientation density function (FOD) using 4th order spherical harmonics, combined with an axially-symmetric Gaussian model [8]. The RSI spectrum was defined as a combination of anisotropic, restricted and free/hindered diffusion compartments as detailed by White et al [8]. For the purpose of this study we focused the analysis on the water signal fraction from the spherically restricted diffusion compartment. Based on the water signal fraction of this compartment, we generated RSI-cellularity index maps, where white and grey matter regions of apparent healthy brain tissue of 15 subjects were used as reference [9].

Segmentation of regions of interest

Tumor segmentation was performed semi-automatically based on region growing algorithm, on 3D volumetric T1 postcontrast sequence using a dedicated software package nordicICE Version 4.0 (NoridcNeuroLab AS, Bergen, Norway) by A.L. in collaboration with A.S., board-certified neuroradiologists (with 5 and 25 years of neuro-oncology imaging experience). Discrepancies were

resolved through a consensus discussion. Both neuroradiologists were blinded for survival data. The volumetric region of interest (ROI) was obtained from the contrast-enhancing tumor core (CET) in all cases. In cases of multifocal and multicentric glioblastoma, the largest enhancing lesion was chosen for segmentation. The peritumoral brain zone (PBZ) is defined as the area surrounding the tumor in the absence of contrast-enhancement in T1 3-dimensional MRI. In addition, this area shows a hyperintense signal in T2-weighted and FLAIR images [18]. ROI with extended margins were generated by means of morphological dilation of the CET using a spherical structuring element Matlab (v.R2017a, MathWorks Inc., Mass., USA). CET substraction provided three concentric volumetric regions with 5 mm thickness in the PBZ. The peri-enhancing zone (PEZ) defined as the area of non-contrast enhancing tumor surrounding the CET at a distance of 5 mm. The near zone (NZ) defined between 5 and 10 mm from the CET and the far zone (FZ) defined between 10 and 15 mm from the CET. ROIs were also drawn in the ipsilateral normal-appearing zone (iNAZ) defined as the area immediately adjacent to the distal edge of the PBZ and in contralateral white matter to the tumor (cWMZ). All ROI's were then co-registered with the RSI-cellularity index, FA and MD respectively maps. Whole-tumor normalized histogram distributions of the RSI-cellularity index, FA and MD were created as described elsewhere [19]. Based on previous studies, MD 10th percentile and RSI-cellularity index 90th percentile values were used for further analysis [20]. The image post-processing workflow is demonstrated in ***Figure 1***.

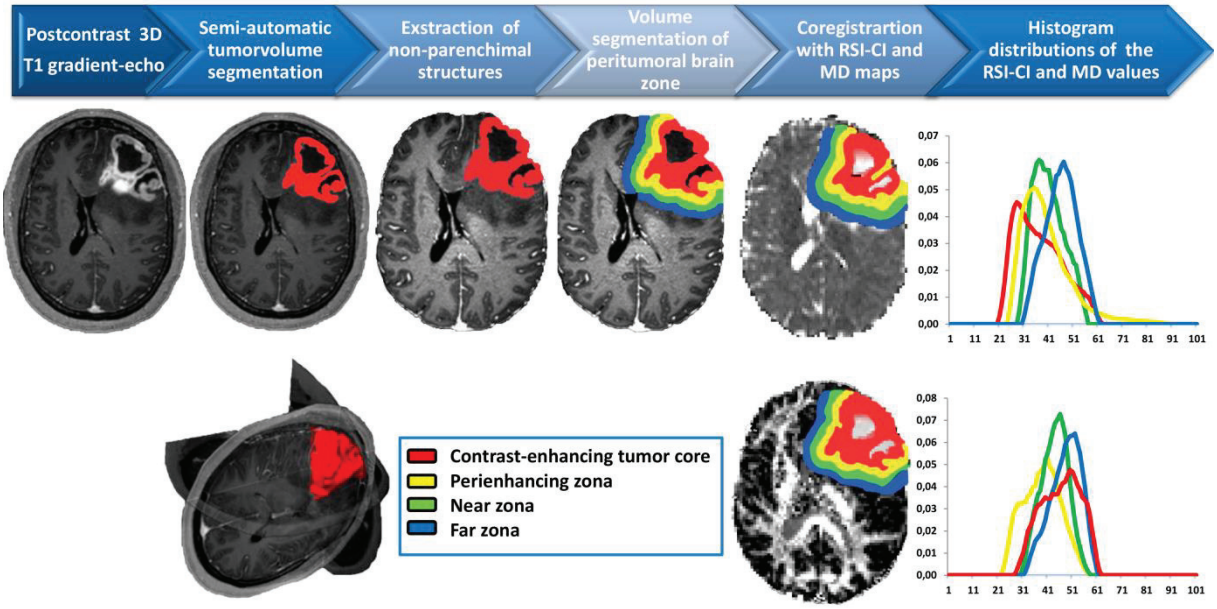

Figure 1. Image post processing workflow. The volumetric region of interest (ROI) was obtained from the contrast-enhancing tumor core and three peritumoral zones. All ROI's were then co-registered with the RSI-cellularity index, FA and MD respective maps and normalized histogram distributions were created.

Survival assessment

Follow-up scans were acquired within 24 hours after surgery, after radiotherapy and at 3-month intervals thereafter. OS and PFS were defined as time interval (number of days) from initial diagnosis

to patient death or tumor progression, respectively. Tumor progression was defined according to updated Response Assessment in Neuro-Oncology criteria [21]. Patients still alive or lost to follow-up were censored for PFS on the date of their last central nervous system imaging study, and for OS on the date of their last clinical follow-up visit.

Statistical analysis

Analysis was performed using SPSS 25 (SPSS, Chicago, USA) and Stata 14 (STATA Corp., Texas, USA). The Mann-Whitney U-test was used to compare diffusion parameters between different ROI inside and outside contrast enhanced tumor core. The independent significance of various predictors (age, extent of resection, Karnofsky performance status scale and genetic profile) on overall survival and progression-free survival were assessed by Univariate Cox proportional hazard regression analysis (CPH). Multivariate CPH analysis, that included significant clinical variables, was performed to evaluate the contribution of diffusion parameters from different tumor compartments to PFS and OS. A classification and leave-one-out cross-validation (LOOCV) algorithm with 10-fold cross-validation was used to calculate optimal cut-off for dichotomize RSI-cellularity index, FA and MD metrics. Kaplan–Meier survival analyses were conducted based on the subgroups obtained from the LOOCV split and compared using a log-rank test. For all cases, a two-tailed P-value of 0.05 or less was considered statistically significant including Holm-Bonferroni correction in the case of multiple comparisons.

Results

Patient characteristics and survival

The median age of the patients with glioblastoma was 65 years (range, 39-87 years). The Median PFS was 184 days, and the median OS was 245 days. Twenty-nine patients had tumor progression following Response Assessment in Neuro-Oncology criteria and nineteen were deceased at the end of the study inclusion time. CPH models revealed that the total resection and Karnofsky performance status over 70 were significantly associated with longer PFS (hazard ratio (HR) 3.5, 95% confidence interval (CI) 1.0-12.1; P=0.04 and HR 4.4, 95%CI 1.6-12.1, P=0.006) respectively, and longer OS (HR 3.8, 95%CI 1.1-12.9, P=0.03 and HR 3.2, 95%CI 1.3 -7.8, P=0.01). These variables were included in subsequent multivariate CPH analyses.

RSI-cellularity index, FA and MD in different glioblastoma compartments

The RSI-cellularity index in CET was on average 24% higher than the value in PEZ (P <0.001) and 28% higher than in NZ (P=0.003) (CET > PEZ > NZ). RSI-cellularity index in FZ retained a higher value, but not significant, compared to those of CET, PEZ and NZ. The lowest MD was estimated in CET with a positive gradient from extern border towards the periphery (CET < PEZ < NZ), but significant differences between any parts of the PBZ were not observed. Moreover, the 25 % lower FA was measured in CET compared with PEZ (P < 0.01) (CET > PEZ). However, notable differences were not registered between FA values in CET and NZ or FZ. Scatter plots in ***Figure 2*** show the distribution of diffusion parameters values for all tumoral and peritumoral zones.

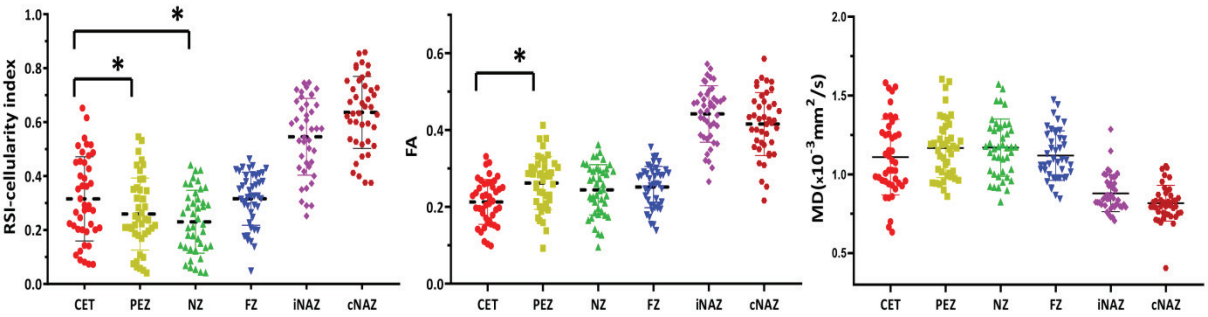

Figure 2. Scatter plot with distribution (median with interquartile range) of a) RSI-cellularity index b) FA and c) MD values in CET, PEZ, NZ,FZ,iNAZ and cNAZ encodet by the colors in patients with glioblastoma. The RSI-cellularity index in CET was significantly higher than those of PEZ (P <0.001) and NZ (P=0.003). Significantly lower FA was measured in CET (P < 0.01) without notable difference between FA values outside CET. No statistical difference was registrated between MD value in any of zones. The asterisks are showing significant differences.

Relationship between survival outcome and diffusion metrics

Higher values of RSI-cellularity index with synchronal lower MD in CET were significantly associated with shorter PFS (177 vs 410 days, p= 0.015; 174 vs 378 days, p= 0.029, respectively) and OS (543 vs 215 days, p=0.002 173 vs 507 days, p=0.008 respectively). This association was also consistent for RSI-cellularity index value measured in PEZ (PFS: 188 vs 429, p<0.048 and OS: 298 vs 572, p=0.041) and NZ (PFS: 150 vs 459, p<0.015 and OS: 166 vs 643, p<0.020). Lower FA values in CET and PEZ were significantly associated with poorer PFS (216 vs 441 days, p= 0.006) and OS (316 vs 601 days, P=0.006). In contrast, no statistical significance was reached between MD values from PEZ, NZ, FZ and survival outcome. The total results of multivariate CPH analyses adjusting for significant clinical covariates (extension of resection, Karnofsky performance status scale) for diffusion image metrics are summarized in ***Table 2***. The most significant survival predictors were RSI-cellularity index in CET, PEZ, NZ and FA in CET with respective hazard ratios of 3.60, 3.60, 3.0, and 5.72. The corresponding Kaplan-Meier survival curves for RSI-cellularity index with cut-off points and log-rank values for each of glioblastomas zones are shown in ***Supplementary figure 2***. Similar survival curves for FA and MD are shown in ***Supplementary figure 3*** and ***Supplementary figure 4.*** RSI-cellularity index in CET, PEZ and NZ stratify both progression free survival and overall survival with highest cut-off value in CET, estimated to 0.210 vs 0.205 for PEZ and vs 0.200 for NZ. Patients with MD in CET under cut-of value 0.83 x 10^{-3} mm^2/s and FA cut-of value under 0.17 had the shortest survival time.

Table 2. Summary of multivariate CPH with included significant clinical covariates (extension of resection and Karnofsky performance status scale).

	Region of interest	Progression – free survival		Overall survival	
		P-value	**HR (95% CI)**	**P-value**	**HR (95% CI)**
RSI-cellularity index	***Contrast-enhanced tumor core***	**0.015**	3.48 (1.2; 9.5)	**0.002**	3.60 (1.3; 9.5)
	Peri-enhancing zone	**0.048**	3.60 (1.0; 12.3)	**0.041**	3.60 (1.0; 12.3)
	Near zone	**0.015**	4.70 (1.3; 16.5)	**0.020**	3.00 (2.0; 24.9)
	Far zone	0.112	2.30 (0.6; 7.9)	0.551	3.30 (0.9; 11.7)
FA	***Contrast-enhanced tumor core***	**0.006**	5.43 (1.2;16.9)	**0.006**	5.72 (1.8-13.5)
	Peri-enhancing zone	0.140	2.21 (0.7; 6.7)	0.058	2.84 (0.9;8.3)
	Near zone	0.416	1.41 (0.5; 3.3)	0.264	1.69 (0.6;4.2)
	Far zone	0.193	2.03 (0.6; 6.0)	0.098	2.44 (0.8;7.3)
MD	***Contrast-enhanced tumor core***	**0.029**	0.37 (0.1; 0.9)	**0.008**	0.31 (0.1; 0.8)
	Per-ienhancing zone	0.301	0.63 (0.3; 1.5)	0.632	0.46 (0.2; 1.1)
	Near zone	0.722	0.85 (0.3; 2.1)	0.912	0.94 (0.4; 2.2)
	Far zone	0.871	1.07 (0.4; 2.6)	0.931	1.04 (0.4; 2.4)

HR = hazard ratio, RSI-cellularity index = restriction spectrum imaging - cellularity index, CI = confident interval, MD = mean diffusivity .

MGMT promoter methylation status and diffusion metrics

Presence of MGMT promoter methylation were significant associated with longer PFS (HR 3.3, 95% CI 1.4;7.9, P=0.006) and longer OS (HR 3.7, 95%CI 1.6;8.7, P=0.002). No statistically significant differences were noted between RSI-cellularity index, FA, nor MD and MGMT promoter methylation status obtained from CET and PBZ.

Discussion

In this work, we studied the ability of RSI to estimate different levels of cellularity in the contrast-enhancing tumor core and in the peritumoral brain zone of patients with glioblastoma. We also evaluated the prognostic value of RSI in order to correlate with the tumor`s potential aggressive behavior and compare it to the clinical established diffusion metrics such as MD and FA.

The highest RSI-cellularity index was measured in CET with a negative gradient from tumor core to the periphery of peritumoral zone (PEZ and NZ). This observation may be explained by the dominant invasion and consequently highest density of glioma cells in perivascular space, leading to a disruption of endothelial tight junctions and leakage of contrast agent in CET[22, 23]. The decline of glioma cellularity from tumor core to periphery reflects an extensively infiltrating pattern in glioblastomas with the highest concentration of invading cells around primary tumor mass[24].

Cellularity in peritumoral zone has been investigated in several studies, in which the MRI findings were corroborated by histopathologic analyses, following stereotactic biopsy obtained from the peritumoral zone. The results of these studies are contradictory [25-28]. Barajas et al investigated 119 tissue specimens and reported that ADC associated with tumoral cellularity in the non-enhancing tumor component, but this was not the case in the contrast-enhanced component of the lesion [26]. Chang et al [27] found that tumor cellularity was inversely correlated with ADC signal by using a voxel-level multiparametric MR imaging model, supporting the theory that water diffusion is restricted in hypercellular neoplastic environments. In contrast, Sadeghi et al [28] did not find negative correlation between ADC ratios and cell density in either tumor core or the peritumoral tissue in examination of the 33 tumor tissue specimens. Discordance between findings may be explained by the inclusion in this study population of both low and high grade gliomas, while Barajas [26] and Chang [27] investigated exclusively glioblastomas. The differences in strategies for obtaining tissue samples (targeted by contrast T1weighted [27, 28] vs by diffusion and perfusion signal [29]) may be an additional reason for discordances.

Shorter survival outcomes were significantly associated with higher RSI-cellularity index in the CET. Interestingly, this correlation was also persistent in the PEZ and NZ. Thus, our findings highlight the importance of the peritumoral areas (PEZ and NZ) in order to predict further tumor expansion and tumor relapse [30]. We did observe a significant association between lower MD in the CET and shorter survival, but in contrast to RSI-cellularity index, MD in the peritumoral zones did not show predictive value to survival outcome. There is still no consensus in literature on how strong relation between the ADC value and tumor cellularity is. Indeed, several studies demonstrate correlation between ADC and cellularity and, as consequence, also between ADC and survival outcome in patients with gliomas [31-33]. But these correlations cannot be generalized. The studies including patients with glioblastomas only, report a weak-to-moderate inverse correlation between ADC and cellularity[34, 35]. Possible explanation for these discrepancies may be found in the high heterogeneity of glioblastoma tissue. Theoretically, any modification of the extracellular matrix can influence the ADC. Glioma cells tend to produce large amount of extracellular matrix component [36], which serves as substrate for cells migration. These structures may exert considerable restriction to diffusion. On the other hand, destruction of normal extracellular matrix by glioma cells and secondary edema increases free diffusion and subsequent ADC. Also necrosis in different stages of microstructural tissue damage can lead to lower and elevated ADC values [37].

FA, which reflects integrity and disruption of white matter fibers, was significantly lower in the CET than PEZ. This finding has been supported by previous studies demonstrating the most extensive loss of fiber connectivity in the aggressive parts of the tumor with highest cellularity [38, 39]. Less variability was found between FA values in PEZ, NZ and FZ than it was observed between RSI-cellularity index values in the same zones. This finding may indicate severe affection of FA value than RSI-cellularity index by extracellular edema in peritumoral zone. Additional explanation may also be found in the

unique invasion pattern that dominates in glioblastoma, tumor cells may migrate along white matter tracks and perivascular spaces [24]. Therefore, despite the differences of cellularity in peri-enhancing areas, the level of diffusion anisotropy is not necessary affected to the same degree. In agreement with previous study, a reduction of FA both in CET and PEZ correlated with shorter survival [39, 40] . In contrast to RSC-cellularity index, FA values in both NZ and FZ had no apparent association to survival, which again highlights the potential of RSI to evaluate tumoral heterogeneity.

Thus, similar to previous studies , our results suggest that RSI may overcome some of the limitations of ADC and FA due to the reduction of sensitivity to the extracellular water. RSI may therefore also provide a more reliable measure of increased cellularity associated with tumor progression.

Several studies have reported that *MGMT* promotor methylated tumors display diffusion MRI features of lower cellularity (high ADC) and severe disruption of white matter tracks (low FA)[41-43]. In contrast, we did not find significant association between any of diffusion metrics and methylation status. These conflicting results may be partially attributed to different methodology (3D ROI analyzed of whole volume tumor in our study versus 2D ROI of the solid part of tumor) [42, 43] and different study populations (*IDH*-wild type glioblastomas versus both *IDH*-mutant and *IDH*- wild type glioblastomas) [43, 44]. In accordance with our results, Ahn S.S.et al [45]and Gupta A. et al [46] did not find any significant correlation between ADC/FA values and *MGMT* promoter methylation status.

Our work has some limitations. First of all, our data were collected from a single institution. Although this approach was selected in efforts to obtain controlled study in which all patients were examined on the same MR scanner with the same tumor protocol. In the future, a cross-site study including data from multiple medical centers needs to evaluate the reproducibility of our results. Furthermore, segmentation of the glioblastomas was performed semimanual that potentially can be a source for sampling bias. However region-grow algorithm for delineation of peritumoral region of interest and extraction of non-brain parenchymal structures was performed automatically. Finally, standard treatment, consisting of radiotherapy and concomitant chemotherapy was started within 4 weeks after surgery. However some differences in radiation doses and timing between radiotherapy sessions were observed, mainly related to patients reduced health status.

Conclusion

In summary, our study demonstrates the importance to analyze structural heterogeneity not only in tumor core but also in the peritumoral brain region. By shedding light on the peritumoral zone, we may better assess the biological behavior of glioblastoma, and thus also its prognosis. In contrast to traditional diffusion metrics, RSI provides a promising prognostic biomarker to depict tumor infiltration in the peritumoral brain zone by removing the hindered diffusion associated with extracellular fluid contents. This characterization of glioblastoma compartments with different levels of cellularity, supplemented by other MRI sequences, can be helpful to optimize the extent of surgical resection, guide optimal biopsy, and radiation field mapping, with significant benefits for patient treatment.

Supplementary material

Supplementary table 1. MRI sequence acquisition parameters .

Sequence	Repetition time (ms)	Echo time (ms)	Field of view (mm)	Flip angle(°)	Matrix	Bandwidth (Hz)
T2	4090	88	230	150	512x435	349
T1	2300	2.98	256	8	256x240	240
FLAIR	5000	387	230	120	256x256	751
DTI	11500	81	280	90	192x192	1446
DSC	1350	30	220	90	130x130	1202
RSI	10600	103	256	90	192x192	1480

FLAIR = fluid-attenuated inversion recovery; DTI = diffusion tensor imaging; DSC = dynamic susceptibility contrast; RSI = restriction spectrum imaging.

Supplementary table 2. Molecular analyses with polymerase chain reaction.

IDH1* and *IDH2	DNA was first amplified in a 10 µl reaction volume using 5 µl of Big Dye Direct PCR Mastermix (Applied Biosystems) and 1.5 µl of the primer combination IDH1-rs1-126F and IDH1-rs1-301R for *IDH1,* and *IDH*2-rs12-63F and *IDH*2-rs12-317R for *IDH2.* The thermal cycling for *IDH1* and *IDH2* was as follows: an initial step at 95°C for 10 min, followed by 35 cycles at 96°C for 3 sec, 62°C for 15 sec, 30 sec at 68°C, followed by a final step at 72°C for 2 min. Mutated and wild-type plasmids for *IDH1* and *IDH2* were used to check the accuracy of our analyses.
TERT	The *TERT* promoter region was amplified using PCR in order to detect the possible mutations −C228T and −C250T which correspond to positions 124 and 146 nt upstream of the *TERT* ATG start site (Killela et al., 2013) [47], respectively. DNA was amplified in 10 µl PCR volume containing 5 µl of Big Dye Direct PCR Mastermix, 0.8 µM of each primers, *TERT*F1 and the reverse primer *TERT*R2, and 4 ng of genomic DNA. The PCR program started with an initial step at 95°C for 10 min followed by 35 cycles at 96°C for 3 sec, 58°C for 15 sec, 30 sec at 68°C, and a final step at 72°C for 2 min.
MGMT promoter methylation	Unmethylated cytosine residues were converted to uracil by bisulfite treatment of 500 ng DNA using the EpiTect Bisulfite Kit (Qiagen, Hilden, Germany) and the QiaCube automated purification system (Qiagen) according to the manufacturer's recommendations. The Therascreen MGMT Pyro Kit and the PyroMark Q24 system (both from Qiagen) were used to assess the methylation status of the MGMT gene promoter. In brief, bisulfite converted genomic DNA was amplified by PCR, the amplicons were immobilized on streptavidin beads, and single-stranded DNA was prepared, sequenced, and finally analyzed on the PyroMark Q24 system. Detailed information about the procedure can be found in the following links: https://www.qiagen.com/no/resources/resourcedetail?id=29031fd2-6d22-4152-b544-288665bc5abc&lang=en, https://www.qiagen.com/no/resources/resourcedetail?id=59f0275de60f-4517-b786-b0e0ca13952e&lang=en, https://www.qiagen.com/no/resources/resourcedetail?id=a06f1196-2bd0-40af-87d5-45c80c285b48&lang=en. According to the company's information, the limit of blank values represents methylation frequencies obtained from healthy blood donor samples with a probability of 95%: 1.5, 1.8, 3.2, and 3.4 for CpG sites 1, 2, 3, and 4, respectively (mean for CpG sites 1 to 4=2.5). In our assays, the cut-off frequency for accepting methylation as positive for all four CpG sites was set to 10%.
IDH1 and IDH2 = Isocitrate dehydrogenase 1 and 2 , TERT = telomerase reverse transcriptase , MGMT = O^6-methylguanine-DNA methyltransferase promoter methylation.	

Supplementary figure 1. Flow diagram demonstrates the patient selection and dichotomization with inclusion and exclusion criteria.

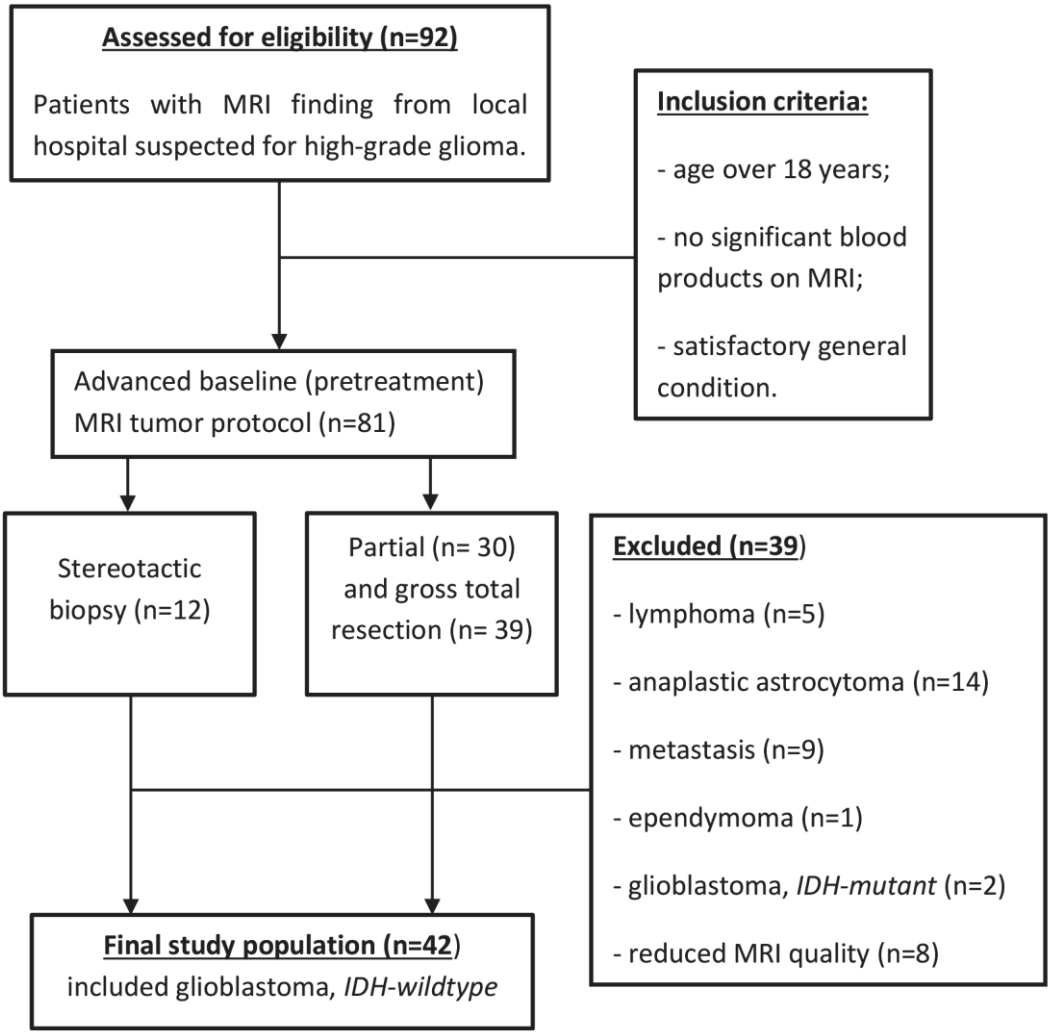

Supplementary figure 2. Kaplan–Meier survival curves stratified by RSI-cellularity index derived from CET, PEZ, NZ and FZ. RSI-cellularity index in CET, PEZ and NZ stratified progression free survival and overall survival, but not RSI-cellularity index in FZ.

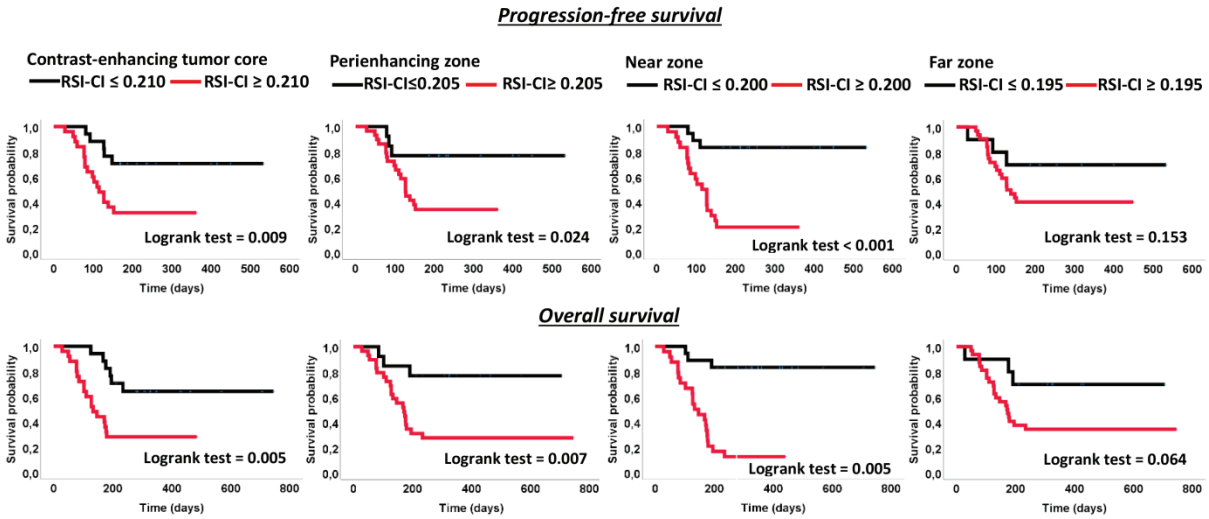

Supplementary figure 3 (on-line). Kaplan-Meier curves of progression-free survival and overall survival in patients with glioblastoma stratified by FA. Only FA in CET was significant associated with both progression free survival and overall survival.

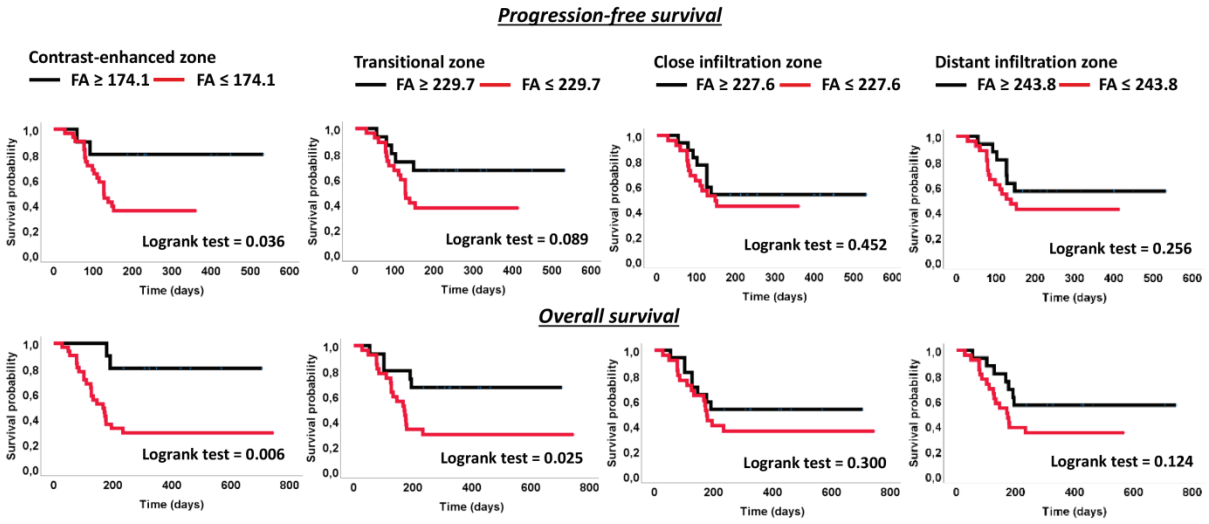

Supplementary figure 4 (on-line). Kaplan-Meier curves of progression-free survival and overall survival in patients with glioblastoma stratified by MD. MD stratified progression free survival and overall survival only in CET, but not in peritumoral brain zones.

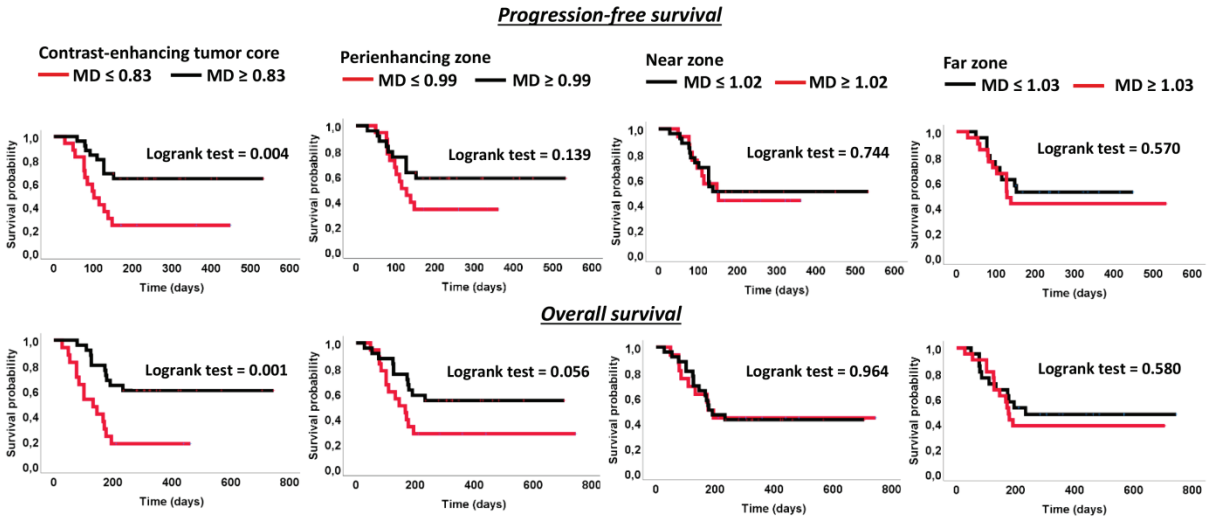

Referanses:

1. Neira JA, Ung TH, Sims JS, et al. Aggressive resection at the infiltrative margins of glioblastoma facilitated by intraoperative fluorescein guidance. *Journal of neurosurgery* 2017;127:111-122
2. Brown TJ, Brennan MC, Li M, et al. Association of the Extent of Resection With Survival in Glioblastoma: A Systematic Review and Meta-analysis. *JAMA oncology* 2016;2:1460-1469
3. Wolf KJ, Lee S, Kumar S. A 3D topographical model of parenchymal infiltration and perivascular invasion in glioblastoma. *APL bioengineering* 2018;2
4. Stupp R, Taillibert S, Kanner AA, et al. Maintenance Therapy With Tumor-Treating Fields Plus Temozolomide vs Temozolomide Alone for Glioblastoma: A Randomized Clinical Trial. *Jama* 2015;314:2535-2543
5. Davis ME. Glioblastoma: Overview of Disease and Treatment. *Clinical journal of oncology nursing* 2016;20:S2-8
6. Sugahara T, Korogi Y, Kochi M, et al. Usefulness of diffusion-weighted MRI with echo-planar technique in the evaluation of cellularity in gliomas. *Journal of magnetic resonance imaging : JMRI* 1999;9:53-60
7. Chenevert TL, Sundgren PC, Ross BD. Diffusion imaging: insight to cell status and cytoarchitecture. *Neuroimaging clinics of North America* 2006;16:619-632, viii-ix
8. White NS, Leergaard TB, D'Arceuil H, et al. Probing tissue microstructure with restriction spectrum imaging: Histological and theoretical validation. *Human brain mapping* 2013;34:327-346
9. Brunsing RL, Schenker-Ahmed NM, White NS, et al. Restriction spectrum imaging: An evolving imaging biomarker in prostate MRI. *Journal of magnetic resonance imaging : JMRI* 2017;45:323-336
10. White NS, McDonald CR, Farid N, et al. Improved conspicuity and delineation of high-grade primary and metastatic brain tumors using "restriction spectrum imaging": quantitative comparison with high B-value DWI and ADC. *AJNR American journal of neuroradiology* 2013;34:958-964, s951
11. McDonald CR, Delfanti RL, Krishnan AP, et al. Restriction spectrum imaging predicts response to bevacizumab in patients with high-grade glioma. *Neuro-oncology* 2016
12. Louis DN, Perry A, Reifenberger G, et al. The 2016 World Health Organization Classification of Tumors of the Central Nervous System: a summary. *Acta neuropathologica* 2016;131:803-820
13. Agostini A, Panagopoulos I, Andersen HK, et al. HMGA2 expression pattern and TERT mutations in tumors of the vulva. *Oncology reports* 2015;33:2675-2680
14. Smith SM, Jenkinson M, Woolrich MW, et al. Advances in functional and structural MR image analysis and implementation as FSL. *Neuroimage* 2004;23:S208-S219
15. Manjon JV, Coupe P, Concha L, et al. Diffusion weighted image denoising using overcomplete local PCA. *PloS one* 2013;8:e73021
16. Kellner E, Dhital B, Kiselev VG, et al. Gibbs-ringing artifact removal based on local subvoxel-shifts. *Magnetic resonance in medicine* 2016;76:1574-1581
17. P.B. K. Introduction to diffusion tensor imaging mathematics: Part III. Tensor calculation, noise, simulations, and optimization. Concepts in Magnetic Resonance Part A.
18. Lemee JM, Clavreul A, Menei P. Intratumoral heterogeneity in glioblastoma: don't forget the peritumoral brain zone. *Neuro-oncology* 2015;17:1322-1332
19. Emblem KE, Pinho MC, Zollner FG, et al. A generic support vector machine model for preoperative glioma survival associations. *Radiology* 2015;275:228-234
20. McDonald CR, Delfanti RL, Krishnan AP, et al. Restriction spectrum imaging predicts response to bevacizumab in patients with high-grade glioma. *Neuro-oncology* 2016;18:1579-1590
21. Sharma M, Juthani RG, Vogelbaum MA. Updated response assessment criteria for high-grade glioma: beyond the MacDonald criteria. *Chinese clinical oncology* 2017;6:37
22. Cuddapah VA, Robel S, Watkins S, et al. A neurocentric perspective on glioma invasion. *Nature reviews Neuroscience* 2014;15:455-465

23. Diksin M, Smith SJ, Rahman R. The Molecular and Phenotypic Basis of the Glioma Invasive Perivascular Niche. *International journal of molecular sciences* 2017;18
24. Claes A, Idema AJ, Wesseling P. Diffuse glioma growth: a guerilla war. *Acta neuropathologica* 2007;114:443-458
25. Akbari H, Macyszyn L, Da X, et al. Imaging Surrogates of Infiltration Obtained Via Multiparametric Imaging Pattern Analysis Predict Subsequent Location of Recurrence of Glioblastoma. *Neurosurgery* 2016;78:572-580
26. Barajas RF, Jr., Phillips JJ, Parvataneni R, et al. Regional variation in histopathologic features of tumor specimens from treatment-naive glioblastoma correlates with anatomic and physiologic MR Imaging. *Neuro-oncology* 2012;14:942-954
27. Chang PD, Malone HR, Bowden SG, et al. A Multiparametric Model for Mapping Cellularity in Glioblastoma Using Radiographically Localized Biopsies. *AJNR American journal of neuroradiology* 2017;38:890-898
28. Sadeghi N, D'Haene N, Decaestecker C, et al. Apparent diffusion coefficient and cerebral blood volume in brain gliomas: relation to tumor cell density and tumor microvessel density based on stereotactic biopsies. *AJNR American journal of neuroradiology* 2008;29:476-482
29. Barajas RF, Jr., Hodgson JG, Chang JS, et al. Glioblastoma multiforme regional genetic and cellular expression patterns: influence on anatomic and physiologic MR imaging. *Radiology* 2010;254:564-576
30. Alieva M, Leidgens V, Riemenschneider MJ, et al. Intravital imaging of glioma border morphology reveals distinctive cellular dynamics and contribution to tumor cell invasion. *Scientific reports* 2019;9:2054
31. Higano S, Yun X, Kumabe T, et al. Malignant astrocytic tumors: clinical importance of apparent diffusion coefficient in prediction of grade and prognosis. *Radiology* 2006;241:839-846
32. Hilario A, Ramos A, Perez-Nunez A, et al. The added value of apparent diffusion coefficient to cerebral blood volume in the preoperative grading of diffuse gliomas. *AJNR American journal of neuroradiology* 2012;33:701-707
33. Kondo M, Uchiyama Y. Apparent diffusion coefficient histogram analysis for prediction of prognosis in glioblastoma. *Journal of neuroradiology Journal de neuroradiologie* 2018;45:236-241
34. Eidel O, Neumann JO, Burth S, et al. Automatic Analysis of Cellularity in Glioblastoma and Correlation with ADC Using Trajectory Analysis and Automatic Nuclei Counting. *PloS one* 2016;11:e0160250
35. Stecco A, Pisani C, Quarta R, et al. DTI and PWI analysis of peri-enhancing tumoral brain tissue in patients treated for glioblastoma. *Journal of neuro-oncology* 2011;102:261-271
36. HJ S. Structural development in gliomas. *American journal of cancer research* 1938
37. LaViolette PS, Mickevicius NJ, Cochran EJ, et al. Precise ex vivo histological validation of heightened cellularity and diffusion-restricted necrosis in regions of dark apparent diffusion coefficient in 7 cases of high-grade glioma. *Neuro-oncology* 2014;16:1599-1606
38. Jellison BJ, Field AS, Medow J, et al. Diffusion tensor imaging of cerebral white matter: a pictorial review of physics, fiber tract anatomy, and tumor imaging patterns. *AJNR American journal of neuroradiology* 2004;25:356-369
39. Flores-Alvarez E, Durand-Munoz C, Cortes-Hernandez F, et al. *Neurology India* 2019;67:1074-1081
40. Saksena S, Jain R, Narang J, et al. Predicting survival in glioblastomas using diffusion tensor imaging metrics. *Journal of magnetic resonance imaging : JMRI* 2010;32:788-795
41. Moon WJ, Choi JW, Roh HG, et al. Imaging parameters of high grade gliomas in relation to the MGMT promoter methylation status: the CT, diffusion tensor imaging, and perfusion MR imaging. *Neuroradiology* 2012;54:555-563
42. Han Y, Yan LF, Wang XB, et al. Structural and advanced imaging in predicting MGMT promoter methylation of primary glioblastoma: a region of interest based analysis. *BMC cancer* 2018;18:215

43. Rundle-Thiele D, Day B, Stringer B, et al. Using the apparent diffusion coefficient to identifying MGMT promoter methylation status early in glioblastoma: importance of analytical method. *Journal of medical radiation sciences* 2015;62:92-98
44. Romano A, Pasquini L, Di Napoli A, et al. Prediction of survival in patients affected by glioblastoma: histogram analysis of perfusion MRI. *Journal of neuro-oncology* 2018;139:455-460
45. Ahn SS, Shin NY, Chang JH, et al. Prediction of methylguanine methyltransferase promoter methylation in glioblastoma using dynamic contrast-enhanced magnetic resonance and diffusion tensor imaging. *Journal of neurosurgery* 2014;121:367-373
46. Gupta RK, Cloughesy TF, Sinha U, et al. Relationships between choline magnetic resonance spectroscopy, apparent diffusion coefficient and quantitative histopathology in human glioma. *Journal of neuro-oncology* 2000;50:215-226
47. Killela PJ, Reitman ZJ, Jiao Y, et al. TERT promoter mutations occur frequently in gliomas and a subset of tumors derived from cells with low rates of self-renewal. *Proceedings of the National Academy of Sciences of the United States of America* 2013;110:6021-6026

Errata

Navn kandidat: *Anna Latysheva*

Avhandlingstittel: *Diffusion and perfusion-weighted imaging in the structural and functional characterization of cerebral tumors for differential diagnosis and treatment planning*

Forkortelser for type rettelser:

Cor – korrektur

Side	Linje	Fotnote	Originaltekst	Type rettelse	Korrigert tekst
0	Tittel til avhandling		…characterization of cerebral tumors for differential diagnosis…	Cor	…characterization of diffuse gliomas for differential diagnosis…
8	10-12		…advanced MR techniques of perfusion and diffusion imaging, to characterize diffuse gliomas utilizing the World Health Organization (WHO) grading systems…	Cor	…advanced MR techniques, as perfusion and diffusion imaging, to characterize diffuse gliomas with respect to WHO grading systems…
9	19		…biomarkers of glioblastoma…		…biomarkers of glioma…
19	20-21		…to further implement these modalities in a diagnostic workflow, multicentre studies…		…to further implementation of these modalities in a diagnostic workflow, multicenter studies…

21	Tittel til Figure 4.		**Figure 4**. Sir Peter Mansfield (to the left)and Paul Lauterbur (to the right), Picture from: Questions and answers in MRI, https://mri-q.com/who-invented-mri.html	Cor	**Figure 4**. Sir Peter Mansfield (to the left) and Paul Lauterbur (to the right), Picture from: Questions and answers in MRI, courtesy of Allen D. Elster, MRIquestions.com.